The Effect of Noisy Protein Expression on *E. coli*/Phage Dynamics

by

Emily Louise Chapman-McQuiston

BS in Physics, George Mason University, 2002

MS in Physics, University of Pittsburgh, 2004

Submitted to the Graduate Faculty of

Arts and Sciences in partial fulfillment

of the requirements for the degree of

PhD in Physics and Astronomy

University of Pittsburgh

2007

UNIVERSITY OF PITTSBURGH

Faculty of Arts and Sciences

This dissertation was presented

by

Emily Louise Chapman-McQuiston

It was defended on

November 13, 2007

and approved by

Xiao-lun Wu, Professor, Department of Physics and Astronomy

Rob Coalson, Professor, Department of Physics and Astronomy & Chemistry

Vladimir Savinov, Associate Professor, Department of Physics and Astronomy

Robert Duda, Research Asst Professor, Department of Biological Sciences

David Swigon, Assistant Professor, Department of Mathematics

Dissertation Advisor: Xiao-lun Wu, PhD Professor, Department of Physics and Astronomy

The Effect of Noisy Protein Expression on *E. coli*/Phage Dynamics

Emily Chapman-McQuiston, PhD

University of Pittsburgh, 2007

It has long been suspected that population heterogeneity, either at a genetic level or at a protein level, can improve the fitness of an organism under a variety of environmental stresses. However, quantitative measurements to substantiate such a hypothesis turn out to be rather difficult and have rarely been performed. We examine the response of *Escherichia coli (E. coli)* to infection by viruses known as phage. In order to inject its DNA into a bacterium, the phage must first bind to a specific receptor protein and consequently the number of receptors per bacterium is related to the bacterial susceptibility to infection. Like many proteins in a bacterial population, the number of expressed receptor proteins in an individual cell is not deterministic but stochastic. In this project, experiments and model calculations are used to study how the noisy expression of phage receptors in a bacterial population changes the short-time population dynamics of an isolated and well-mixed *E. coli*/phage system. We find that when phage are present in the system, the selective killing of bacteria expressing high numbers of phage receptors creates a phenotype selection and the bacterial population can no longer be considered as having a homogeneous susceptibility to the phage pressure. It is shown that a heterogeneous bacterial population is significantly more fit compared to a homogeneous population when confronting a phage attack. We find that a small percentage of cells which are expressing few phage receptors become important because these bacteria persist despite the presence of phage. In view of their important roles in environmental adaptation, in various diseases and potentially

in evolution, a fundamental understanding of this minority of cells remains a significant challenge.

TABLE OF CONTENTS

LIST OF TABLES

LIST OF FIGURES

1.0 INTRODUCTION

1.1 *E. COLI* AS A MODEL CELL

Cells are the basic unit of life and yet are composed of non-living chemicals. Biologists separate cells into three classes; prokaryotes, eukaryotes and archaea. Prokaryotes are single celled organisms which do not have a membrane-bounded nucleus. Like prokaryotes, archaea are single-celled organisms that do not contain a nucleus, but are more closely related to eukaryotes. Eukaryotes are more complex cells and have compartments with specialized functions such as the nucleus which contains the DNA (Mader 2004).

Inside the cell, DNA is generally considered the "information manual" of the cell, the amount of DNA content, though, does not necessarily correlate with the amount of genetic information or the complexity of the organism. For example, the worm *C. elegans* has 100 Mb (where b here stands for basepairs), a common fern has ~307,000 Mb, and *Homo sapiens* have a mere 3,000 Mb (Capy 2000). The DNA content is not a good indicator of complexity because biological organisms use a variety of methods to develop complexity. Even though different organisms seem incomparable, all organisms are composed of cells. Within cells, the genes are encoded into the DNA. In all cells, DNA is transcribed into RNA, which is translated into proteins. There are many other cell to cell similarities in highly varying organisms. While it is advantageous to study specific processes that have developed in specific organisms, there are

general processes which are common to many if not all living organisms. These similarities are what allow for the use of simple microorganisms such as *E. coli* as a model to study the basic processes of cells such as DNA replication and protein expression.

1.2 λ PHAGE AND THE PHAGE λ RECEPTOR PROTEIN

A phage is a virus which infects bacteria. Most phages are comprised of two basic components, DNA and protein. As can be seen in the cartoon in Figure 1, the phage has a head or capsid which contains the DNA, a long tail and a tail fiber which is responsible for binding to a receptor (a bacterial protein). The relative simplicity of phage makes them an ideal tool in studying some of the basic questions of biological systems. The famous Hershey-Chase experiment used T2 phage to determine that DNA, not protein, is the material that contains genes (Weaver 2002, Hershey and Chase 1952).

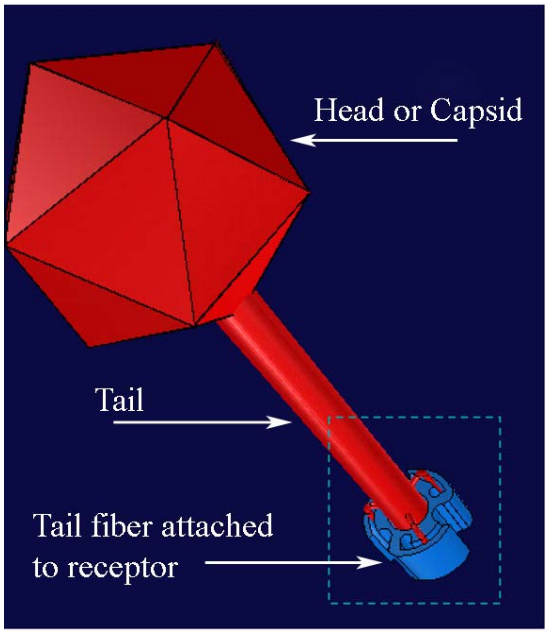

Figure 1 Lambda phage cartoon depicting the possible key lock mechanism in phage adsorption. A variation of this figure was presented in Moldovan et. al. 2007.

We have chosen to study the particular phage shown in cartoon form in Figure 1. λ, a phage which infects *E. coli*. λ is a temperate phage because after infecting a cell it can follow one of two pathways. The first pathway is the lytic pathway in which the phage transcribes and translates most of its genes, replicating its DNA quickly, forming heads and tails and leading to cell lysis in order to release new phages. The second pathway is the lysogenic pathway in which the phage incorporates its DNA into the bacterial genome and is replicated passively along with the bacterial genome (Weaver 2002, Ptashne 2004). A bacterium that has an incorporated phage genome is called a lysogen. The phage DNA remains integrated into the genome because a phage protein called CI, represses the ability to make most of the phage proteins and the phage genome remains passive inside the bacterial cell. A useful lambda phage mutant is known as the CI857 mutant. This mutation was isolated in the 1960s by Sussman and Jacob (Brooks and Clark 1967). This mutation is useful because it causes the repression system (the CI protein) of the lambda phage to become temperature sensitive. This mutation allows for complete repression of the lytic cycle at 30°C and complete induction of the lytic cycle at 40°C (Ptashne 2004).

In order to infect cells and replicate, the λ phage must first bind to the lambda receptor protein (also known as the maltoporin protein) on *E. coli*. The functional receptor is composed of three individual protein subunits that are transcribed from the lamB gene. The lamB gene is located on a genetic network called the maltose regulon which will be discussed in detail later in Section 1.5.1. Figure 2(a) is an electron micrograph of an *E. coli* bacterium which has been adsorbed with a high MOI (multiplicity of infection=$\frac{phage/cm^3}{bacteria/cm^3}$). The phage irreversibly binds to the receptor on the outside of the bacterium and then can be visualized using an electron microscope. Each bound phage indicates the presence of a maltoporin protein.

The space filling structure of the trimeric maltoporin protein is depicted in Figure 2(b) (from Schirmer et. al. 1995). The trimeric protein allows the passive diffusion of maltose and maltodextrins through the outer membrane (Boos and Shuman 1998). Maltose (a disaccharide of two glucose molecules) has other methods of getting into the cell such as through the Omp proteins when maltose is present at high concentrations (>10μM). Therefore, the number of maltoporin receptors is only limiting to cell replication when maltodextrins (4 or more glucose molecules) or a low concentration of maltose (<10μM) is present (Szmelcman and Hofnung 1975).

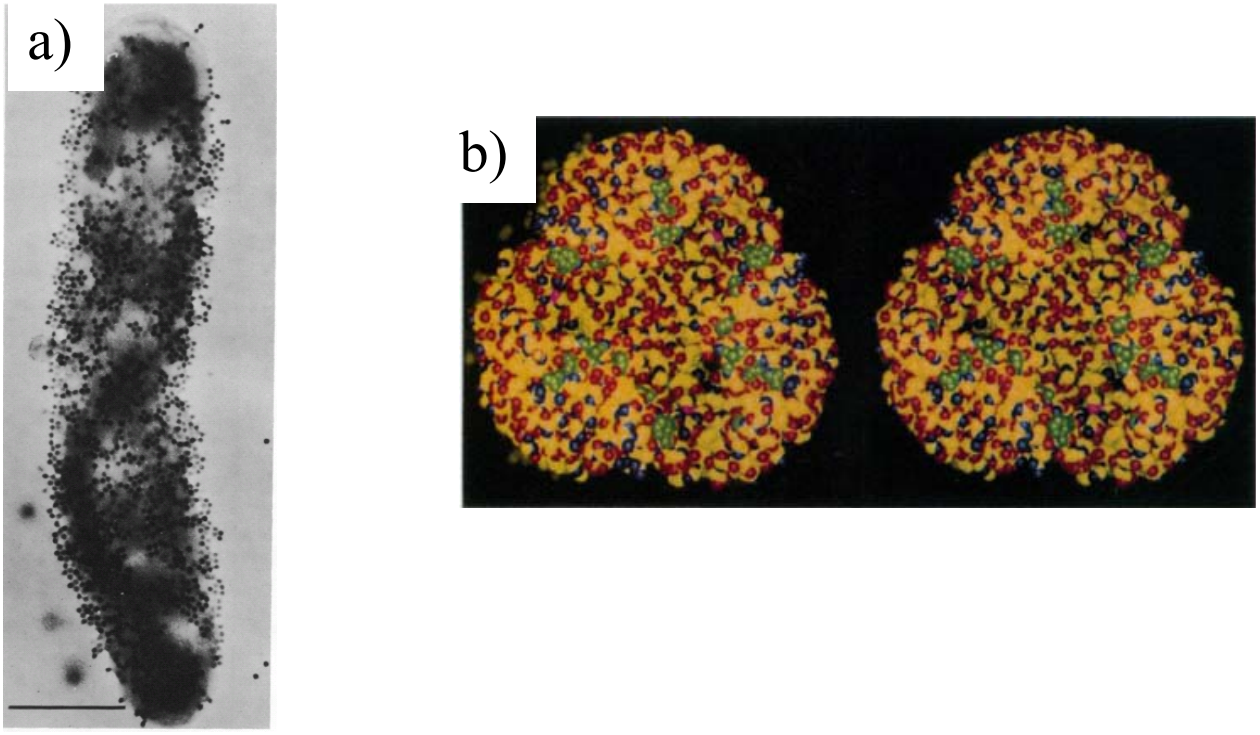

Figure 2 λ phage infection of *E. coli*
(a) electron micrograph of *E. coli* with attached phage, from Ryter et. al. 1975. Reprinted with permission from the Journals Department of the American Society of Microbiology. (b) Depiction of the space filling structure of the trimeric lambda receptor protein, from Schirmer et. al. 1995. Reprinted with permission from AAAS.

1.3 ADSORPTION: THE FIRST STEP IN INFECTION

Phage λ must attach to the lambda phage receptor before infection can occur. Phage have no active motility so the infection of bacteria by phages is diffusion-limited. The phage diffuses until a random collision causes it to contact a receptor. At this point, the phage binds, injects its DNA and phage replication proceeds.

Berg and Purcell (1977) developed a quantitative model describing how the number of receptors per bacterium relates to the rate of adsorption when receptors can be modeled as perfect sinks. Berg later described this model in a more understandable derivation which will be summarized here (Berg 1993). The Berg and Purcell model begins with Fick's first law in one-dimension:

$$J_x = -D\frac{\partial C}{\partial x} \tag{1}$$

Where J_x is the flux of a particle, D is the diffusion coefficient of the particles, C is the concentration of the particles and x is a measure of distance. This implies that a net flux of particles occurs when a concentration gradient exists. In an experiment, a gradient can only be maintained if there is a source at one point and an adsorber at another point (such as the case when there is a bath of phage at infinity and bacterial receptors that act as phage sinks). Now considering a small area where particles are not created or destroyed the number conservation law applies:

$$\frac{\partial C}{\partial t} = -\frac{\partial J_x}{\partial x} \tag{2}$$

Filling equation (1) into equation (2) gives rise to Fick's second law:

$$\frac{\partial C}{\partial t} = D\frac{\partial^2 C}{\partial x^2} \tag{3}$$

When sources and adsorbers are present this will reach a steady-state when $\frac{\partial C}{\partial t} = 0$. Generalizing Fick's 2nd equation to three dimensions and assuming a steady-state condition, we find that $\nabla^2 C = 0$. Because this equation is analogous to Gauss's equation from electromagnetism in the absence of charge, well known solutions from electromagnetism can be used to solve these problems.

For phage adsorption, a bacterium is an ellipsoid with N adsorbing disks. For simplicity, here, we will look at a sphere and later generalize to an ellipsoid. Using an electrical analogy Berg and Purcell showed that the diffusion current to a sphere with N disks has the form:

$$\frac{I}{I_0} = \frac{1}{1 + \frac{\pi a}{Ns}} \tag{4}$$

Where I is the diffusion current, $I_0 = 4\pi DaC_o$, C_o is the concentration of the particle at infinity, a is the radius of the sphere, D is the diffusion coefficient of the particle, N is the number of disk adsorbers and s is the radius of the disk adsorber. The adsorption coefficient for a phage is $\gamma = \frac{I}{C_o}$, and generalizing to an ellipsoid where $a^2 >> b^2$ we can find an equation for the adsorption coefficient γ of a phage to a bacterium with N disks:

$$\gamma = \gamma_o \frac{Ns}{Ns + \frac{\pi a}{\ln(2a/b)}} \tag{5}$$

where,

$$\gamma_o = \frac{4\pi Da}{\ln(2a/b)} \tag{6}$$

There are two limits to note with this result. First, we look at the low coverage limit (N is small). When N is small (Ns<< πa), we find that equation (5) becomes $\gamma = N\frac{\gamma_o s \ln(2a/b)}{\pi a}$. The adsorption coefficient becomes linear with N. In the opposite limit, when Ns>>πa then $\gamma \to \gamma_o$, where γ_o is the maximum theoretical adsorption coefficient. When we place realistic numbers for a, b, s and D, we find the crossover between the two regimes occurs at ~750 receptors, meaning that for a fairly low coverage of the receptors on a bacterial cell, γ saturates to its maximal value.

1.4 EPIGENETICS AND PERSISTENCE

Since DNA sequences were discovered to encode for the information passed from cell to cell, it was thought that only DNA could pass information from one generation to another. More recently, scientists have begun to study other methods of information transfer such as how DNA methylation gives cells the ability to maintain varying phenotype characteristics over many rounds of cell division despite the fact that they contain the same genomic sequence. The presence of varying phenotypes with identical genotypes is known as epigenetics.

A specific type of interesting epigenetic state in bacteria is called bacterial persistence. It has been known since the 1980s that bacteria that were not genetically resistant to antibiotics could still persist in the presence of antibiotics for extended periods. Ampicillin, for example, kills growing bacteria. Therefore, bacteria which are not in a rapidly growing state are not killed by ampicillin. Such cells are persistors because once the antibiotics were lifted from the medium the bacteria has a probability of recovering the rapidly growing phenotype. The resistance to the

antibiotics is temporary and not a genetic mutation. Figure 3 shows an example of such a persister. In this experiment fluorescent bacteria were placed in microfluidic channels such that the length of the cells in the channel was proportional to the number of bacteria present. In panel A the red arrow is pointing to a bacterium which does not appear to be growing quickly over the first 1.5 hours. Other bacteria in the panel are growing and the length in the microfluidic channel becomes larger between panels A and C. Between C and D, ampicillin is added for 5 hours, killing and lysing most of the bacteria. The ampicillin is then washed out and fresh medium was flowed through the microfluidic channel. Even though before the addition of the antibiotics the cells were in a non-growing state, afterwards the antibiotic is removed and the cells have a probability of recovering their growth ability and growing again in the microfluidic channel.

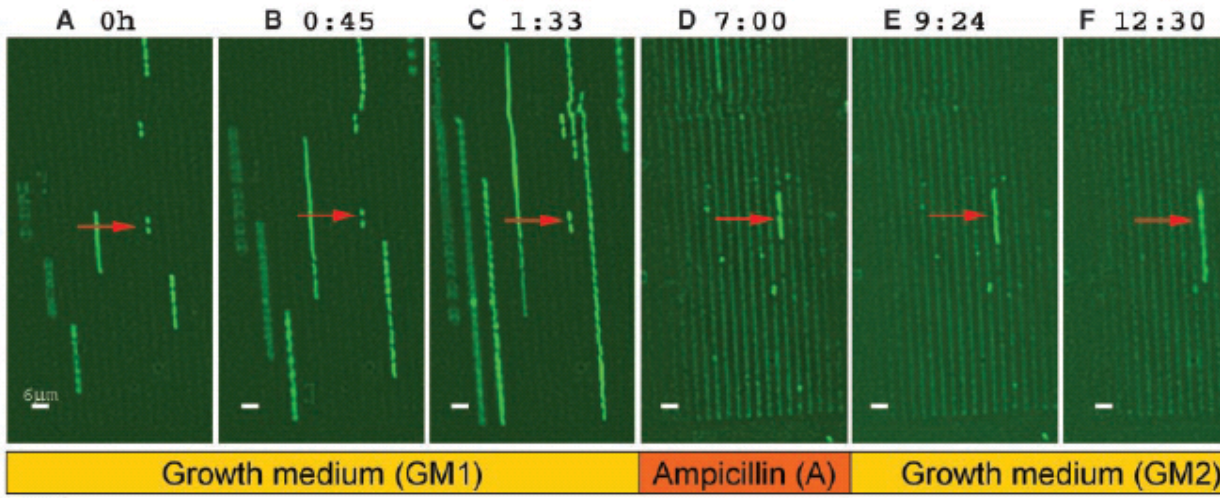

Figure 3 Bacterial persistence in a microfluidic channel.
From Balaban et. al. 2004. Reprinted with permission from AAAS. The red arrow points to a slowly growing bacteria that persists through the 5 hours of antibiotic treatments.

In this particular study, antibiotic persistence was shown to act as a phenotypic switch as is pictured in Figure 4. In other words, the cells existed in one of two epigenetic states, the normal state or the persister state. The cells have a probability of switching from the persister to the normal state and regaining the phenotype of the normal state cells. Normal cells also have a

small probability of switching from the normal to the persister state, gaining the phenotypes of the persister cells.

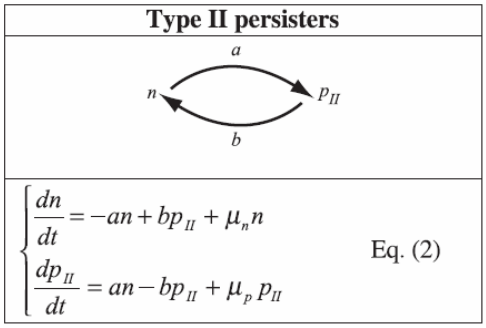

Figure 4 Bacterial persistence can be modeled as a two state switch, from Balaban et. al. 2004. Reprinted with permission from AAAS.

1.5 PROTEIN EXPRESSION IS INHERENTLY NOISY

To begin to understand bacterial persistence, we must first understand how different genetically identical cells can express different phenotypes. A basic understanding can begin at the process of protein expression. When describing the process of protein expression it has been hypothesized that the general flow of information in most organisms follows the path DNA→RNA→protein (Crick, 1970). In this description, the flow of information and process of protein expression is seemingly a deterministic process. If we place protein expression into its environmental context, we find that the process of protein expression occurs on a microscopic scale and is subject to kT fluctuations and to large number fluctuations when proteins are expressed in small quantities (Raser and O'Shea 2005).

Classifying noisy behavior, Elowitz et. al. (2002) and Swain et. al. (2002) mathematically defined two types of noise when studying the stochastic expression of a particular protein. First,

known as extrinsic noise, is the variation in cell-to-cell expression level of proteins due to the fact that individual cells experience fluctuations in the amount of protein making machinery and vary at different points in the individual cell's growth cycle. Second, known as intrinsic noise, is the variation in protein expression due to its inherent stochastic nature. In other words, the protein expression of two identical promoters in the same cell have the possibility of expressing different levels of protein because RNA polymerases and repressor proteins compete for binding sites on promoters. In the experiment, Elowitz and coworkers placed two different colors of fluorescent protein under the expression of identical inducible promoters on the genome in the same cell. Cells expressing the same amount of the two colored proteins appear as yellow in Figure 5. Cells expressing more of one protein are seen as either green or red in the figure. Notice when the cells only have small numbers of proteins (panel A), different cells (and the same promoter in the same cell) express very different amounts of protein. Cells which have highly expressed protein numbers tend to appear fairly homogeneous as can be seen in panel B of the figure.

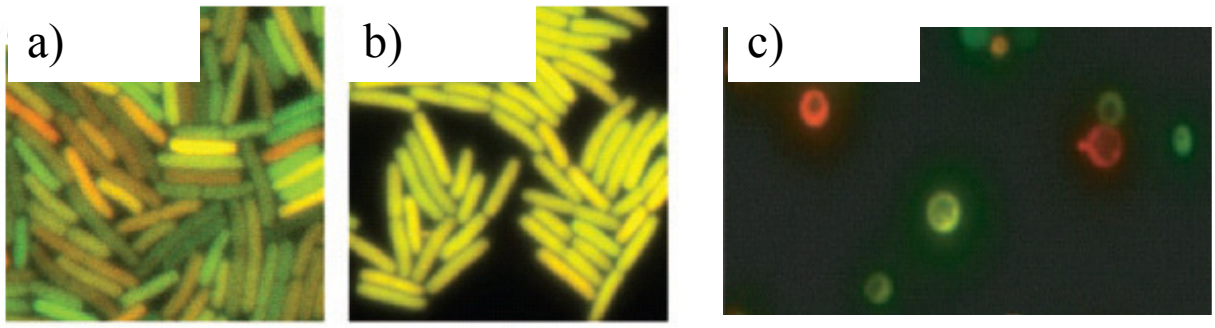

Figure 5. Noisy (a) and homogeneous (b) gene expression in bacteria. (c) Noisy gene expression in yeast. (a) and (b) are a from Elowitz et. al. (2002). Reprinted with permission from AAAS. (c) is from Raser and O'Shea (2004). Reprinted with permission AAAS.

Raser and O'Shea (2004) classified noise in eukaryotes, by using the method of Elowitz et. al. (2002) in *Saccharomyces cerevisiae* (budding yeast) which is depicted in Figure C. They showed that stochastic gene expression is similar in eukaryotes and prokaryotes and can be placed into three classes depending on the relative rates of promoter reactions. In class I, the promoter is activated infrequently but is stable once activated. Using simulations they showed that for class I promoters, the intrinsic noise is highly dependent on the steady-state mean number of proteins and changing the promoter activation rate, transcriptional efficiency or translational efficiency, changes the amount of intrinsic noise dramatically. In class II, the promoter is activated infrequently and the activated state is unstable. In this class the amount of intrinsic noise is fairly independent of the promoter activation rate, but as the transcriptional or translational efficiency increases, the intrinsic noise strength increases. In class III, the promoter is activated frequently but the activated state is unstable. In this class, the intrinsic noise strength is fairly independent of the strength of the promoter activation rate, the transcriptional efficiency or the translational efficiency.

Other experiments have studied the source of noise in a population of cells when the promoter is highly repressed. These studies looked directly at the effects of both transcriptional and translational bursting and the protein distribution that develops (Cai et. al. 2006, Yu et. al. 2006, Golding et. al. 2005). While most of these experiments are specific to one promoter inside the cell, an experiment by Bar-Even et. al.(2006) attempted to show that the general source of noise for many promoters in natural conditions is due to mRNA fluctuations. In the experiment, the authors clone the fluorescent protein GFP behind many natural promoters and use flow cytometry to study protein distributions in a population after a chemical perturbation which induces expression of the protein. While the advantage of flow cytometry is its high throughput

capability, the disadvantage is the loss of resolution. In this experiment, the integrated autofluorescence of the cells dominated the fluorescent signal of the protein of interest until >1000 fluorescent proteins were present inside the cell.

Like all cells, *E. coli* is not constantly making all proteins in the DNA sequence. Instead, the DNA encodes genetic networks that can either turn the expression of particular proteins on so that they are highly expressed or off so that there is only minimal expression.

In a classical paper, Novick and Weiner (1957) discovered using chemical kinetics that *E. coli* cells when placed in the presence of a chemical called TMG (thiomethyl β-D-galactoside) could be described as either "on" or "off." In other words, the proteins needed for metabolization of lactose known as the lacZYA proteins in each cell were either expressed maximally or expressed minimally but cells were not generally expressed at an intermediate state. So, even though in situations where only small concentrations of inducer were added and the population averaged expression of the lacZYA proteins increased slowly, the inducer actually only turned "on" a percentage of cells (that were maximally induced) instead of inducing each cell at an intermediate level as can be seen in Figure 6.

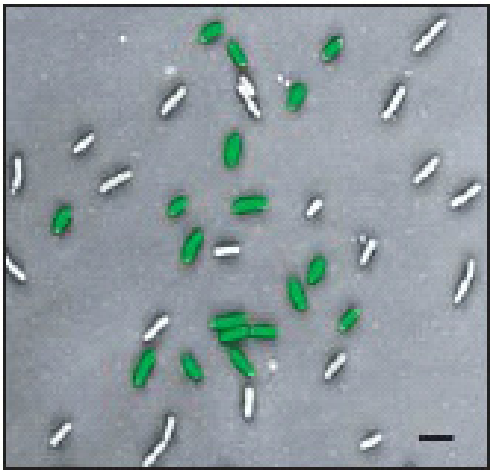

Figure 6 *E. coli* cells grown in intermediate concentrations of the chemical TMG, a lactose analog. Notice the cells are either highly expressing the lac operon (green) or not expressing (white). Reprinted by permission from Macmillan Publishers Ltd: Nature Ozbudak et. al. (2004), copyright 2004.

The lactose network is one metabolism network which is turned off when glucose is present but turned on when only lactose is present. Many metabolism networks have this all-or-none behavior, for the study described in this dissertation a more complicated network, the maltose regulon, is involved.

1.5.1 The Maltose Regulon

In the previous section, there was discussion about the classical lac operon which is one of the best studied model genetic networks. Here we discuss a different regulatory network known as the maltose regulon. Regulons are composed of several genes or operons which are under control by the same regulatory protein, while operons are genes with a common function that are transcribed on the same mRNA. A regulon is generally more complex than an operon and typically consists of a few operons at different loci on the chromosome.

The λ-phage receptor is composed of 3 LamB proteins. The gene which encodes for the LamB protein is located on the maltose regulon. As can be seen in Figure 7, the LamB protein is transcribed along with the malK and malM proteins. While the function of the malM protein is still mainly unknown, the malK protein is involved with the transport of maltose molecules through the inner membrane of the *E. coli*. The genes of the maltose regulon have two things in common. They are all involved in the metabolization of maltose and maltodextrins and are all regulated by the protein malT which becomes an activator when it binds with the inducer maltotriose (a molecule composed of 3 glucose molecules). An activator is a protein that binds near a promoter (such as the malK promoter in Figure 7) and increases expression of the genes downstream but when it is absent those genes are repressed completely or only expressed at

basal levels. A second, more global regulator of metabolization operons is the cAMP/CRP complex. This complex is known to have a large effect on the expression of many carbon metabolization operons such as the maltose regulon, lac operon and the PTS operon which effects glucose metabolization.

Figure 7 Activators of the maltose regulon.
Green boxes are malT binding sites, blue boxes are cAMP/CRP binding sites. Both activators are necessary for the efficient transcription of the malE and malK promoters. The cAMP/CRP binding sites are important for the transcription of malK and malE promoter. malEFG, malK, lamB and malM are all involved in the transport of maltose and maltodextrins into the cell, the diagram was inspired from a figure in Boos and Shuman (1998).

It has been hypothesized that malT is activated at low levels even in the absence of the inducer maltotriose, preparing the cell for efficient use of low concentrations of maltose or maltodextrins, if available. It is interesting to note that only the transport proteins expressed by the malK and malE promoters need cAMP for high expression while other promoters such as malS, malP and malZ only need the activator malT. The malK promoter initiates transcription of three genes malK, lamB and malM (Boos and Shuman 1998).

1.6 PREDATOR-PREY MODELS

When the phage and *E. coli* are mixed, it is simple to describe the dynamics using a predator-prey model. The general predator-prey model was first developed independently by Lotka (1925) and Volterra (1926) and is now known as the Lotka-Volterra model:

$$\frac{dx}{dt} = rx - \alpha xy \tag{7}$$

$$\frac{dy}{ct} = \beta xy - Dy \tag{8}$$

Here, x is the prey density, y is the predator density, r is the unimpeded growth rate of the prey, D is a constant of mortality for the predators, α is a proportionality constant linking the mortality of the prey to the number of predator, and β is a proportionality constant linking the increase in predator to the number of prey. While these equations, do produce oscillations seen in experiment, the amplitude of the oscillations depends completely on the initial conditions of the system rather than the intrinsic parameters making them unrealistic to biological systems (May 1972). An important theorem by Kolmogorov stated that 2-dimensional nonlinear dynamic systems give rise to stable and unstable fixed points. The unstable fixed points give rise to limit cycles. This theorem was tested in biological systems and gave support to the notion that most predator-prey systems actually have oscillations due to limit cycles as found in the more specific Lotka-Volterra model (May 1972). In another interesting paper, Robert May reviewed the rich spectrum of solutions that can be found in simple nonlinear difference equations, once again to give more support to the notion that simple difference equations (modeling simple interactions) could give rise to complicated and possibly chaotic behavior (May 1976)

As a variation to the Lotka-Volterra model, Wangersky and Cunningham (1957) added a time delay to equations (7) and (8) changing the dynamics of the system:

$$\frac{dx}{dt} = rx(t) - \alpha x(t)y(t) \tag{9}$$

$$\frac{dy}{dt} = \beta x(t-\tau)y(t-\tau) - Dy(t) \tag{10}$$

This is a more biologically relevant equation because predators do not instantly increase in numbers when an abundant prey is present; more realistically there is a time delay which can be thought of as the gestation period. This equation has no stable solutions, however, because adding a finite time delay creates oscillations growing to infinity. For $\tau=0$ in the Lotka-Volterra model, a growing oscillation is not possible and the well-known stable oscillations occur. In a more realistic biological system where τ is finite, this implies that if predation is linear, such as the term $-\alpha x(t)y(t)$ in equation (9), then predation cannot be the only limit on prey growth. Stability in the system does arise when a carrying capacity K (which implies a resource limited environment) is added to the equations:

$$\frac{dx(t)}{dt} = rx(t)(1-\frac{x(t)}{K}) - \alpha x(t)y(t) \qquad (11)$$

$$\frac{dy(t)}{dt} = \beta x(t-\tau)y(t-\tau) - Dy(t) \qquad (12)$$

While the time delay is destabilizing, the density-dependent carrying capacity is stabilizing and creates the necessary limit on prey growth which allows for both stable and unstable solutions.

1.7 PHAGE/*E. COLI* POPULATION DYNAMICS

The discussion above of prey-predator models were introduced as a general form for prey-predator relationships and the solutions that are possible. Because there are many different types of prey-predator interactions, when the specific interactions between the prey and predator are known, detailed versions of the above equations can be written down.

In 1960, Campbell developed a model using differential equations describing the specific interactions between bacteria and phage in order to predict equilibrium values of bacteria and

phage in a chemostat culture (Campbell 1960). A chemostat is a constant volume growth vessel where nutrients flow into the reaction chamber at a constant rate and debris/phage/bacteria flow out of the reaction chamber at the same constant rate. They found solutions which allow for the coexistence of phage and bacteria in the chemostat. This equilibrium condition, though, requires the inactivation of phage either through natural decay or by being washed out of the chemostat. Stewart and Levin (1973) developed a model based on two organisms competing for the same resource in a chemostat community. This model included the specific density-dependent interactions between phage and *E. coli* and was experimentally testable. In 1977, Levin et. al. modified the model of Campbell (1961) and Stewart and Levin (1973) and tested the model results against their experimental findings when bacteria and bacteriophage competed in a chemostat. This group showed that by varying the concentration of nutrients and the flow rate of the chemostat, they could find regions where stable oscillations and stable equilibrium of the bacteria and bacteriophage occur. This original experiment served as the basis for a series ecology studies in bacteria/bacteriophage systems in chemostats. Chao et. al. (1977) showed that in the chemostat community, bacteria-phage interactions were stable, and even after the introduction of phage resistant mutants, a low level of phage sensitive bacteria remained which kept the phage from becoming extinct. They hypothesized that in their system, that this low level of sensitive bacteria only persisted if phage resistance had a cost, in other words had a lower growth rate than the sensitive cells.

Lenski (1988) wrote an extensive review of many of the studies and models used to describe the interaction of bacteria and bacteriophage. In this review, Lenski raised two important points: (1) the Lotka-Volterra-like models are not stable in serial cultures and (2) that a non-heritable refuge (that is when bacteria become transiently resistant to phage) could explain

the fact that bacteria/phage cultures are much more stable than the Stewart and Levin (1973) model predicts. He shows evidence that a model which includes an individual stage of non-heritable refuge (either spatial or physiological) could produce stable interactions.

Schrag and Mittler (1996) tested the four hypotheses for long term coexistence of bacteria and phage discussed in Lenski (1988). The four hypotheses were:

(1) Numerical refuge hypothesis:

The bacteria will coexist in a chemostat purely due to the development of stable limit cycles due to the natural interactions between bacteria and phage. This hypothesis is only realized in specialized conditions.

(2) Arms-race hypothesis:

Coexistence is achieved through mutations in the bacteria and corresponding mutations in the phage over an endless arms-race. It was later shown, though, that in general the host will prevail (Hofnung et. al. 1976).

(3) Physiological refuge hypothesis:

The bacteria have a physiological state which they switch to which is temporarily resistant to phage infection.

(4) Spatial refuge hypothesis:

The bacteria use spatial heterogeneity for protection against phage attack, such as wall growth in chemostats.

The authors concluded that while there was some indirect evidence for physiological refuge in chemostats, spatial refuge was the hypothesis that explained their experimental results in both the chemostat and serial culture experiments.

Later, a theoretical group used the basic phage/bacterium model to examine how the addition of phage adsorbing to bacterial debris affects long-term co-existence (Rabinovitch et. al. 2003). This group found that in order to create coexistence between bacteria and phage, viral decay must occur either by natural inactivation or through adsorption to debris. The viral decay is necessary to change the unstable focus of the original model to a possibly stable one (Rabinovitch et. al. 2003). In their analysis, this group used an adsorption coefficient of 10^{-12} min^{-1} ml^{-1} which is approximately two orders of magnitude lower than values later measured for λ phage and *E. coli* (Moldovan 2006, Moldovan et. al. 2007). In Chapter 2.0 , we discuss that within realistic parameter values, the model always predicts extinction of the bacterial population.

2.0 MODELING PHAGE/*E. COLI* DYNAMICS

As was discussed in Sections 1.6 and 1.7, predator-prey relationships and more specifically bacteria-phage interactions have been studied for many years. Recently, though, studies of stochastic protein expression and fluorescent detection of single proteins have become common. It is this new information that has led us to study the effect of stochastic receptor expression on bacteria-phage dynamics. As an introduction, in Figure 8, we show *E. coli* K-12 bacteria which have been adsorbed with high concentrations of fluorescently labeled λ phage and visualized under a fluorescent microscope. Each phage indicates the presence of a maltoporin protein. While most bacteria appear to be covered with fluorescent particles, (Figure 8a), there are minority populations that due to their stochastic phenotype express very few proteins and therefore can only adsorb a few fluorescent phage (circled in Figure 8b).

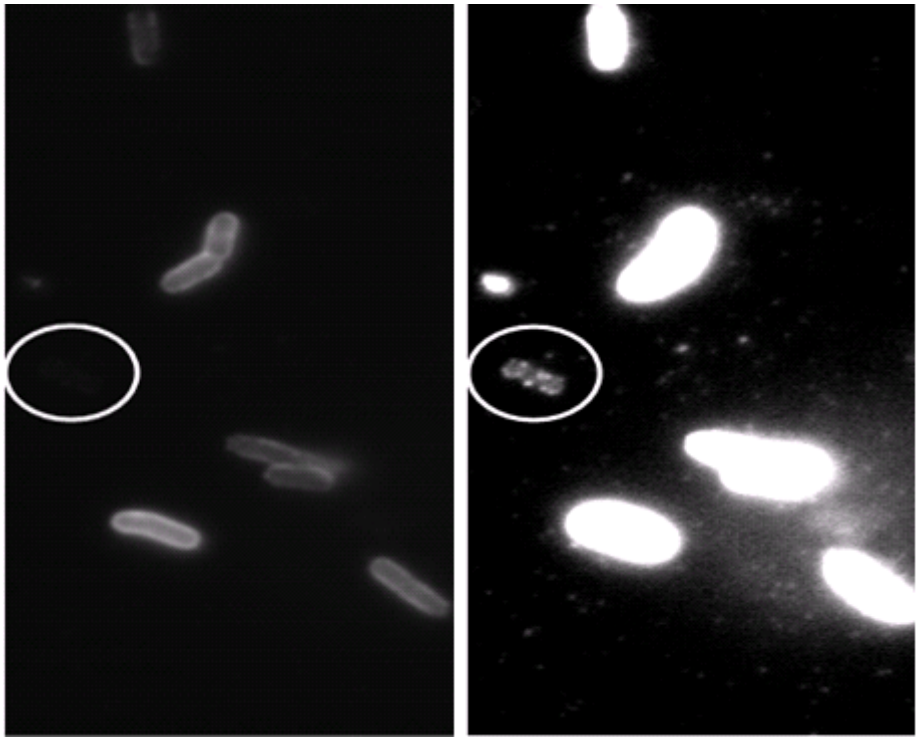

Figure 8 Example of a minority phenotype present in a genetically homogeneous population of bacteria. The picture is of Ymel adsorbed with fluorescent phage, (a) and (b) are the same picture with different contrast settings. The heterogeneity of individual bacteria is shown in this picture. The circled bacterium has fewer phage adsorbed than many of the other bacteria in the picture. The number of attached phage can be counted as they appear as individual diffraction limited disks on the bacteria.

2.1 PHYSICAL PICTURE: THE SIMPLIFIED MODEL

In this section, we present a simplified version of the models introduced in Section 1.7 which describes the phage/*E. coli* interactions and assumes that the average adsorption coefficient of the bacterial population is constant in time. These equations are based on the previously developed models used for the population dynamics of *E. coli* and phage (Levin et. al. 1977, Schrag and Mittler 1996, Rabinovitch et. al. 2003). In order to simplify the equations we leave out some of the interactions normally modeled in phage/*E. coli* dynamics such as limited resources and mutations which only dominate the system when studying the long-term dynamics of the system which is considered to be greater than ~10 hours. We focus on the short term

behavior of the bacterial population before mutations dominate the system and resources become limited.

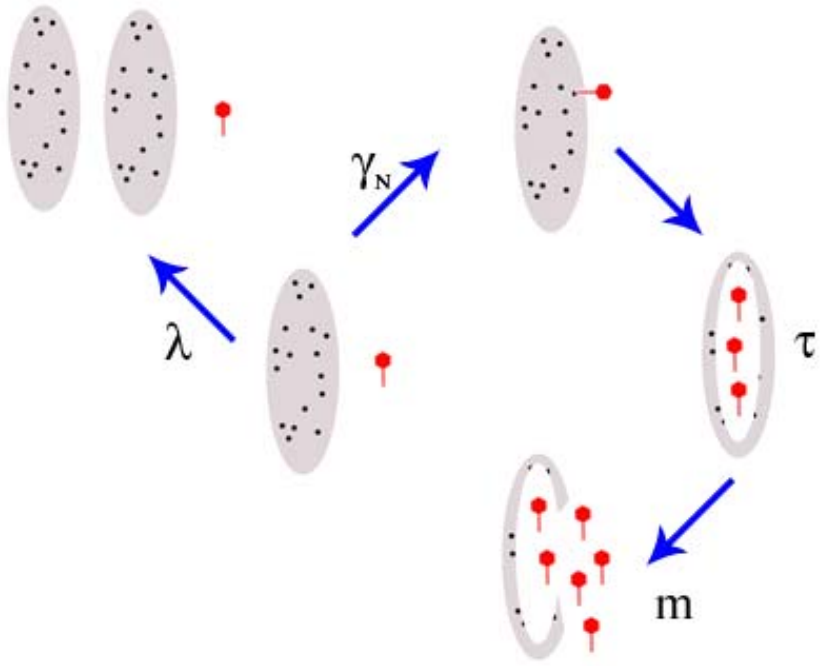

Figure 9 Cartoon depiction of phage/*E. coli* dynamics.
Bacteria naturally grow in a certain chemical environment with a growth rate λ, when bacteria and phage are mixed, the phage adsorb to the bacteria with a rate γ_N which is dependent on the number of receptors per bacteria. Once a phage adsorbs, the phage replicates inside the cell and τ minutes later an average of m phage burst out of the infected cell.

In our model, we assume that the bacteria are contained in a closed system with unlimited resources. Depicted in Figure 9, the bacteria replicate at a rate of λ. In the presence of phage, a bacterium can adsorb a phage with a rate that is proportional to the uninfected bacterial concentration B(t) and phage concentration P(t) as well as the adsorption coefficient γ. After a latent period of time τ, the bacteria burst producing on average m new phage. More than one phage, though, can attach to a bacterium. This has been included into the model by adding the term I(t) which describes the "debris" in the system. The debris is defined as infected or dead

bacteria that still have the ability to adsorb phage. The debris degrades with some rate ε. The equations which describe this simplified system are:

$$\frac{dB(t)}{dt} = (\lambda - \gamma P(t))B(t) \tag{13}$$

$$\frac{dI(t)}{dt} = \gamma P(t)B(t) - \varepsilon I(t) \tag{14}$$

$$\frac{dP(t)}{dt} = m\gamma P(t-\tau)B(t-\tau) - \gamma P(t)(B(t) + I(t)) \tag{15}$$

This set of equations will be referred to as the homogeneous model. Notice the adsorption coefficient γ is the average adsorption coefficient of the initial bacterial population. As will be discussed later, the adsorption coefficient is dependent on the number of receptors per bacteria but in this model this value has been set as a constant determined by the initial population. These equations generally predict extinction unless the parameters are finely tuned. The addition of the debris term has been shown computationally to create a parameter space where bacteria and phage may coexist (Rabinovitch et. al. 2003). We find, however, that when using our measured values for all of the rate constants, these equations still predict extinction of the bacterial population even though experiments show otherwise. This can be seen in Figure 10, where a) is an experimental population dynamics experiment performed by Radu Moldovan and described in his thesis (Moldovan 2006). When the homogeneous model is simulated using the measured constants from Table 1, (Figure 10b)) the model predicts extinction of the bacterial population in <10 hours, but this never occurs in actual measurements. Surviving bacteria were isolated and individual surviving colonies were regrown from hour 25 of population dynamic experiments similar to the one presented in Figure 10a). The colonies were checked for their ability to support phage growth. We found that the bacteria that regrew are just as sensitive to phage infection as bacteria that were never exposed to phage. The number of plaques formed through

addition of phage was measured for 50 colonies (10 colonies from 5 experiments), binned and presented in Figure 10c). When the normalized PDF (probability density function) was fit with a Gaussian it was found that $\sigma \approx \sqrt{(mean)}$, implying that the plate to plate variations in colony number can be explained completely by the random sampling error of the phage stock. The mean value found in this experiment was approximately equal to the mean found when using bacteria that had never been exposed to phage pressure previously.

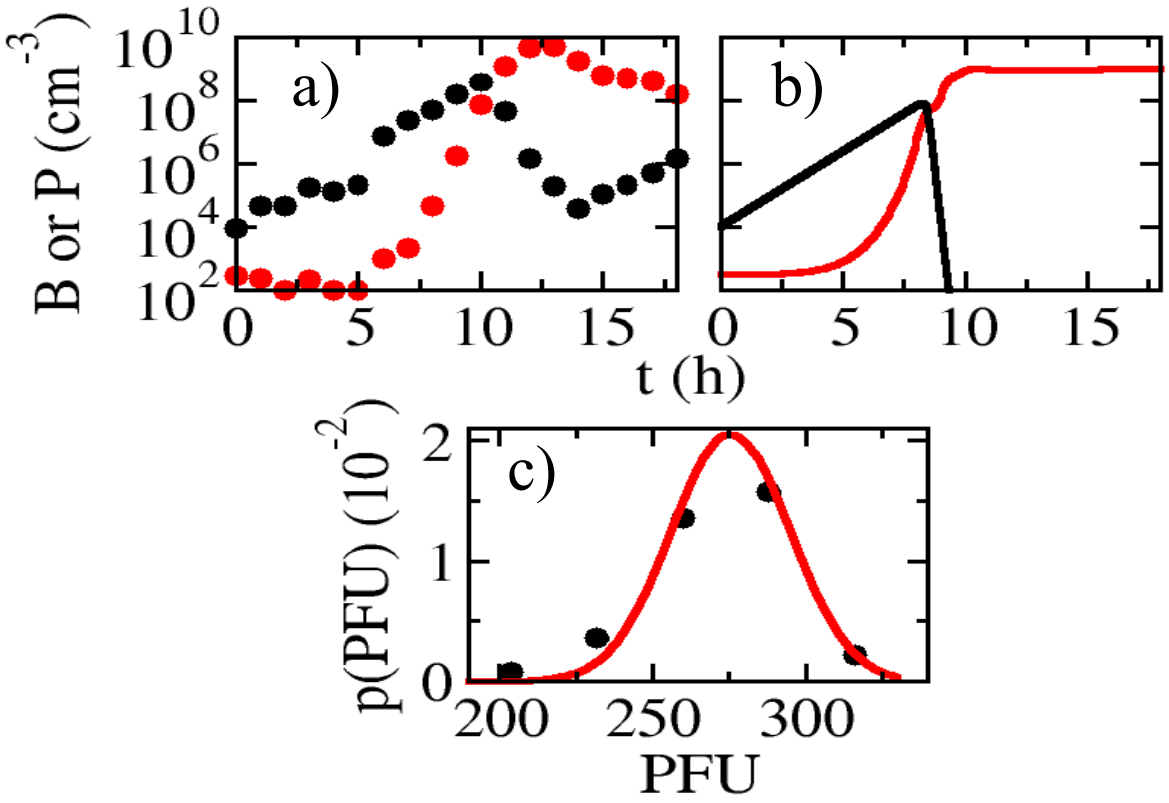

Figure 10 Low MOI population dynamics experiment.
(a) Experimental population dynamics experiment, the bacterial concentration (black circles) and free phage concentration (red squares) are measured over a period of 30 hours (only 20 presented). (b) The homogeneous model predicts extinction for the bacterial population (black line) when the phage (red line) overtake the bacterial population. (c) The bacteria at about 25 hours are regrown with no phage pressure and the ability to form plaques is tested. Using 50 separate colonies over 5 experiments the number of plaques on each plate is counted and the PDF is shown (black circles). The PDF is fit with a Gaussian (red line). We find $\sigma \approx \sqrt{(mean)}$ implying that the plate to plate variations are due to the sampling error.

2.2 MODEL DEPENDENCE ON RECEPTOR HETEROGENEITY

Bacteria develop resistance to phage infection, reaching all levels of the infection process. Because phage need to attach to a specific receptor, the disruption of the attachment process is a common target for bacterial resistance and mutations of the receptor compose 70% of isolated phage resistant mutants (Hofnung et. al. 1976). In the next section we will study the effect of a bacterial population having a broad, continuous susceptibility to phage infection due to varying numbers of receptors present on different genetically identical bacteria in the same population. Different susceptibilities arise due to the varying adsorption rates that are dependent on the number of receptors of each bacterium.

2.2.1 Dependence of Adsorption Coefficient on Receptor Number

As was discussed in Section 1.3, the adsorption coefficient of an ellipsoid with N receptors was derived to be:

$$\gamma_N = \gamma_0 \frac{Ns}{Ns + \frac{\pi a}{\ln(2a/b)}} \tag{16}$$

Here s is the receptor radius, a is the length of the semi-major axis and b is the length of the semi-minor axis of the elliptical cell as is depicted in Figure 11. γ_0 is the maximum adsorption rate for a perfect sink:

$$\gamma_0 = \frac{4\pi Da}{\ln\left(\frac{2a}{b}\right)} \tag{17}$$

Here, D is the diffusion coefficient of the phage particle. By electron microscopy it has been shown that the phage head has a radius of ~30 nm. The diffusion coefficient measured by light scattering shows the phage particle to have an equivalent hydrodynamic radius of ~35 nm (Moldovan et. al. 2007). The cell dimensions needed to calculate γ can be measured using light microscopy techniques and are described in the Appendix.

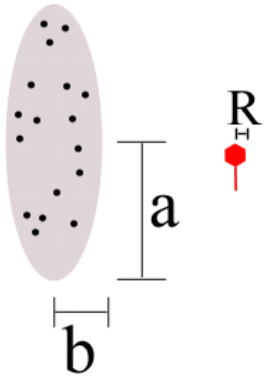

Figure 11 The parameters which determine the maximum adsorption coefficient.
The radius of the phage head is used to approximate the diffusion coefficient of the phage particle, which we have previously measured using light scattering.

2.2.2 Heterogeneous Adsorption Model

The receptor dependence of the adsorption coefficient will now be incorporated into the homogeneous model presented by equations (13), (14) and (15). Because bacteria with different receptor numbers have different adsorption coefficients, as depicted in Figure 12, each bacterial subpopulation with N receptors $B_N(t)$ adsorbs phage with an adsorption coefficient of γ_N. We assume here that the growth rate λ is independent of the number of receptors, this is a valid assumption when the maltose concentration is >10μM because it has previously been shown that maltose can enter the cell through other porins when a large concentration of maltose are present

(Szmelcman and Hofnung 1975). A bacterium with N free receptors that adsorbs a phage now becomes debris with N-1 free receptors $I_{N-1}(t)$. Debris with N+1 free receptors adsorbs a phage to become debris with N receptors $I_N(t)$. Because we are studying the individual subpopulations of bacteria, we have to take into account the ability of bacteria to gain receptors through protein production and to lose receptors through degradation or simply through dilution during bacterial replication. For example, bacteria in the subpopulation B_1 can create a receptor and move to subpopulation B_2 at the rate α_{12}. All these interactions can be described with the following mathematical model:

$$\frac{dB_N}{dt} = (\lambda - \gamma_N P)B_N + \sum_i (\alpha_{iN} B_i - \alpha_{Ni} B_N) \tag{18}$$

$$\frac{dI_N}{dt} = \gamma_{N+1} P(B_{N+1} + I_{N+1}) - \gamma_N P I_N - \varepsilon I_N \tag{19}$$

$$\frac{dP}{dt} = mP(t-\tau) \sum_{N=0}^{N_{max}} \gamma_N B_N(t-\tau) - P \sum_{n=0}^{N_{max}} \gamma_N (B_N + I_N) \tag{20}$$

where $N=0..N_{max}$.

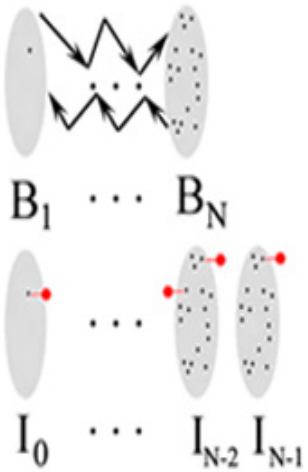

Figure 12 Definition of bacterial subpopulations.
A subpopulation of bacteria with N receptors in the model is labeled as B_N. Bacteria that have adsorbed at least one phage and have N-1 free receptors are labeled as I_{N-1}

The observable quantity in the system is the total uninfected bacterial concentration:

$$B_{tot} = \sum_{N=0}^{N_{max}} B_N \tag{21}$$

When bacteria switch between subpopulations, there are no sink or source terms, so the switching must obey a conservation rule, $\sum_N \sum_i (\alpha_{Ni} B_i - \alpha_{iN} B_N) = 0$. Therefore, when we sum over all the individual bacterial subpopulations, we find:

$$\frac{dB_{tot}(t)}{dt} = \lambda B_{\text{tot}}(t) - P(t) \sum \gamma_N B_{\text{N}}(t) \tag{22}$$

We can then define $\overline{\gamma(t)} = \frac{\sum_N \gamma_N B_N(t)}{B_{tot}(t)}$ and rewrite equation (22) as

$$\frac{dB_{tot}(t)}{dt} = \lambda B_{\text{tot}}(t) - P(t) \overline{\gamma(t)} B_{\text{tot}}(t) \tag{23}$$

Equations (19) and (20) can be rewritten in a similar manner:

$$\frac{dI_{\text{tot}}}{dt} = \overline{\gamma(t)} P(t) B(t) - \varepsilon I_{\text{tot}}(t) \tag{24}$$

$$\frac{dP}{dt} = mP(t-\tau)\overline{\gamma(t-\tau)} B_{\text{tot}}(t-\tau) - P(t)\left(\overline{\gamma(t)} B_{\text{tot}}(t) + \overline{\gamma_{\text{I}}(t)} I_{tot}(t)\right) \tag{25}$$

Here, $\overline{\gamma(t)}$ is the average adsorption coefficient of the uninfected bacteria as a function of time and $\overline{\gamma_I(t)}$ is the average adsorption coefficient of the debris as a function of time. Notice that equations (23), (24), (25) are almost identical to equations (13), (14), (15). The difference is that in the heterogeneous model the adsorption coefficient is allowed to vary as a function of time. When first looking at equation (23), it seems that all the switching between subpopulations is no longer contained in these equations. In actuality, it is now implicitly contained in the time

dependence of the average adsorption coefficient, rather than explicitly contained in the equations themselves.

2.2.3 Insights Gained in the Limit of Negligible Switching

In equations (18), (19) and (20), the unknown parameters are the switching terms. As a first step in studying the effect of receptor heterogeneity, we assume that the system is in the limit of negligible switching and examine the results of this assumption. Subpopulation switching will be examined extensively in Section 3.8 and Chapter 4.0 . When $P >> \sum_N N(B_N + I_N)$ and t is small, the phage concentration is approximately constant, $P \approx P_o$, and switching can be neglected ($\sum_i (\alpha_{Ni} B_i - \alpha_{iN} B_N) = 0$). Under these conditions, the term $\lambda - \gamma_N P_o$ is constant, and we can solve the differential equation for each subpopulation B_N.

$$B_N = B_N(0) e^{(\lambda - \gamma_N P_o)t} \tag{26}$$

Notice that the subpopulation B_N is either growing or decaying exponentially depending on whether the term $\lambda - \gamma_N P_o$ is positive or negative, respectively. This indicates that if the term is positive, the subpopulation of bacteria with N receptors is effectively growing while if the term is negative, then the subpopulation is effectively decaying. The critical point occurs when $\lambda - \gamma_N P_o = 0$. We fill in equation (16) for γ_N and solve for P_o, we find that

$$P_o = \frac{\lambda}{\gamma_0}\left(1 + \frac{\pi a}{\ln(2a/b)s}\right) \tag{27}$$

Using the values from Table 1 for the Ymel strain in equation (27), we obtain the graph shown in Figure 13. Figure 13 depicts the phage concentration-receptor number parameter space. A

bacterial subpopulation with N receptors will decay if the phage concentration rises above the curve and will grow if the phage concentration falls below the curve. It is important to note that the phage concentration can range over three orders of magnitude and still have a subpopulation with at least one receptor effectively growing and another subpopulation with N receptors effectively decaying.

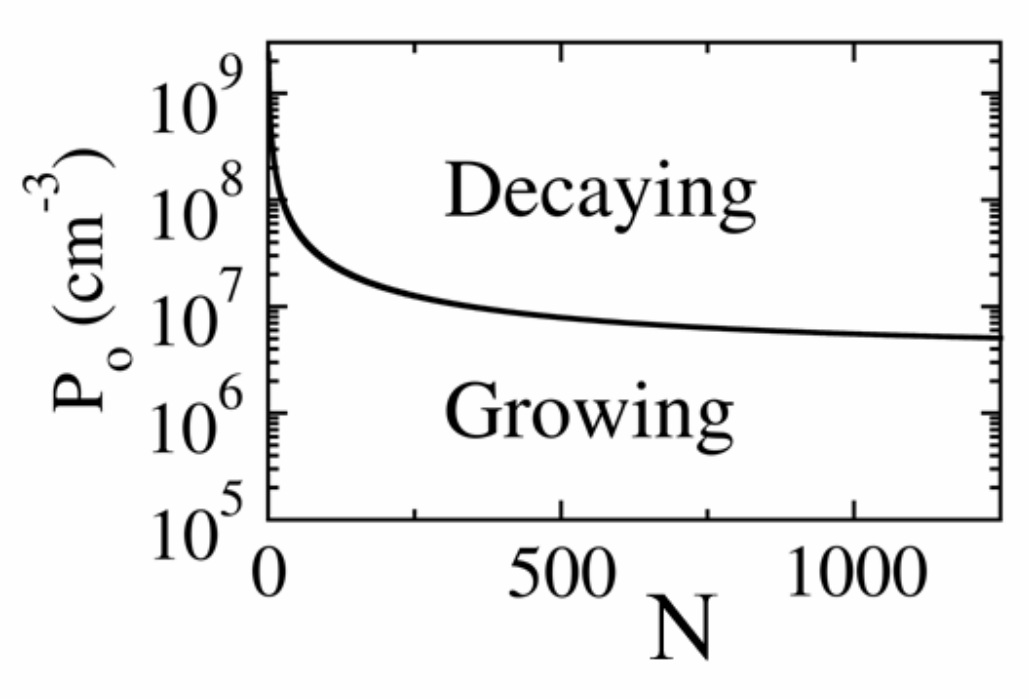

Figure 13 Different subpopulations can be exponentially growing or decaying under constant conditions. In an approximately constant phage concentration, a bacterial subpopulation with N receptors will grow exponentially if it falls above the line in parameter space and will exponentially decay if it falls below the line. Notice that this line ranges over 3 orders of magnitude for sensitive bacterial subpopulations.

2.3 ANALYTICAL SOLUTION: INITIAL GAUSSIAN RECEPTOR DISTRIBUTION

It is difficult to gain an understanding about the response of the system with many coupled differential equations. We choose to make assumptions that simplify the calculation.

We looked again at the solution to the differential equations at a time when the phage concentration P is constant and switching is negligible. Once again this gives us a solution for a subpopulation of bacteria with N receptors to be equation (26). Summing over all subpopulations, we find:

$$B_{tot} = \sum_{N=0}^{N_{max}} B_N(0) e^{(\lambda - \gamma_N P_o)t} \tag{28}$$

For simplicity, we assume that the initial distribution can be described by a Gaussian of the form:

$$B_N(0) = \frac{2B_o}{erfc(-\frac{N_o}{\sqrt{2}\sigma})} \sqrt{\frac{1}{2\pi\sigma^2}} e^{\frac{-(N-N_0)^2}{2\sigma^2}} \tag{29}$$

The factor $\frac{2}{erfc(-\frac{N_o}{\sqrt{2}\sigma})}$ is included to normalize the Gaussian for the range $N = 0 \to \infty$.

The erfc(x) is the complementary error function which goes to 0 as the argument goes to positive infinity and goes to 2 as the argument goes to negative infinity. Substituting equation (29) into equation (28):

$$B_{tot} = \sqrt{\frac{2}{\pi\sigma^2}} \frac{B_o}{erfc(-\frac{N_o}{\sqrt{2}\sigma})} \sum_{n=0}^{N_{max}} e^{\frac{-(N-N_0)^2}{2\sigma^2}} e^{(\lambda - \gamma_N P_O)t} \tag{30}$$

We also assume that we are studying a distribution in the limit where Ns<<πa which means that the surface area of the receptors is much smaller than the surface area of the bacteria. When this assumption is made, we find that $\gamma_N = \gamma_o \frac{Ns}{\pi a}$. Using the linear approximation into equation (30) and (turning the sum into an integral from 0 to ∞) we can solve this equation exactly with the result:

$$B_{tot}(t) = B_o \frac{erfc\left(\frac{\gamma_1 P_o \sigma t}{\sqrt{2}} - \frac{N_o}{\sqrt{2}\sigma}\right)}{erfc(-\frac{N_o}{\sqrt{2}\sigma})} e^{(\lambda - \gamma_1 P_o N_o)t + \frac{1}{2}(\gamma_1 P_o \sigma)^2 t^2} \qquad (31)$$

Here $\gamma_1 = \frac{s\gamma_0}{\pi a}$ is the adsorption coefficient of a bacterium with one receptor. Notice that the mean and width of the initial distribution completely determines the response of the bacterial system at some constant phage concentration P_o because without subpopulation switching the bacterial population is composed of many subpopulations that are exponentially growing or decaying at varying rates. At short times, the argument of erfc(x) is negative and therefore the erfc(x) is just a constant between 1 and 2. During these small times the term $\lambda - \gamma_1 P_o N_o$ determines whether the exponential will be positive or negative. The average receptor density of the initial distribution accurately determines whether the population will experience either exponential growth or decay. This suggests that at short times the average homogeneous model is an accurate description. At intermediate times, the second order term $\frac{1}{2}(\gamma_1 P_o \sigma)^2 t^2$ (which is quadratic in t) will dominate and the bacterial concentration will increase. At long times, the quadratic term competes with the complementary error function and we find that as $t \to \infty$ the bacterial concentration goes to:

$$B_{tot}(t) \to \left(\frac{B_o}{\sqrt{\pi}\gamma_1 P_o \sigma}\right) \left(\frac{e^{-\frac{N_o}{2\sigma^2}}}{erfc(\frac{-N_o}{\sqrt{2}\sigma})}\right) \frac{e^{\lambda t}}{t} \qquad (32)$$

Notice that the rate of growth at longer times is independent of the phage pressure P_o. That is because in this model we have assumed the limit of no switching which as will be discussed later

causes the average adsorption coefficient to asymptotically approach zero which implies that the assumptions used to derive this result fail completely at longer times. Therefore as t becomes large, the bacterial growth rate should be independent of phage pressure.

To check the validity of the derivation in an obvious limit, let's look at the situation where $\sigma \to 0$. The equation reduces to:

$$B_{tot}(t) = B_o e^{(\lambda - \gamma_1 P_o N_o)t} \tag{33}$$

This is the solution to the homogeneous model when P_o~constant which is expected. As a graphical way of looking at the different solutions found and the times at which they are consistent, in Figure 14 the analytical solution for a Gaussian distribution, equation (31), is presented as the solid lines for a phage pressure of $P_o=2x10^7$ cm^{-3} (blue) and $P_o=5x10^7$ cm^{-3} (black). The homogeneous model is presented as the dashed lines, and the short time approximation (see Section 3.2) (which is equation (31) without the complementary error function) is presented as the dotted line. Notice, the homogeneous solution is valid for a short period of time but eventually the full solution begins to recover while the homogeneous solution only exponentially decreases and the two solutions eventually separate. The short time approximation on the other hand (the dotted line) is consistent with the full solution for a longer period of time but eventually as it begins to recover, the behavior rises much more quickly than the full solution. This is because the quadratic term in the exponential takes over the behavior of the system because there is no competition from an erfc term. This is consistent with our assertion in Section 3.2 that the short time approximation is a second order correction to the homogeneous solution. While, this analytical solution for an initial Gaussian distribution is illuminating, protein distributions are rarely if ever Gaussian. A much more common distribution used to describe protein distributions is the log-normal distribution.

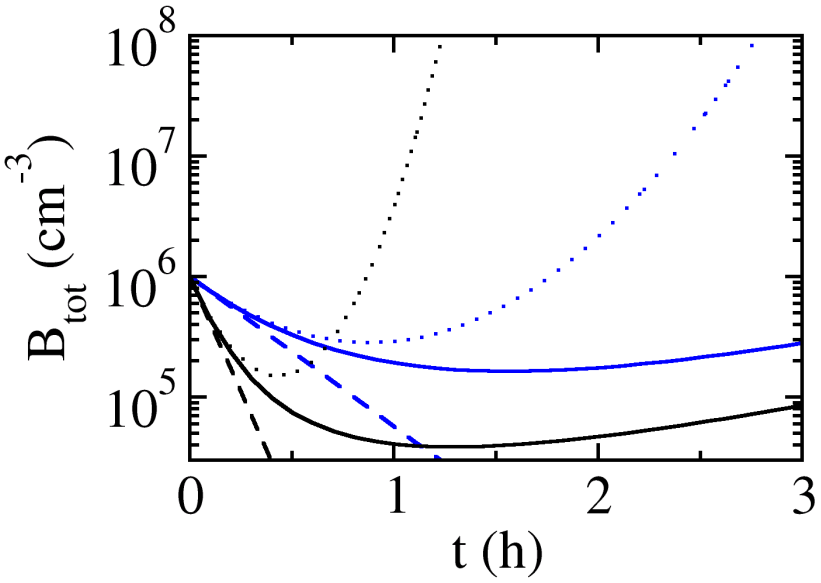

Figure 14 Comparing analytical solutions for an initial Gaussian protein distribution.
The blue lines are solutions for a constant phage pressure of P_o=2x10^7 cm^{-3}, whereas the black lines are for a constant phage pressure of P_o=5x10^7 cm^{-3}. For both phage pressures the homogeneous solutions drops down to extinction, (dashed line), but is valid for short times. The short time second order correction (no erfc terms, dotted line) is consistent with the full analytical solution until it minimizes and starts to increase in which case the increase is much greater than is actually possible due to the quadratic term in the exponential. The simulation of equation (31) where at long times the quadratic term in the exponential competes with the erfc function, is valid at all times as long as the assumptions made in the derivation remain valid.

2.4 ANALYTICAL SOLUTION: INITIAL LOG-NORMAL RECEPTOR DISTRIBUTION

In this section, we use the saddle-point approximation to derive an analytical solution for the dynamical behavior of the bacterial population, when the receptor distribution is initially distributed log-normally:

$$p(N) = \frac{1}{\theta N\sqrt{2\pi}} e^{-\frac{(\ln(N)-\ln(\mu))^2}{2\theta^2}} \qquad (34)$$

Once again we know the solution in the limit when P_o~constant and switching can be neglected:

$$B_{tot}(t) = \sum_{N>0}^{N\max} B_N(0) e^{-(\lambda-\gamma_N P_o)} \qquad (35)$$

Then we can replace:

$$B_N(0) = B_{tot}(0) * p(N) \tag{36}$$

Assuming a majority of the distribution is in a subpopulation with high enough N that we can replace the sum with an integral, we find:

$$B_{tot}(t) = \frac{B_{tot}(0)}{\theta\sqrt{2\pi}} e^{\lambda t} \int_0^{\infty} e^{-(\frac{(\ln(N)-\ln(\mu))^2}{2\theta^2} + \gamma_N P_o t)} dN \tag{37}$$

We can substitute, $N_o = \frac{\pi a}{s \ln(2a/b)}$

$$\begin{aligned} &\ln(N/N_o) = y \\ &\frac{dN}{N} = dy \end{aligned} \tag{38}$$

We then substitute y and $\bar{y} = \ln(\frac{\mu}{N_o})$ and find:

$$B_{tot}(t) = \frac{B_{tot}(0)}{\theta\sqrt{2\pi}} e^{\lambda t} \int_{-\infty}^{\infty} e^{-f(y)} dy \tag{39}$$

where, $f(y) = \frac{(y-\bar{y})^2}{2\theta^2} + \frac{\gamma_o P_o t}{1+e^{-y}}$. We assume that we can estimate the solution using the saddle point approximation to expand the function around the minimum of f(y). This implies that: $f(y) \approx f(y^*) + \frac{1}{2} f''(y^*)(y-y^*)^2$. y* is the point where the function is a minimum, which can be found by taking the first derivative of f(y) and solving for the point where it is 0.

$$\frac{(y^*-\bar{y})}{\theta^2} + \frac{\gamma_o P_o t}{4\cosh^2(y^*/2)} = 0 \tag{40}$$

This is a transcendental equation which we can use to find the solution for y* numerically. Now to finish the saddle point approximation we have to find the second derivative of the f(y) evaluated at y*:

$$f''(y^*) = \frac{1}{\theta^2} - \frac{\gamma_o P_o t}{4} \frac{\sinh(y^*/2)}{\cosh^3(y^*/2)} \tag{41}$$

Using the saddle point approximation we find that,

$$B_{tot}(t) \approx \frac{B_{tot}(0)}{\theta} \sqrt{f''(y^*)} e^{(\lambda t - \frac{(y^* - \bar{y})^2}{2\theta^2} - \frac{\gamma_o P_o t}{1+e^{-y^*}})} \tag{42}$$

Because the curves are completely determined by the mean and standard deviation of the initial log-normal distribution we can now use this equation to approximate the shape mean and standard deviation of the initial receptor distribution. Here we would like to emphasize the approximations which were incorporated into the derivation of the above analytical solution:

1) We are only studying the situation when the term f(y) can be expanded around a minimum which approximately corresponds to where y*~y when time is small.
2) We are studying the situation when the phage concentration is approximately constant.
3) We are assuming that the switching between subpopulations is slow.

Since protein expression distributions tend to be log-normal (Figure 17b, blue lines), this analytical solution will allow us to extract the mean and standard deviation of the initial receptor distribution using the heterogeneous model. The results can be compared with direct measurements of the initial receptor distribution measured using fluorescent microscopy and flow cytometry.

2.5 CONCLUSION

We have developed a mathematical model which separates a population of bacteria into individual bacterial subpopulations dependent on the number of functional maltoporin proteins that are being expressed. While the model is complicated, we have developed several simplified solutions using limits of varying rigor which allow us to understand the impact of receptor heterogeneity on the population dynamics. In Chapters 3.0 and 4.0 this theory will be compared with experiment using several assumptions of varying rigor. Throughout these chapters, there will be continual discussion about the study of receptor heterogeneity and its molecular origins in *E. coli*.

3.0 COMPARISON OF MODEL WITH EXPERIMENT

The two parameters used to compare the model discussed in Chapter 2.0 with experimental observations are the mean (<N>) and standard deviation ($\sigma_{<N>}$) of the initial unperturbed receptor distribution. In this chapter, model independent and model dependent measurements of these two quantities are made. First, a model independent measurement of the receptor distribution using fluorescently labeled phage as an "anti-body" for the receptors is presented. Second, we use **a** correction to the homogeneous model and short time experiments to extract <N> and $\sigma_{<N>}$. Next, we fit killing curves which satisfy the P_o~constant assumption with the analytical solution derived in Section 2.4, as a model dependent way to extract the mean and standard deviation of the initial receptor distributions. Finally, the full set of nonlinear differential equations (assuming negligible switching) described in Chapter 2.0 is numerically integrated using the constants measured in the Appendix and shown in Table 1. For the full integration, the measured receptor distributions, phage and bacterial concentrations are used as the initial conditions of the system. Throughout this chapter, we use the term killing curves which is defined as measurements of the bacterial concentration when phage are in excess under the initial conditions that MOI>1 (multiplicity of infection, MOI=$\frac{P_o}{B_o}$).

Constant	*Description*	*Ymel*	*LE392*
a (μm)	Semi-major axis	2.1	2.7
b (μm)	Semi-minor axis	0.46	0.48
γ_0 (cm^3/s)	Maximum effective adsorption rate	$9.0x10^{-11}$	$1.1x10^{-10}$
λ (h^{-1})	Growth rate	1.1	1.1
m (phage/infected bacteria)	Burst size	14	12
τ (minutes)	Latent period	47	45

Table 1 Table of constants.
The description of the measurement of each constant is described in the Appendix and used in all simulations. This table contains all the constants used in both the fit to the analytical solution and the full simulation. The constant ε was treated as an adjustable parameter but must be larger than the latent period. It was found that numerical integration at the initial conditions used was fairly independent of ε and $\varepsilon(=\tau^{-1})$ was fixed as the latent period. Each constant was independently measured for both strains.

3.1 INITIAL RECEPTOR DISTRIBUTIONS

We have developed a method to measure the maltoporin receptor distribution in a bacterial population using fluorescent lambda phage particles as a fluorescent probe with a strong affinity for the maltoporin receptor. Lambda phage tails were previously used as a fluorescent probe for the receptors and were found to remain bound to the receptor for extended periods of time allowing visualization by fluorescent microscopy (Gibbs et. al. 2004). Here we choose to use the full virus because we can attach many more fluorescent dye molecules to an individual probe. For cells with only a few attached phage, we can visualize individual phage which appear as diffraction limited spots in Figure 8. An attached fluorescently labeled virus indicates the presence of a maltoporin protein. We assumed that approximately each available receptor had an attached phage because at the phage concentration that was used to infect the cells, a bacterium

with a single free receptor will adsorb a phage after on average 4 minutes of incubation in 10mM $MgSO_4$. The size of the phage head could possibly block the attachment of another phage, but this steric hindrance should only by a factor when ~2000 phage particles are attached.

3.1.1 Receptor Labeling Procedure

The phage were labeled with AlexaFluor 488 (see Appendix). Exponentially growing cells were washed twice and resuspended in 10mM $MgSO_4$ with no carbon source. A bacterial population was incubated with a high fluorescent phage concentration (>$4x10^{10}$ cm^{-3}). The cells and phage were allowed to adsorb in the dark for 30-35 minutes at 37 °C. The cells were then washed twice with 10 mM $MgSO_4$ to clear out the excess free phage. A 50 µl sample was taken out and diluted into 2 mls of 10 mM $MgSO_4$. This sample was used to do fluorometry as described below. The remainder of the cells were kept on ice in the dark until the flow cytometry was performed.

3.1.2 Fluorometry

The flow cytometer used to study fluorescently attached phage was unable to distinguish individual quantized phage attached to bacteria and therefore a calibration scheme using a fluorometer was used to determine how the arbitrary fluorescent units of the flow cytometer related to the number of attached phage.

The fluorometry measurements were performed on a Bio-Rad VersaFluorTM Fluorometer. The brightness of a known concentration of labeled λ phage was found in FLUs or FLuorometer Units. The same sample was diluted by a known amount and a new reading was

taken, this process continued for at least 4 readings. The data was fit with a straight line using the least squares method in OriginPro 7.5 with a y-intercept value of 0 (Figure 15).

The above procedure was repeated with 1μm yellow-green IDC spheres. Because the illumination volume remained constant, by dividing the two slopes (FLU/phage and FLU/bead) we can find the multiplicative factor phage/bead which can be used to calibrate the flow cytometer. It is important to note here that the fluorescence spectra of the IDC spheres and of the dye (AlexaFluor488) used to label the phage are very similar, so different filter sets will not greatly affect the ratio of the fluorescence readings.

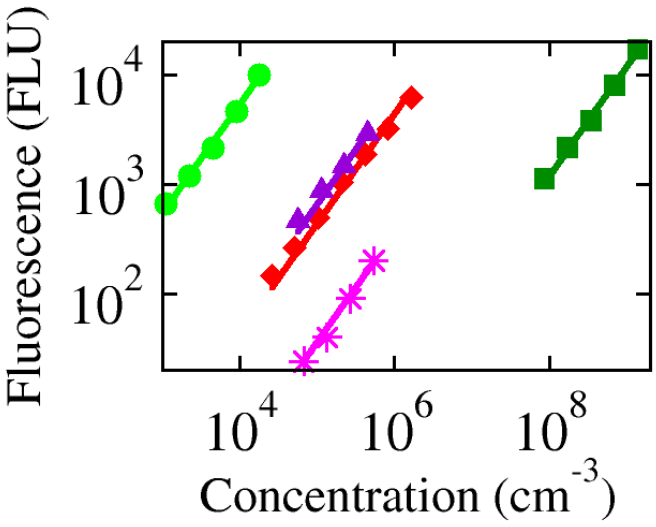

Figure 15 Fluorometry dilution curves.
Fluorescence readings at different dilutions were taken for phage (dark green squares), fluorescent IDC spheres (light green circles), fluorescent phage adsorbed Ymel (red diamonds), fluorescent phage adsorbed LE392 (purple triangles) and LE392 autofluorescence (pink stars). After background subtraction the dilution curve was fit with a straight line with a zero y-intercept. These values were used to calculate average receptor numbers as shown in Table 1.

3.1.3 Average Receptor Values

We calculated the average receptor number for both Ymel and LE392 strains using the flow cytometer and the fluorometer to check the validity of the calibration described in the previous section. The results of several methods to calculate <N> are presented in Table 2. The calculation of the average receptor number using the fluorometer is independent of the ratio of bead fluorescence and phage fluorescence whereas the calculation of the average receptor number using the flow cytometer is completely dependent on the ratio of the beads and phage allowing us to check the validity of the calibration

The fluorometry dilution procedure was repeated with a sample of bacteria which had been adsorbed with saturating concentrations of fluorescent phage (MOI>4000). After cell autofluorescence was subtracted, the slope of the linear fit (FLU/bacteria) was divided by the phage dilution slope (FLU/phage) to find the average number of phage/bacteria. Example dilution curves for both Ymel and LE392 can be seen in Figure 15. After averaging over 3 independent measurements of the Ymel strain and 5 independent measurements of the LE392 strain, an average of <N>=270±30 receptors/bacteria and <N>=550±80 receptors/bacteria were found for Ymel and LE392, respectively. These values are consistent with individual measurements of the average receptor number for both strains of bacteria.

3.1.4 Flow Cytometry

The flow cytometry measurements were performed on a Becton Dickinson FACS DiVa Flow Cytometer and Cell Sorter or a DAKO Cyan ADP Analyzer. It was found that the Cyan instrument had better resolution between the attached phage signal and the cell autofluorescence,

but both instruments yielded similar results. Only the fluorescence intensity in the green channel excited with 488nm laser was considered in this experiment. The forward and side scatter were used to discriminate debris from live bacteria.

The same samples that were run on the fluorometer were also run on a flow cytometer, along with a sample of fluorescent latex spheres. After correcting for autofluorescence (see Section 3.1.5), we calculated the receptor distribution in FCUs (arbitrary Fluorescent Units on flow cytometer scale) (shown as the red line in Figure 16). Using the fluorometry measurements, it was determined that each phage is a factor of 2.2×10^{-5} the fluorescence of a bead on the Becton Dickinson machine. Using the average fluorescence value for the beads on the flow cytometer scale, it was found that each phage is on average 20 FCUs. The cells were infected with a very high phage concentration so we assume that all receptors have a fluorescent phage attached. In other words, the fluorescent phage distribution is the same as the receptor distribution, and therefore the receptor distributions of the two cell strains were measured (Figure 17).

3.1.5 Correction for Autofluorescence

Deconvoluting the signal and the autofluorescence of cells is a common problem in fluorescent studies in biology (Corsetti 1988, Havilio 2006). The standard Fourier transform technique was found not to be useful here because the mean value of the large peak of the maltose grown cells is 2-3 orders of magnitude larger than both the minor peak and the autofluorescence peak (green line in Figure 16). The numerically deconvoluted functions always had false oscillations in place of the minor peak. Due to this difficulty, we present an alternative method of deconvolution below.

Because we want to know the distribution of the minority population with a low fluorescence, the deconvolution of the signal from the autofluorescence is important. While the majority of the fluorescent phage distribution was only slightly affected by the autofluorescence of the cells, the distribution of the cells with very few attached fluorescent phage were highly affected by the autofluorescence of the cells. The low receptor concentration bacteria are the bacteria which will remain alive in the presence of very high concentrations of phage pressure while the bacteria with high receptor concentrations will quickly be killed. So, it is of much less importance to know the exact distribution of the cells with high receptor concentrations but may be of greater importance to know the distribution of cells with low receptor concentrations.

All fits in this section were done using a nonlinear regression algorithm in OriginPro 7.5. The autofluorescence distributions are shown on Figure 16 as the green line. The autofluorescence distribution has been scaled to fit on the graph. This distribution was fit with a log-normal function to give the autofluorescence probability density function (PDF) $p_A(A)$. The probability density function that we measured using the flow cytometer, is the probability of a cell having a total fluorescence T=A+R where A is the autofluorescence of the cells and R is the fluorescence of the attached phage. The total measured fluorescence distribution $p_T(T)$ was fit using the Origin Pro Multi-Peak Fitting Module. The PDF of the total fluorescence $p_T(T)$ of each cell was fit with the function

$$p_T(T) = \frac{H}{\left(T\sigma_1\sqrt{(2\pi)}\right)} e^{\frac{-\left(\ln(T)-\ln\left(\overline{F_1}\right)\right)^2}{\left(2\sigma_1^2\right)}} + \frac{(1-H)}{\left(\sigma_2\sqrt{(2\pi)}\right)} e^{\frac{-\left(T-\overline{F_2}\right)^2}{\left(2\sigma_2^2\right)}} \qquad (43)$$

In this equation, H is the percentage of cells in the first peak. This function, which is a combination of a log-normal function and Gaussian function, was chosen because it most closely describes the data. While two log-normal functions fit the upper tail of the larger peak better for

both the Ymel and LE392 distributions, it is more important to describe accurately the mid to low receptor subpopulations and equation (43) more closely describes the data from the average value of the larger peak down to the low receptor number subpopulations.

We know $p_T(T)$ and the $p_A(A)$ therefore we need to deconvolute these two PDFs in order to figure out the fluorescence due to the attached phage $p_R(R)$. The measured distribution $p_T(T)$ is a convolution of the autofluorescence of the cells and the receptor PDF. This is described by the equation:

$$p_T(T) = \sum_{A=0}^{F_{max}} p_R(R) p_A(A) \tag{44}$$

We assume that the autofluorescence and phage fluorescence are uncorrelated. The total fluorescence, then, is just a sum of the autofluorescence and the phage fluorescence, T=A+R. Filling this into equation (44) we find that

$$p_T(T) = \sum_{A=0}^{F_{max}} p_R(T - A) p_A(A) \tag{45}$$

An error metric minimization method is used to deconvolute the two functions (Mignotte et. al. 2002). The first assumption is that the PDF of the signal $p_R(R)$ has the same functional form as the total measured data $p_T(T)$. The second assumption is that H in equation (43) remains constant. In other words, the percentage of cells in each peak does not change under the deconvolution. The other four constants $\overline{F_1}$, σ_1, $\overline{F_2}$, σ_2 are then fit by minimizing the left hand side of the equation:

$$\sum_{T=0}^{T_{MAX}} \left[p_T(T) - \sum_{A=0}^{F_{max}} p_R(T - A) p_A(A) \right]^2 = 0 \tag{46}$$

The LHS of equation (46) was minimized using the amoeba algorithm in Numerical Recipes in C. The amoeba algorithm uses a simplex method to minimize a function in N dimensional parameter space (Press et. al. 1988).

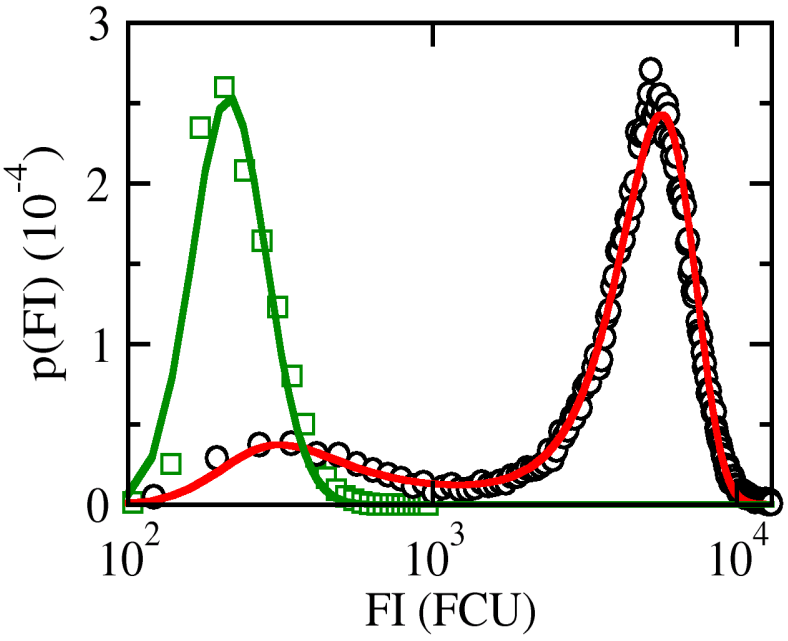

Figure 16 Flow cytometry data with fits to the distribution.
Fluorescent phage adsorbed cells were measured through a flow cytometer. The binned PDF for more than 50,000 cells can be seen for Ymel (black circles). The autofluorescence curve is scaled to fit on the graph and is presented as the green squares along with a scaled fit to a log-normal distribution (green line). The total convolution of the phage adsorbed signal $P_R(R)$ (calculated using the deconvolution algorithm) signal and the $P_A(A)$ autofluorescence is the red line, it agrees very well with the measured distribution.

In Figure 16, the black circles are the binned experimental flow cytometry data, the green squares the experimental autofluorescence data, the green line is a log-normal fit to the autofluorescence and the red line is the convolution of the autofluorescent background and the minimized function $P_R(R)$. To change this PDF from FCUs into a quantitative receptor distribution, the relationship that 1 phage=20 FCUs is used. Using the fact that:

$$p_R(R)dR=p_R(N)dN \qquad (47)$$

Here, R is the fluorescence of the deconvoluted signal and N is the number of receptors. On average R=20N, therefore,

$$p_R(R)=20p_R(20N) \quad (48)$$

The receptor distribution for Ymel found using this method is shown in Figure 17. It was found that this deconvolution has very little effect on the shape of the killing curve simulation when compared to pure subtraction of the autofluorescent background. In Figure 17b), the binned flow cytometry data for Ymel (black) and LE392 (red). Therefore, the receptor distribution used to initialize the set of nonlinear differential equations for cells grown in maltose is just the original data subtracted by the average value of background fluorescence. The distributions are also fit with log-normal functions (blue line) for later comparison with results using the analytical solution found in Section 2.4 for a log-normal distribution.

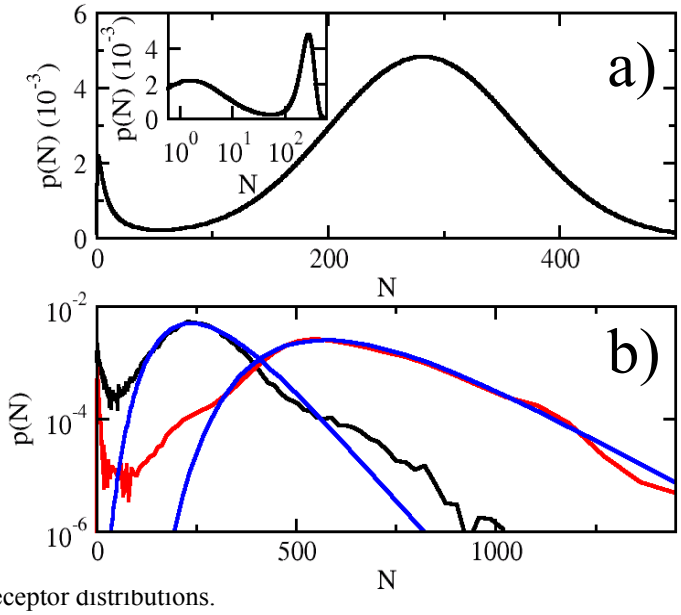

Figure 17 Initial receptor distributions.
a) Through the fluorometer measurements it was deduced that one phage on average equaled 20 flow cytometer fluorescent units. Therefore we were able to deduce the receptor per bacteria PDF for Ymel. The inset is the same PDF but presented on a log scale. b) The PDF for Ymel is depicted as the black line whereas the LE392 PDF is the red line. The blue lines are fits to a log-normal distribution. These fits will be used for comparison with the log-normal analytical model in Section 3.3.

3.2 SHORT TIME APPROXIMATION

One of the results derived in Chapter 2.0 is that at short times the homogeneous model is valid. In this chapter, a short-time correction to the homogeneous model is presented. By the definition of the averaged adsorption coefficient:

$$\overline{\gamma(t)} = \frac{\sum_N \gamma_N B_N(t)}{B_{tot}(t)}, \tag{49}$$

we can derive the equation:

$$\dot{\bar{\gamma}} = -\sigma_\gamma^2 P(t) + D(t), \tag{50}$$

where $\sigma_\gamma^2 = \overline{\gamma^2} - \bar{\gamma}^2$ and $D(t) = \sum_N \sum_i (\gamma_N - \gamma_i)\alpha_{Ni} B_i$. As a correction to the homogeneous model, at short times D(t) is negligible, P_o~constant and σ_γ^2~constant. We assume D(t) is negligible because the α terms are smaller than the killing. While the standard deviation is not necessarily constant we find this to be a valid approximation in this system. We find experimentally that the standard deviation remains approximately constant after selective killing by phage pressure (see Figure 42). Using these assumptions, we find that $\dot{\bar{\gamma}} \approx -\sigma_\gamma^2 P_o$. Taking the integral, $\bar{\gamma}(t) = -\sigma_\gamma^2 P_o t + \gamma_{<N>}$. Filling this into equation (23) and taking the integral again:

$$B(t) \approx B_o e^{(\lambda - \gamma_{<N>} P_o)t + \frac{1}{2}(\sigma_\gamma P_o)^2 t^2} \tag{51}$$

This is the same as the Gaussian solution presented in Section 2.3 without the erfc terms. This implies that if $\gamma_{<N>} >> \sigma_\gamma$, the selective killing does not greatly change the width of the distribution. Equation (51) can be parameterized as:

$$B(t) \approx B_o e^{\Lambda_{eff} t + Ct^2} \tag{52}$$

As an example, two experiments fit with equation (52) are shown in Figure 18. The red circles are the Ymel strain and the purples squares are the LE392 strain, both experiments were inoculated with an initial phage concentration of $5x10^8 cm^{-3}$. The black lines are the fits to equation (52).

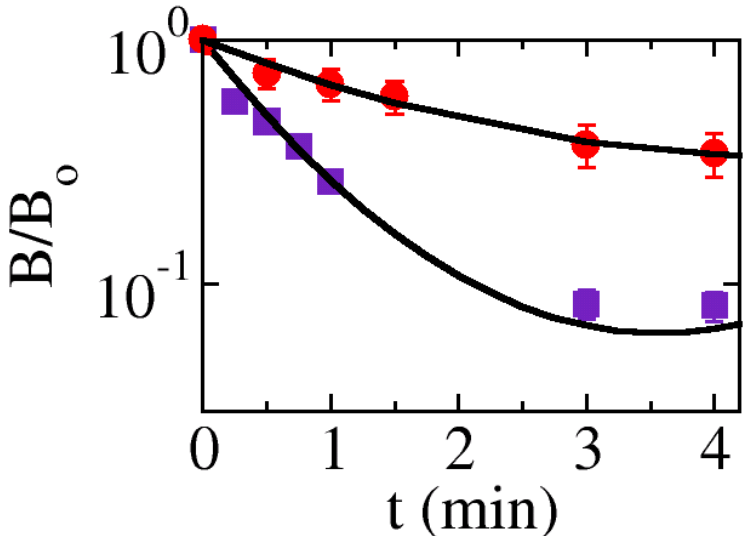

Figure 18 Fitting the short time (<5 minutes) experimental data with equation (52).
The red circles are a run for Ymel and purple squares are for LE392, both experiments had a P(0)=$2x10^8$ cm^{-3}.

The short term experiments were performed with a variety of initial phage concentrations. The phage concentration was kept $>10^8$ phage/cm^3 (MOI>100) to ensure it remained approximately constant on this timescale. The next assumption used is the short time assumption, which means we are only concerned with a first order correction to the homogeneous model. This is in the region where $(\lambda - \gamma_{<N>} P_o)t > \frac{1}{2}\sigma_\gamma^2 P_o^2 t^2$ which means this assumption is valid when $t < \frac{2(\lambda - \gamma_{<N>} P_o)}{\sigma_\gamma^2 P_o^{\,2}}$, which sets a limit on the P_o that can be used because experiments need to be ~5 minutes in length in order to take enough measurement points. Λ_{eff} was plotted as a function of P_o and C was plotted as a function of P_o^2 because both of the relationships should be linear for

validation of the model. Both were fit with a straight line allowing $\gamma_{<N>}$ and σ_γ to be extracted. The experiments for Ymel (red circles) and LE392 (purples squares) are presented in Figure 19.

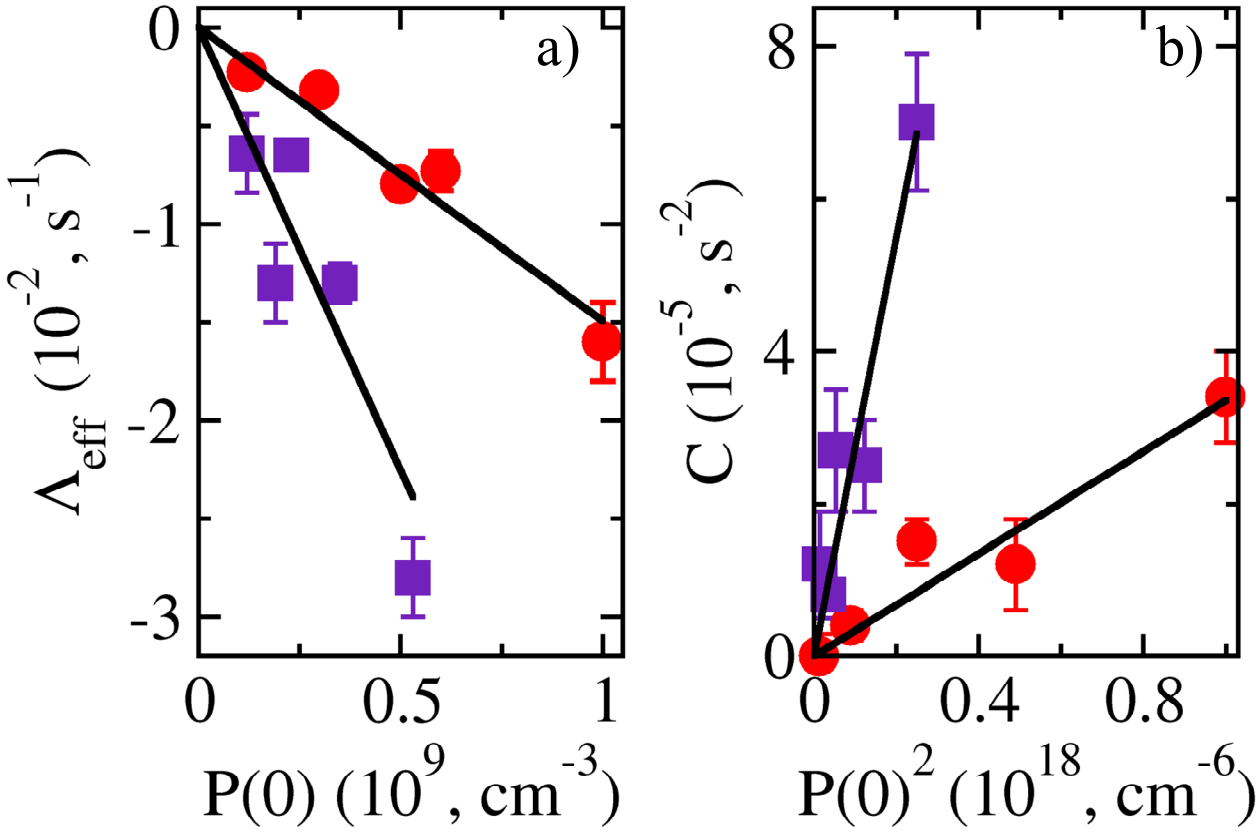

Figure 19 Calculation of model-dependent value for the average and width of the distribution in the short time approximation. In these graphs the color coding is the same as Figure 18 (a) The slope of the Λ_{eff} vs P(0) line is equal to $\bar{\gamma}$. (b) the slope of the C vs. $P(0)^2$ is equal to $0.5\sigma^2$

For the two strains, $\gamma_{<N>}$ was used to calculate <N> while σ_γ was used to calculate $\sigma_{<N>}$ for comparison with flow cytometry results as given in Table 2. For this experiment, LE392 was found to have <N>=660±170 and $\sigma_{<N>}$=250±30. For Ymel it was found that <N>=140±20 and $\sigma_{<N>}$=80±10. While the measured <N> for Ymel was lower than flow cytometry measurements, all other measured values were found to agree with the flow cytometry data within the error.

3.3 FIT TO THE LOG-NORMAL MODEL DERIVED IN 2.4

In Section 2.4, we derived an analytical solution for the bacterial concentration B(t) when switching is neglected, P_o~constant and the initial distribution is a log-normal distribution. Once again, a log-normal distribution is defined as:

$$p(N) = \frac{1}{\theta N\sqrt{2\pi}} e^{-\frac{(\ln(N)-\ln(\mu))^2}{2\theta^2}}$$

The analytical solution equation (42) derived in Section 2.4 is used to fit killing curve experiments. For this experiment, killing curves with an MOI >80 and $B_{tot}<3x10^6$ cm^{-3} were fit with equation (42) using the OriginPro v7.5 Fitting Module with log-weighting. From this fit, the parameters $\mu=\langle\ln(N)\rangle$ and $\theta = \overline{\left[\ln(N) - \left\langle \ln(N) \right\rangle\right]^2}^{1/2}$ from the log-normal equation were extracted. An example of a typical fit using equation (42) can be seen in Figure 20a). The black circles are the experimentally measured concentration of a population of bacteria which was initially inoculated with a phage concentration of ~$1.5x10^8$ PFU/cm^3. In order to keep the phage concentration approximately constant the bacteria had a low concentration of ~$1x10^6 cm^{-3}$, which under these conditions only decreased below this level. While the MOI of this system is ~100, the low bacterial concentration kept the phage concentration approximately constant. μ and θ were converted into the traditional mean and standard deviation for comparison with the measured receptor distributions. For the log-normal distribution the mean <N> and standard deviation $\sigma_{<N>}$ are defined as:

$$< N >= \mu e^{\frac{\theta^2}{2}} \tag{53}$$

$$\sigma_{<N>} = \mu e^{\frac{\theta^2}{2}} \sqrt{e^{\theta^2} - 1} \tag{54}$$

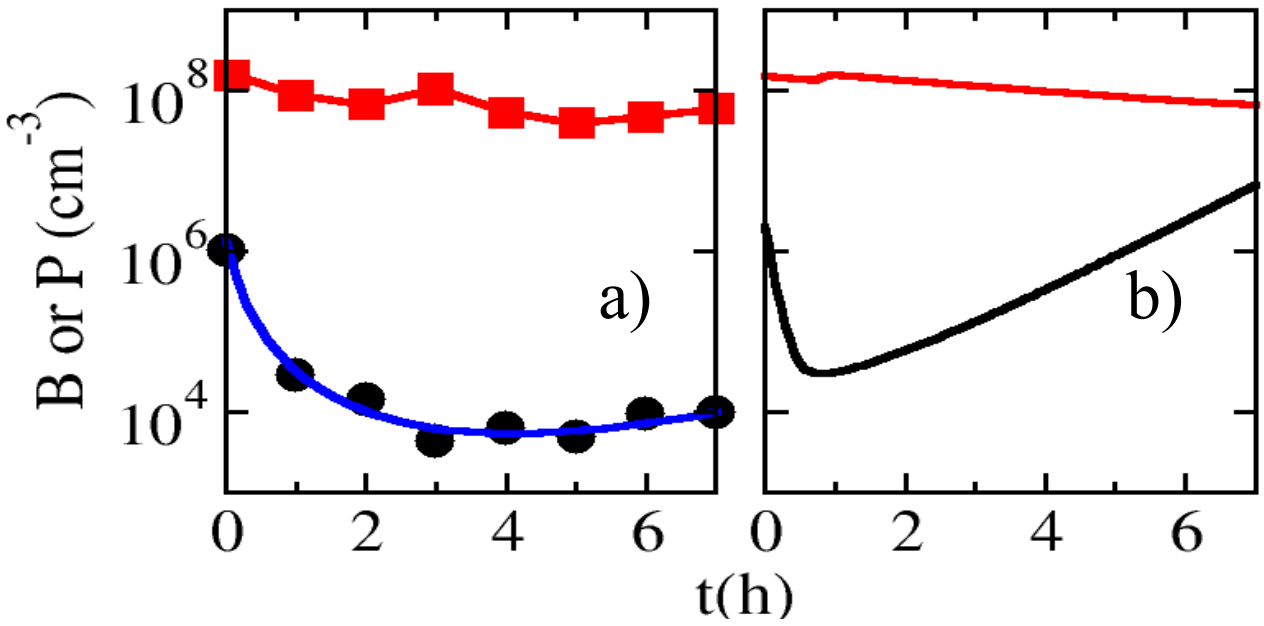

Figure 20 A killing curve with an approximately constant phage concentration.
(a) Experimental curve with bacterial concentration (black), phage concentration (red) and the fit to the log-normal analytical model (blue) (b) For comparison purposes, the full model simulation for both the phage (red) and bacteria (black) are presented. The long period of low effective growth cannot be explained by the no-switching model.

	Short Time Fits		**Fit to Analytical Solution**		**Flow Cytometry**		**Fluorometry**
	$\langle N \rangle$	σ	$\langle N \rangle$	σ	$\langle N \rangle$	σ	$\langle N \rangle$
LE392	660±170	250±30	600±120	610±130	570±50	200±10	550±80
Ymel	140±20	80±10	310±20	320±30	240±30	140±60	270±30

Table 2 Comparing the model dependent and model independent measurements of the distributions.

The average mean and standard deviation for more than four different fits can be seen in Table 2 for both the LE392 and Ymel strains. The mean and standard deviation of the actual receptor distributions were measured as:

$$< N >= \frac{\sum_{i=1}^{I_{\max}} N_i}{I_{\max}} \tag{55}$$

$$\sigma_{<N>} = \sqrt{< N^2 > - < N >^2} \tag{56}$$

For both strains the mean is estimated relatively well, but the variance is overestimated using this procedure. The full simulation of the model (described in detail in Section 3.4), using the measured receptor distributions as the initial conditions, shows that that the mean correctly estimates the killing over shorter times in this case ~1 hour but the experimental curve is flatter than the full simulation between hour 1 to hour 7 causing the overestimation of the standard deviation. The flatness of the curve could be due to the fact that the log-normal distribution does not accurately mimic the minority populations. Also, we fit curves over a period of ~10τ and the assumption that switching is negligible becomes suspect as we allow the system to evolve over longer times. In Figure 20b), the full simulation of the heterogeneous model using the measured bacterial distribution as initial conditions is presented assuming negligible switching and the inclusion of the minority bacterial subpopulations does not fully explain the flat region hinting at the importance of the switching terms.

3.4 RESULTS: KILLING CURVES WITH HIGH $MgSO_4$ CONCENTRATIONS

Exponentially growing bacteria were inoculated with phage at varying concentrations ranging more than two orders of magnitude from MOI~1 to 400. For the Ymel strain (~300 receptors/bacteria initially), the homogeneous model, which consistently predicts the initial behavior of the bacterial population, predicts that the population should decay when the initial phage concentration is greater than ~$1x10^7$ cm^{-3} and the population should grow when the initial phage concentration is less than ~$1x10^7 cm^{-3}$. Figure 21 shows this range of behaviors. For example, the killing curve with an initial phage concentration of $2x10^7$ cm^{-3} initially decays and the killing curve with an initial phage concentration of $4x10^6$ cm^{-3} initially grows. The critical point where the bacterial replication and death due to infection is on average equal, $\lambda = \gamma_{<N>} P_o$ =>P_o~$1x10^7$ cm^{-3} which is in-between these two values. A similar pattern is apparent for the LE392 strain that has an average ~600 receptors per bacteria. The initial part of the curve should decay when P_o>$8x10^6 cm^{-3}$. In Figure 21, the killing curve with P_o= $3x10^7$ cm^{-3} decays and the killing curve with P_o=$5x10^6$ cm^{-3} grows, as is expected.

As shown in Figure 21, the homogeneous, heterogeneous models and experimental results are presented and tend to agree with each other for times less than ½ hour. The length of time that the heterogeneous and homogeneous models agree is dependent on the strength of the initial phage perturbation. For the Ymel strain in Figure 21a), b) and c) the homogeneous and heterogeneous models agree for ~5 hours for the curve with an initial phage concentration of $4x10^6 cm^{-3}$, whereas the two models of the curve with an initial phage concentration of $4x10^8 cm^{-3}$ only agree for times less than about half an hour.

We used the two different strains LE392 and Ymel in order to compare the change of the initial PDF on the shape of the killing curves. The simulation of the heterogeneous models for the two strains (Figure 21b), d)) shows that the Ymel curve and LE392 curve do exhibit subtle differences. In the experiment, besides the comparisons made above, there are no systematic differences that can be seen between the killing curves of the two strains. The run to run variations in the shape of the killing curves vary as much as the differences between the two strains.

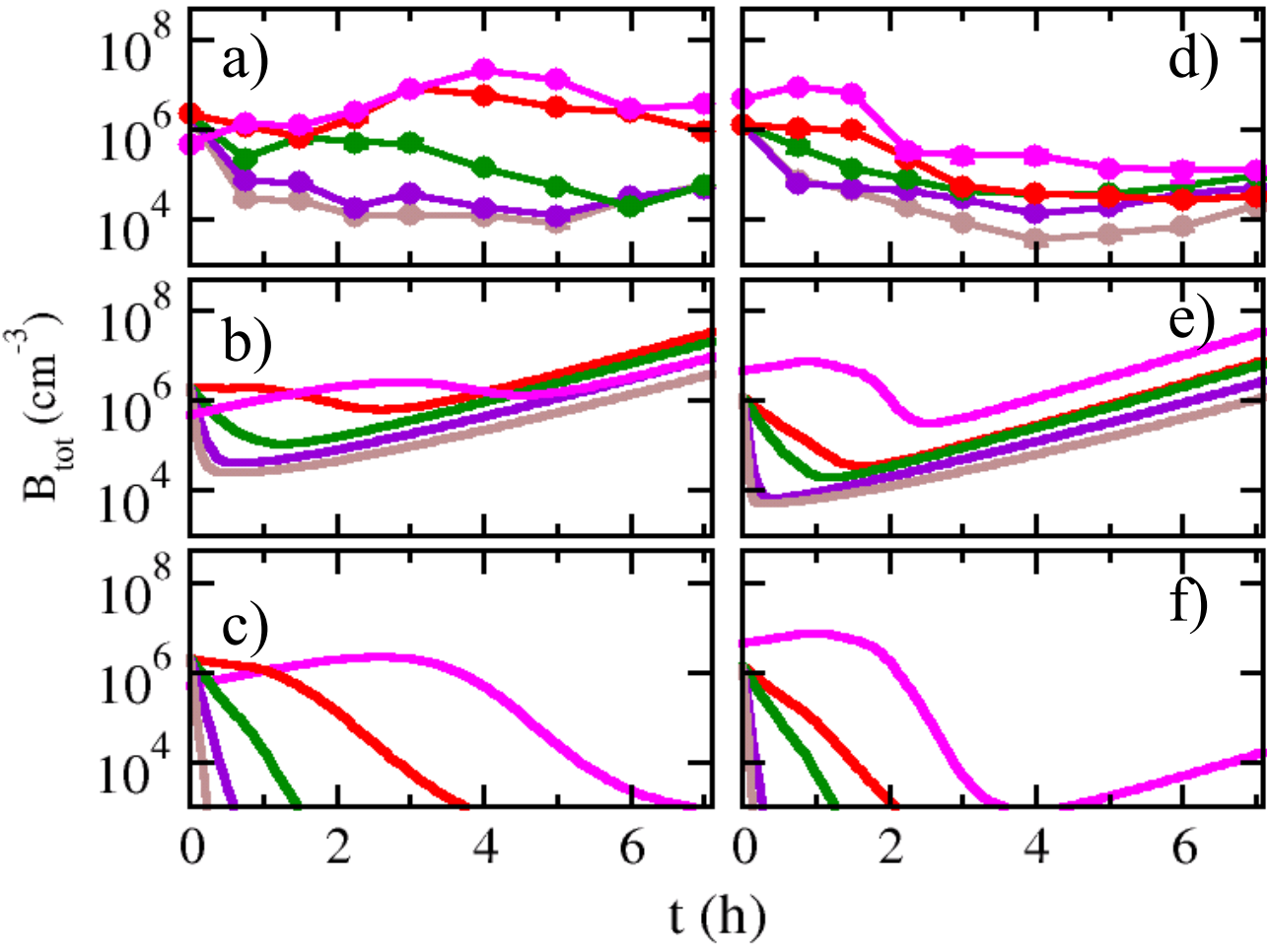

Figure 21 Killing curves of Ymel and LE392**.**
These graphs are (a, d) experimental, (b, e) theoretical heterogeneous model and (c, f) theoretical homogeneous model killing curves for Ymel and LE392 respectively. The curves show the evolution of B_{tot} for a system with an initial phage concentration of $4x10^6$ (pink), $2x10^7$ (red), $7x10^7$ (green), $2x10^8$ (purple), and $4x10^8$ (brown) cm^{-3} for Ymel; and a phage concentration of $5x10^6$ (pink), $3x10^7$ (red), $5x10^7$ (green), $2x10^8$ (purple), and $4x10^8$ (brown) cm^{-3} for LE392.

3.5 RESULTS: KILLING CURVES WITH LOW $MgSO_4$ CONCENTRATIONS

By decreasing the $MgSO_4$ in the media, we can decrease the rate of adsorption (Moldovan et. al. 2007). The main issue with decreasing the salt concentration is that the validity of the Berg-Purcell model is now called into question. In the Berg-Purcell model, the receptors are assumed to be perfect sinks and by decreasing the salt concentration this is not necessarily true, because the adsorption is no longer diffusion-limited. We found that by changing the $MgSO_4$ concentration in the media from 10mM to 1mM decreases the phage adsorption by a factor of ~4 (see Appendix). The only way to be consistent with the Berg-Purcell model is to assume that the number of "functional" phage binding receptors is decreased by a factor of 4 in this low salt condition. We model this decrease in adsorption simply as a factor of 4 decrease in the number of receptors measured in the 10 mM $MgSO_4$ condition. We can then determine the effect of a decrease in adsorption on the killing curves.

Because we find similar results for Ymel and LE392, we only present the results of decreasing the salt concentration on the LE392 strain, although both strains were examined. Figure 22 is the experimental killing curves for the LE392 strain in 1mM MgSO4. The curves range from an initial phage concentration of $3x10^6$ cm^{-3} to $3x10^8$ cm^{-3}. According to the homogeneous model the bacterial population should exponentially increase at phage concentrations $<3x10^7$ cm^{-3}. Once again the experimental results confirm that the initial curves grow exponentially until the initial phage concentration reaches the critical point of ~$3x10^7 cm^{-3}$. The bacterial population can no longer be described by the average homogeneous model because the high phage concentrations are on average selectively killing the bacteria with high receptor numbers.

This particular experiment also contributes to the evidence that the decrease in the rate of adsorption of phage in the middle of a killing curve is the main factor in the persistence of the bacterial population and suggests that the number of available receptors is an important factor in explaining bacterial persistence to phage. In the Appendix, we present an experiment where we add the plasmid pTAS1 which constitutively expresses receptors and the number of persistent cells decreases. This evidence emphasizes the idea that persistence occurs as a result of receptor heterogeneity.

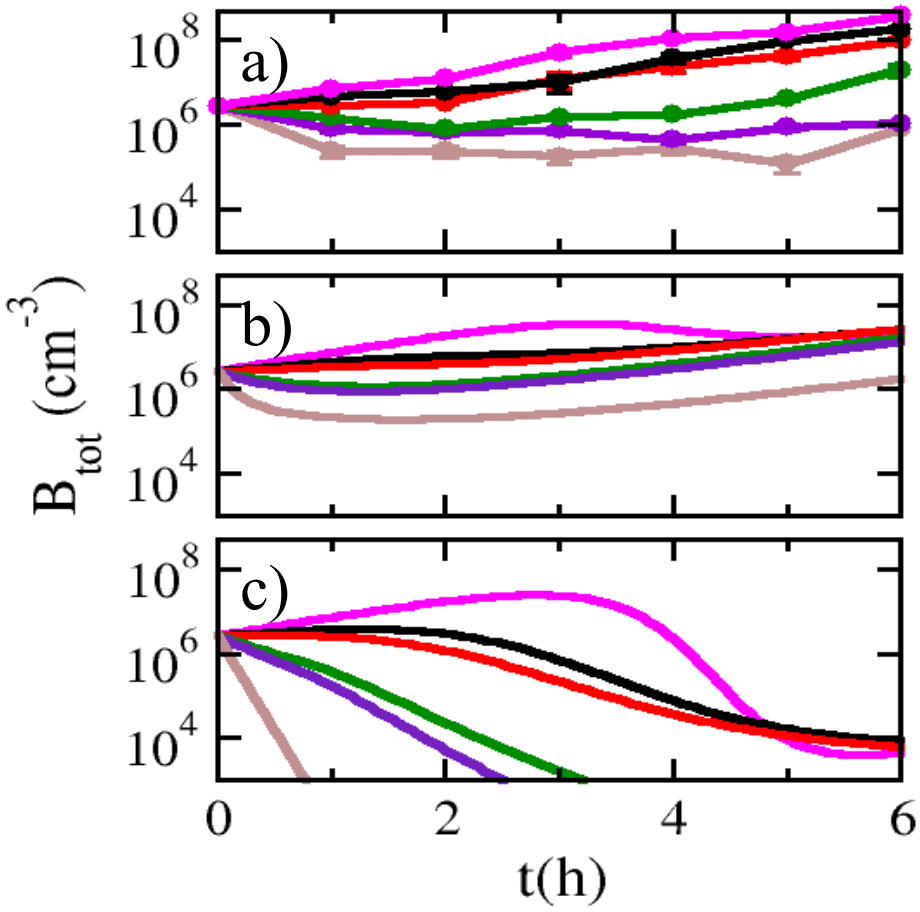

Figure 22 Killing Curves of LE392 in 1mM MgSO4
These graphs are (a) experimental, (b) theoretical heterogeneous model and (c) theoretical homogeneous model killing curves for LE392. The media in this experiment has only 1mM $MgSO_4$ rather than the 10mM in the previous experiment. In the model, the number of functional receptors is decreased by ¼ while every other parameter remains the same as the previous experiment. The curves show the evolution of B_{tot} for a system with an initial phage concentration of $3x10^6$ (pink), $2x10^7$ (black), $3x10^7$ (red), $8x10^7$ (green), $1x10^8$ (purple), and $3x10^8$ (brown) cm^{-3}.

3.6 *E. COLI* IN GLUCOSE AND GLYCEROL

As a last, extreme example of the effects of phenotype heterogeneity, we present the killing curves of *E. coli* in two different carbon sources which induce the maltose regulon to different receptor expression levels. As can be seen in Figure 23, glucose grown cells have very few attached phage and correspondingly few receptors, causing the autofluorescence and signal distributions to have a large overlap. Because of the large overlap, deconvolution of the distribution is important for determining the actual receptor distribution and numerical Fourier transform techniques do work. In Chapter 4.0 , the Fourier transform technique was used to deconvolute the two distributions but here we use the deconvolution method (described in Section 3.1.5), using simple log-normal distributions to characterize the experimental data. In Figure 23a), the experimental data (black circles) is presented along with the convolution of the autofluorescence distribution and the signal distribution (purple line). The deconvolution was essentially the same if we used a quantized distribution (red line) or a continuous distribution (blue line).

Killing curves were performed (Figure 23b)) for over one order of magnitude of phage concentrations ($7x10^8 cm^{-3} < P_o < 10^{10} cm^{-3}$) including a concentration so high only the subpopulation with zero receptors should be able to grow. Notice when $P_o < 2x10^9$ cm^{-3} there is almost no killing which is expected with both heterogeneous and homogeneous models, whereas when $P_o \geq 2x10^9$ cm^{-3} there is some killing (Figure 23b) inset) but this killing very quickly becomes independent of the phage pressure. The quantized distribution in Figure 23a) (red line) was used as the initial receptor distribution to simulate the killing curves of the glucose grown cells. The parameters in Table 1 were used for the glucose simulation except for the growth rate (λ=1.3 h^{-1}) and bursting coefficient (m=30 phage/bacteria) which were both larger in glucose

grown cells. Measurements of these parameters were identical to those presented for maltose grown cells in the Appendix.

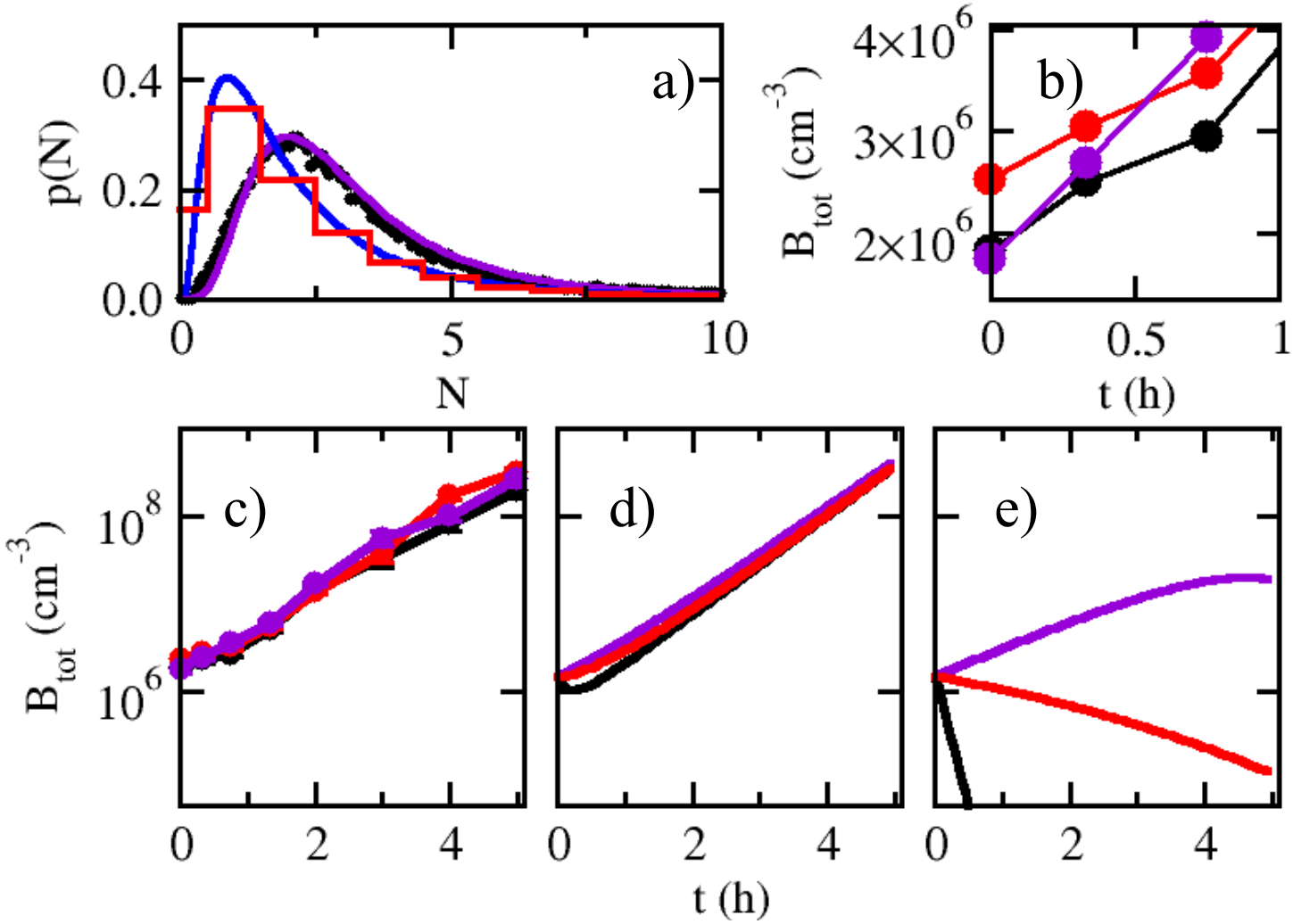

Figure 23 Effect of heterogeneity on LE392 cells grown in glucose.
(a) The receptor distribution of LE392 cells grown in glucose. The blue line is the continuous, deconvoluted distribution, the red line is the quantized deconvolution distribution. The black circles are the experimental data and the purple line is the convolution of the autofluorescence and the quantized distribution. (b) The LE392 killing curve in glucose zoomed into the first hour. The glucose cells exposed to P_o=7x10^8 cm^{-3} (purple) of phage show almost no killing, whereas the cells exposed to P_o=2x10^9 cm^{-3} (red) and P_o=10^{10} cm^{-3} (black) do show some minor killing but it seems to be independent of the phage Pressure. In (c) the experimental killing curves are presented for 5 hours until the bacteria becomes saturated. (d) LE392 heterogeneous model simulation which mimics the experimental killing curves well. (e) the homogeneous simulation which shows a large dependence on the phage pressure, an effect not seen in experiment or the heterogeneous model.

According to the our measurement, LE392 cells grown in glycerol do not have a well-defined steady state. Instead, two different distinct distributions were found which are presented

in Figure 24a) as the purple and black PDFs. Because of the ill-defined steady state, the simulation of the heterogeneous model is meaningless. Therefore, we just note here that all states of receptor expression in glycerol are intermediately expressed between the glucose grown LE392 cells (blue line, Figure 24a)) and maltose grown LE392 cells. As expected, the experiment shows intermediate levels of killing and persistence which reflects the large percentage of cells with few receptors. Because of both the strain dependence and the media dependence of p(N), the mean and standard deviation of the receptor distributions that were measured with different strains and in different media have been tabulated in Table 3.

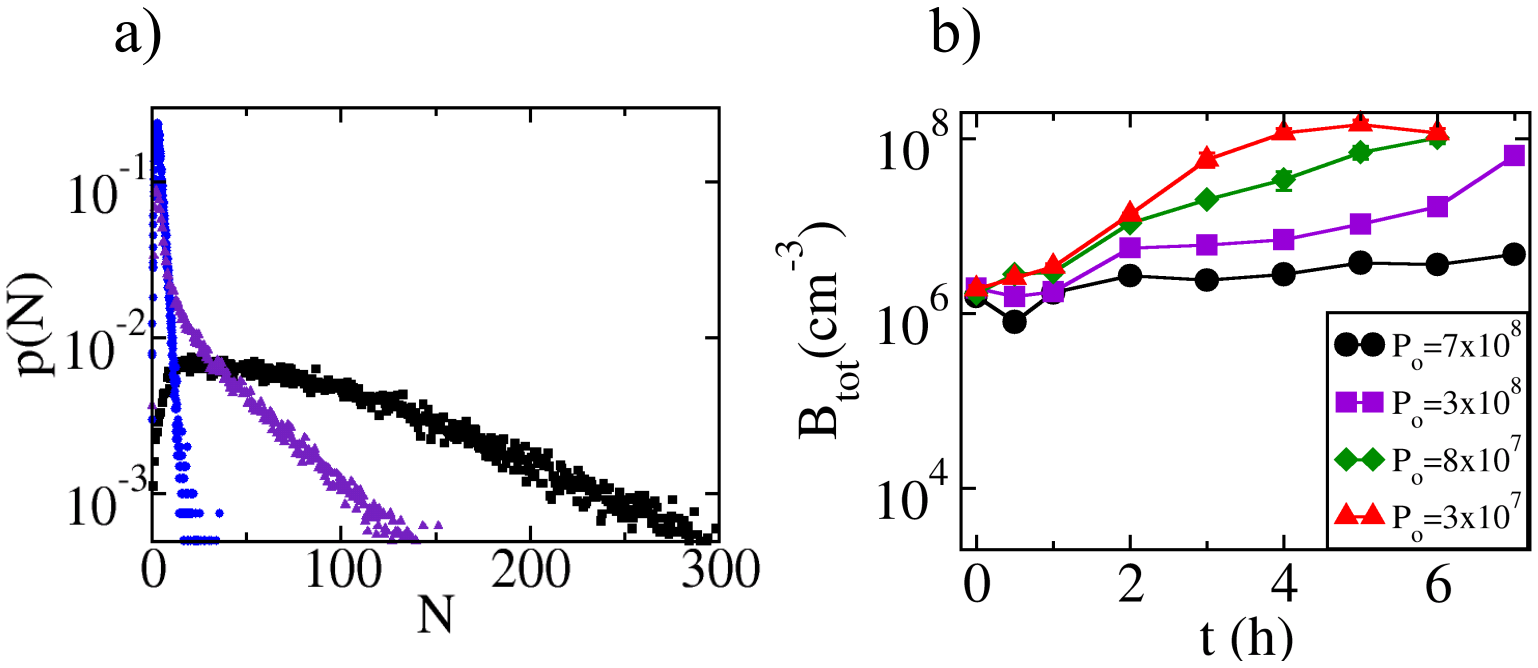

Figure 24 Persistence in LE392 cells grown in glycerol.
(a) The glycerol grown LE392 distributions (black and purple) are compared against the glucose grown distribution (blue). The glycerol distributions express values higher than glucose and lower than Ymel but a well-defined steady state was not found. (b) The killing curves for glycerol grown LE392 show an intermediate level of persistence. For example not much killing or growing is seen in the glycerol distribution with $P(0)=7x10^8$ cm^{-3} (black).

	LE392 (glucose)	LE392 (glycerol)	LE392 (glycerol)	LE392 (maltose)	Ymel (maltose)
$\overline{n}$	2	20	100	570	240
σ_n	2	25	75	200	140

Table 3 The mean and standard deviation of p(N) in different media.
p(N) is highly strain and media dependent.

3.7 UNDERSTANDING PHENOTYPE HETEROGENEITY

Here we strive to understand the response of the bacterial system during times of immense killing pressure by phage. The bacterial population is generally modeled as a homogeneous population which is a valid assumption when the bacteria outnumber the phage but once the phage concentration increases above the critical point ($P_0 > \frac{\lambda}{\gamma_N}$) this assumption is no longer valid. The homogeneous model predicts extinction of the bacterial population in most cases which is at odds with experimental observations. LamB heterogeneity greatly increases the fitness of the bacterial population when phage are present. This increase, though, is associated with the cost of the decreased ability to transport maltodextrins into the cell, but when the carbon source is maltose (not maltodextrins), low lamB expression has been found to only decrease cell fitness when the maltose is present at limiting concentrations (Boos and Shuman 1998).

After a large percentage of the bacterial population has been killed the average receptor density is no longer the same as it was under lack of stress. The bacteria with higher receptor densities are more likely to be killed and therefore the average receptor density of live bacteria is

lower than it would be under no pressure. It is also important to note that the bacteria with high receptor densities do not adsorb just one phage, they adsorb many phage. The high receptor subpopulations act as a phage sink. For example, in the λ phage/Ymel system the high density bacteria have an average of around 250 receptors while they only burst to produce around 10 phage. The majority of these bacteria have the possibility of adsorbing 25x more phage then they produce.

During times of high phage pressure, selective killing of high receptor number subpopulations creates a cell state selection gaining time for genetic selection. In this experiment, though, the observable quantity is always $B_{tot} = \sum_N B_N$ which does not provide much information about the behavior of individual subpopulations. While we have provided a simple mathematical model of bacteria which includes switching between subpopulations, fluorescent phage techniques could be used to study how the individual subpopulations responds after a pulse of high phage pressure, rather than just observing the sum over the subpopulations.

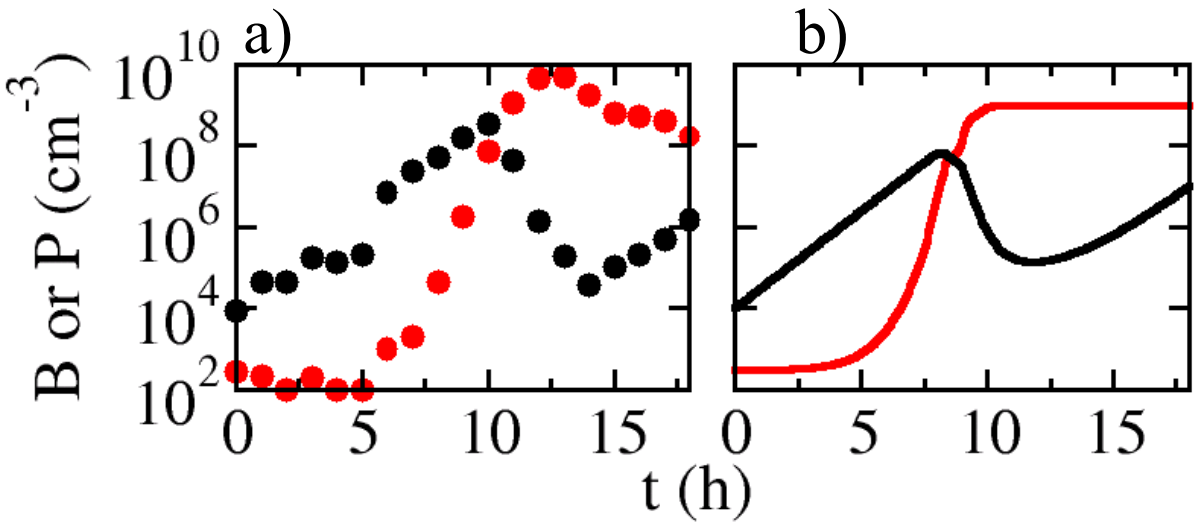

Figure 25 Revisiting the experiment which originally motivated the study.
The heterogeneous model predicts that the effective average receptor number of the bacterial population will decrease until the bacterial population has a chance to recover. The heterogeneous model closely resembles the experimental findings in (a). These experiments and simulations had the same growth conditions and parameters as the killing curves. The only difference is the initial conditions.

In Figure 25, we revisit the experiment that originally motivated the study. In this experiment, a low initial phage concentration is added and the phage are allowed to amplify during the experiment. Phenotype heterogeneity does explain the increase of the sensitive bacterial population at around hour 13 of the experiment as can be seen in the full simulation Figure 25b). Phenotype heterogeneity increases the ability of the bacterial population to respond to the environmental phage pressure.

3.8 WHAT IS THE EFFECT OF THE SWITCHING TERMS?

All the model/experiment comparisons above have neglected the effect of switching between subpopulations. As a beginning study of the effect of subpopulation switching, we first rearrange equation (23):

$$\overline{\gamma(t)} = \frac{\lambda B(t) - \frac{dB}{dt}}{P(t)B(t)} \tag{57}$$

In this equation, all the terms on the right hand side are observable quantities so the average adsorption coefficient can be calculated. Phage at varying initial concentrations were added to exponentially growing bacteria. The phage and bacterial concentrations were measured over a periods of time around 4 hours. The bacterial concentration was interpolated for measurements so that the derivative $\frac{dB}{dt}$ can be evaluated. The derivative was calculated using the difference method:

$$\frac{1}{B}\frac{dB}{dt} \approx \frac{\Delta \ln B_{tot}}{\Delta t} \tag{58}$$

Figure 26a) shows a typical experiment where $B_o=3x10^7$ cm^{-3} and $P_o=1x10^8$ cm^{-3} where the blue circles are the measured bacterial concentration, the red circles are the measured phage concentration and the black line is the interpolation of the curves, which was used to calculate the derivative. The average adsorption coefficient was calculated using equation (57) and the average receptor number was calculated using the Berg and Purcell relationship (equation (5)). Figure 26b) shows three independent measurements of the average receptor number with three different initial phage concentrations, $P_o=4x10^7$ (purple line), $P_o=1x10^8$ (red line) and $P_o=1x10^9$ (black line) cm^{-3}.

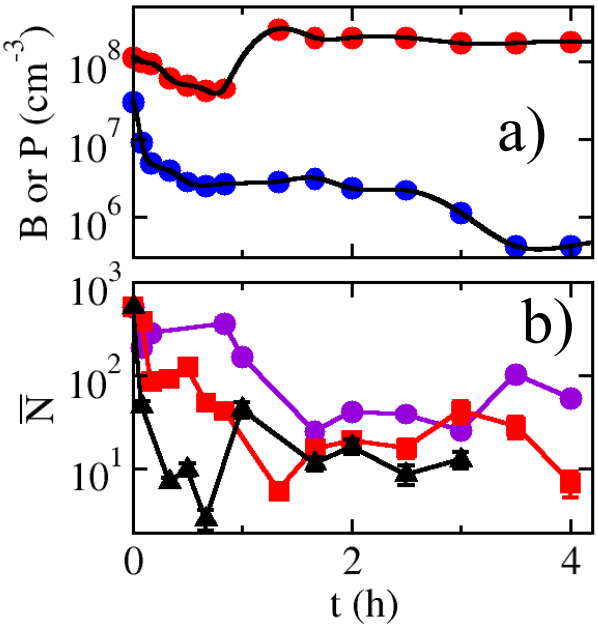

Figure 26 Testing the change in the adsorption coefficient as a function of time.
(a) A highly sampled killing curve. Blue circles are the bacterial concentration and red circles are the phage concentration and the black line is the interpolation used to calculate dB/dt. (b) Change in the average receptor number as a function of time for an initial phage concentration of $4x10^7$(purple), $1x10^8$(red) and $1x10^9$(black) cm^{-3}.

There are two important observations from this figure. First, as is expected, the higher the initial phage concentration the smaller that the average receptor number is after about ½ hour of killing. This is expected from the prediction that an introduction of phage creates a process of selective killing and the higher the pressure the more severe the selective killing is. The second important

aspect to notice is that the average adsorption coefficient does not drop down to zero. This gives information about the switching terms. Revisiting equation (50):

$$\dot{\bar{\gamma}} = -\sigma_{\gamma}^{2} P(t) + D(t)$$

If the switching terms are negligible and D(t)~0 then the adsorption coefficient can never increase and can only monotonically decrease in the presence of phage. In the experiment (Figure 26), we find that the average adsorption coefficient does not continually decrease but can remain stable for an extended period of time. This indicates that after extensive killing the switching terms are no longer negligible and do become important to the dynamics of the system. The next chapter will study the subpopulation switching explicitly.

4.0 STUDYING THE LamB RESPONSE AFTER A PERTURBATION

Cells have evolved at least two schemes to respond to fluctuating environments. The first method is to sense the environmental change and adapt when a variation occurs. This is at the cost, though, of maintaining the sensing machinery. The second method known in ecology as "bet-hedging" is to use population diversity as a strategy of survival. In other words, organisms which are genetic clones use stochastic switching mechanisms to create different subpopulations that are phenotypically more fit in different environments. Theoretically, several groups have developed models to explain the fitness advantages and costs due to the use of these two mechanisms (Thattai and van Oudenaarden 2004, Kussell and Leibler 2005, Kussell et. al. 2005). The mechanism that is advantageous has been shown to depend on the type and timescale of the natural environmental fluctuations.

In this experiment, we study the changes in expression of the functional lambda phage receptors under two different environmental perturbations by taking advantage of two functions of the LamB trimer. The protein is both a transporter of maltose/maltodextrins as well as a point of attack for λ phage. It is well known that the maltose regulon is "off" in the presence of glucose, expressing very few LamB proteins. The regulon can "sense" the presence of maltose and responds by inducing the maltose regulon. On the other hand, λ phage bind to this protein in order to infect cells and a large majority of the bacterial population die. In order to survive, we found in Chapter 3.0 that a minority population of bacteria express very few receptors even

under full induction. When isolated, though, the minority bacteria with a small number of receptors do eventually recover and exhibit the same phenotypes as the majority population. In this chapter, we study the dynamics as the receptor distribution of the LE392 strain responds after two different environmental perturbations. In the first environmental perturbation we change the carbon source from glucose to maltose. This carbon source change induces the maltose regulon. The majority of the population initially is expressing very few proteins due to repression of the regulon in the glucose environment. Once placed in the maltose environment the regulon becomes induced and the cells begin expressing many proteins. We assay the change in the receptor distribution of the population as the regulon becomes induced. In the second case, the regulon is initially fully induced. We select the cells with very few receptors by selectively killing cells highly expressing LamB receptors. The selective killing decreases the average number of LamB receptors in the bacterial population. The minority population we selected which are expressing low levels of LamB eventually recovers the initial steady-state receptor distribution. We find that the recovery dynamics after the two perturbations are very different. While the chemical induction of the regulon causes a quick response and relaxation into the steady-state of the environment containing the maltose carbon source, the bacteria that were able to survive phage attack tend to maintain very few receptors for many generations and the relaxation is approximately an order of magnitude slower.

4.1 USING FLOW CYTOMETRY TO STUDY MINORITY POPULATIONS

In Section 3.1, a method to quantitatively characterize the LamB protein distribution was described in detail. This method is used extensively in this chapter. The AlexaFluor

(succinimidyl ester) dyes are available in a variety of colors with different emission and excitation spectra and because the dyes react with primary amines (a functional group located on a subset of amino acids), amine-reactive dyes will generally conjugate with most proteins. It had been found previously that AlexaFluor 488 nonspecifically binds to the phage without affecting the infectivity of >99% of the phage; therefore the phage can be labeled in a variety of colors with each color signifying a different role in an experiment (Moldovan 2006). In this experiment, we use phage labeled with either AlexaFluor 488 or AlexaFluor 633. These two colors were chosen because their emission and excitation spectra are well separated and the excitation maxima correspond to standard excitation lasers (488 nm and 635 nm) used in commercial flow cytometers. A false color photo of the labeled phage attached to bacteria can be seen in Figure 27.

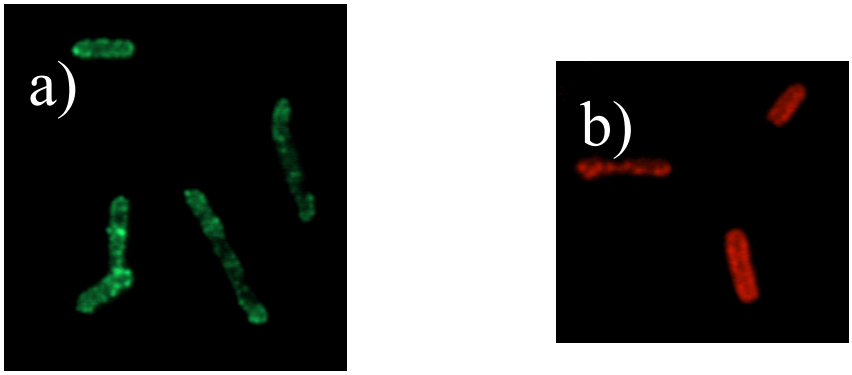

Figure 27 Phage can be labeled in a variety of colors to signify their role in the experiment.
a) A picture of *E. coli* grown to exponential phase and adsorbed with phage labeled with AlexaFluor 488.
b) A picture of *E. coli* cell grown to exponential phase and adsorbed with phage labeled with AlexaFluor 633.

The picture of the bacteria with adsorbed green phage (Figure 27a)) appears sharper than the picture of bacteria with adsorbed red phage (Figure 27b)). Using microscope objectives with the same numerical aperture, the resolving power of two objects is described by; $\theta_{\min} \propto \lambda$,where θ_{min} is the minimum angle in which two objects can be resolved (which can be related to the distance between two objects) and λ is the wavelength of light. The emission maximum of the

AlexaFluor 633 is ~650nm while the emission maximum for AlexaFluor 488 is ~515nm. Therefore the resolution of the phage attached with AlexaFluor 488 is ~1.3 times better than the resolution of the phage attached with AlexaFluor 633. This effect is apparent when comparing Figure 27 a) and b).

4.1.1 Verifying the Receptor Distribution Calibration

The two different colors of phage allow us to determine whether the calibration for the receptor number distribution described in Section 3.1.5 is dependent on different emission wavelengths and sets of excitation/emission filters. Low intensity fluorescent beads with excitation and emission spectra highly similar to AlexaFluor 488 (green phage) and AlexaFluor 633 (far red phage) were bought from Molecular Probes (product #L14823, green), (product #L14818, deep red). These are spherical polystyrene beads with a 2.5 μm diameter and have been labeled with fluorescent dye to varying intensities.

In the following calibration the beads marked 0.1% (green) and 0.2% (far red) were used. This fluorescent intensity was chosen because it is close to the fluorescent intensity of the phage and still far away from the autofluorescence of the polystyrene spheres. The following fluorometry measurements were performed on the BioRad TM fluorometer using the same method described in Chapter 3.0 . For the following green measurements an excitation filter of 480±10 nm and an emission filter of 520±5 nm were used, while for the far red measurements an excitation filter of 620±30 nm and an emission filter of 700±33 nm were used. As in Section 3.1, dilution curves were taken for phage/bacteria/beads. The background media fluorescence was subtracted and each set of dilution data was fit with a straight line with a y-intercept of 0. An

example run for the green phage (Figure 28a) and for the red phage (Figure 28b) are presented. As was done in Chapter 3.0 the approximate average receptor value was calculated by taking the slope of bacteria+phage subtracting autofluorescence and dividing by the slope of the phage. For this particular run, in the green channel the calculated average receptor number was ~650 receptors/bacteria while in the red channel the calculated average receptor number was ~700 receptors/bacteria which is in reasonable agreement with Table 2.

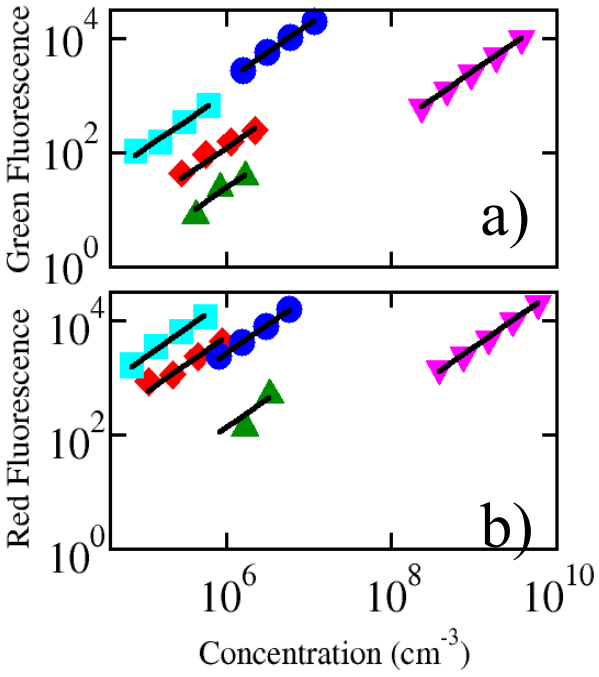

Figure 28 Fluorometry dilution curves with green emission (a) and red emission (b). The symbols represent bacteria adsorbed with saturating phage concentration (blue circles), 0.1% or 0.2% beads (cyan squares), polystyrene spheres with no fluorescent labeling (red diamonds), cell autofluorescence (green up triangles), labeled phage (pink down triangles). The black lines are the fits to a line with a zero y-intercept value.

Each new stock of fluorescent phage was independently calibrated and the level of error in the multiplicative factor between beads and phage varies from calibration to calibration. After three separate runs for each phage stock, it was found that for the green channel the relative fluorescence of the phage is 400±100 phage/bead when compared to the green beads labeled as

0.1%, while the far red phage were found to be approximately 2000±1000 phage/bead when compared to 0.2% far red beads.

All the following flow cytometry data was taken on a Dako Cyan ADP 9-color analyzer. The green beads were run on the flow cytometer, excited with the 488 nm laser line and analyzed from the FITC emission channel. The beads were found to create an approximate Gaussian distribution with an average value of 1070 FCUs. After several runs, it was then calculated that for this particular set of phage on this flow cytometer each phage was equal to 3±0.7 FCUs/phage. LE392 was adsorbed with saturating concentrations of green phage and run on the flow cytometer. The FCUs were then calibrated into receptor numbers using the multiplicative factor of 3±0.7 FCUs/phage. This corresponds to a measured $\langle N \rangle = 650 \pm 160$ and $\sigma = 200 \pm 50$ which can be seen in Figure 29a).

The far red beads were run on the flow cytometer, excited with the 635 nm laser line and analyzed from the APC emission channel. The beads were measured to be 2050 FCUs, which on average is 1±0.5 FCUs/phage. LE392 was adsorbed with saturating concentrations of red phage and run on the flow cytometer. The FCUs were then calibrated into receptor numbers using the multiplicative factor of 1±0.5 FCUs/phage which corresponds to a measured $\langle N \rangle = 660 \pm 300$ and $\sigma = 240 \pm 100$ which is presented in Figure 29b). In Figure 29c), it is shown that the distribution calculated from measurement in the red and green channels are highly similar for the same bacterial population separated into two aliquots and assayed with the two colors of phage.

As a verification of the calibration accuracy for low receptor numbers, the receptor distribution of LE392 cells grown in glucose was calculated using a fluorescent microscope and the flow cytometer. A sample of cells grown in glucose and assayed with green fluorescent phage were run on the flow cytometer which can be seen in Figure 30a) (black line) along with

the autofluorescence curve (red line). Because of the large overlap, the cells were deconvoluted using the standard Fourier transformation technique (described in detail in the Appendix). The deconvolution of the two measured distributions of Figure 30a) is presented in Figure 30b).

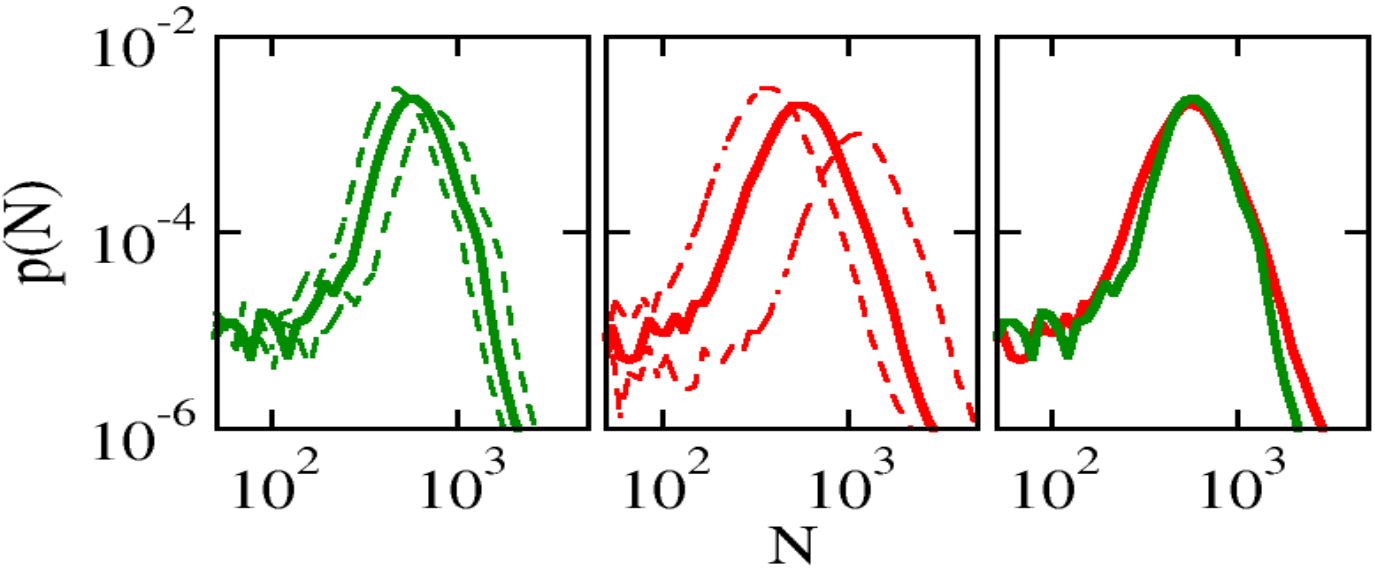

Figure 29 Comparing red and green flow cytometry calibration.
(a) Green flow cytometry curves. The solid line is the average calibration; the dashed lines are ± the error of the mean. (b) Far red flow cytometry calibrations, dashed lines are ± the error of the mean. (c) The average calibration for the red and green curves are consistent but the red calibration has about 2x greater error.

To compare this observed distribution using a second method of calculation, LE392 cells grown in glucose and adsorbed with fluorescent phage were viewed under a fluorescent microscope while being illuminated with a xenon arc lamp and video images were taken of different groups of bacteria. The depth of field for a 100x, 1.3 NA oil immersion objective is ~0.5 μm, which is approximately ½ of the width of a bacterial cell. Because the entire depth of field is 0.5 μm we can place one face of the bacteria in focus at a time, the face attached to the glass and the face that is away from the glass, which can be seen in Figure 30c, panel ii and iii. First, a picture of a group of bacteria attached to the glass was taken using phase contrast. A fluorescent picture was then taken of the bacteria ensuring that the phage which attached to the

glass outside of the region of the bacteria were in focus, Figure 30c) (panel ii). The focus was then shifted by approximately 1μm to place the side of the bacteria that is located away from the glass cover slip in focus (panel iii). The phage attached to the glass are no longer visible but the phage attached to the face of the bacteria located away from the glass are in focus. Each fluorescent disk was counted as one phage and the number of phage attached to each bacterium was counted for 244 bacteria. A bacterium with up to 11 phage was placed in the appropriate bin and all bacteria with >11 phage were lumped into a bin which ranged from 12-100. The hand counted PDF is the red line, the average of seven deconvoluted glucose signals is the black line, and the deconvoluted signal using the least squares fitting method in Section 3.1.5 is the purple line in Figure 30d). The three PDFs appear to be highly similar which verifies the reproducibility of the low number receptor calibration of the PDFs.

The distribution calculated above (hand counting fluorescent disks; Figure 30d, redline) can also be used as a calibration method to determine the relationship between average attached fluorescent phage number and the integrated grey level. The same group of cells used to measure the receptor PDF by hand counting were also used to measure the fluorescent intensity PDF. The phase pictures like the example in panel i in Figure 30c) was used to identify a Region Of Interest (ROI). The grey level was integrated over the ROI of the corresponding fluorescence picture. In the hand counting measurement, each face of the bacteria was treated separately. This was because the eye needed to recognize each disk. This is unnecessary for the ROI measurement because even though the eye does not recognize a disk, the diffuse light which is slightly out of focus is still present from both sides and will be calculated in the integrated grey level of the picture even if the Airy disk is not completely in focus. The grey level distribution was then minimized to fit the hand counting distribution using the equation, $N = \frac{F - \Phi}{\varphi}$.

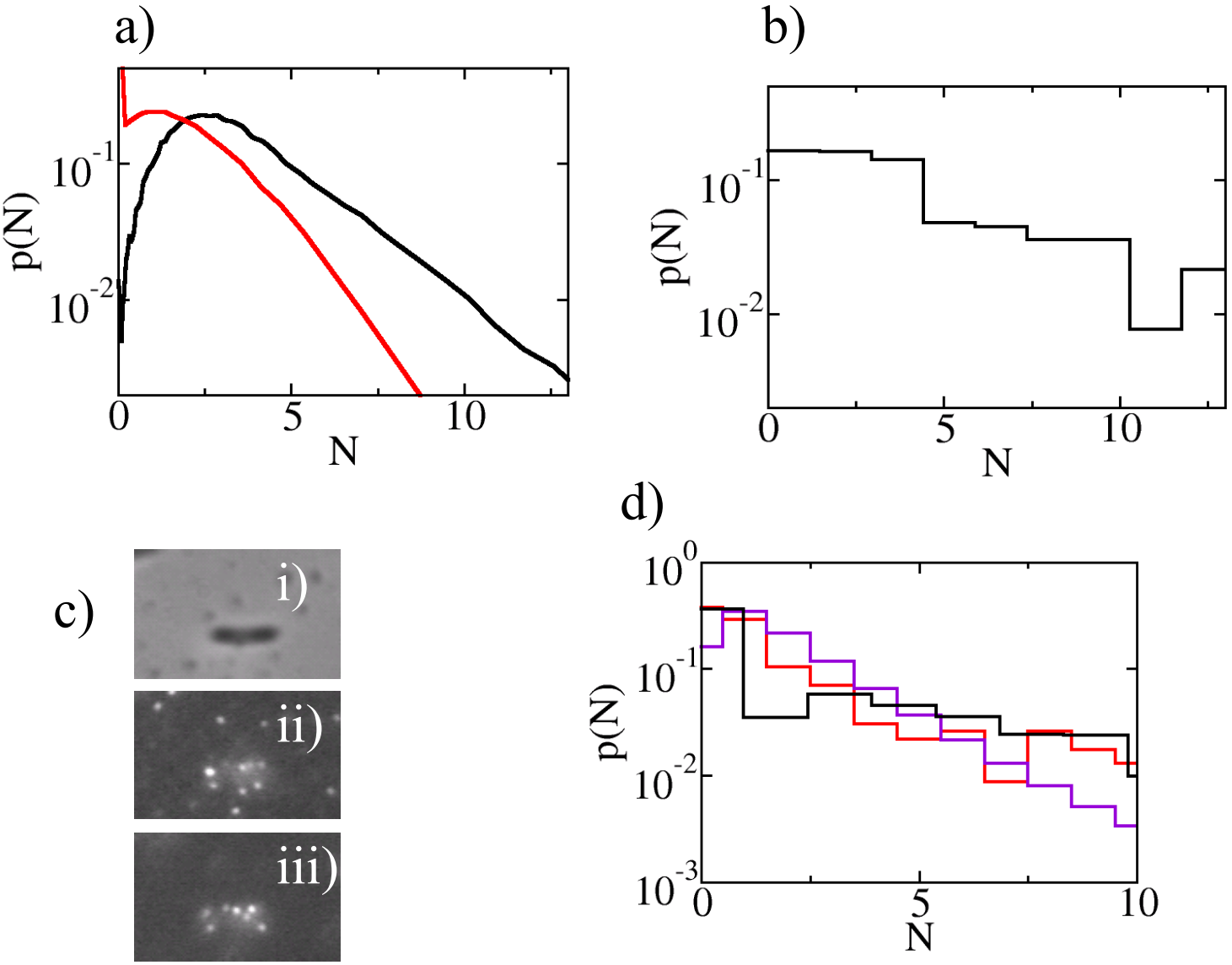

Figure 30 Distribution deconvolution of glucose grown LE392 using the microscope and flow cytometry. a) the signal from LE392 grown in glucose and adsorbed with fluorescent phage (black line) and the autofluorescence of LE392 (red line), b) the signal from a) is deconvoluted using standard Fourier transform techniques c) fluorescent phage attached to bacteria can be counted by hand in the low receptor number limit (top panel) a picture of a bacteria taken using phase contrast, (middle panel) the same bacteria, this time a fluorescent picture is taken ensuring phage attached to the glass are in focus, (bottom panel) the same bacteria with a 1 μm shift in the focus of the lens, d) red line is the receptor distribution measured using the hand counting technique, black line is the average of seven deconvoluted signals and the purple line is the deconvoluted distribution found in Section 3.1.5 using the method presented there.

Correspondingly, to ensure the normalization of the PDF, we use the relationship $p(N)dN = p(F)dF$, after simple algebra we find, $\varphi p(N) = p(F)$. Here, N is the number of receptors, F is the integrated grey level, Φ is the background grey level, and φ is the number of

fluorescent units per phage. The value for Φ was found to be approximately equivalent to 2620 grey level per pixel which is consistent with individual measurements of the background level of 2550 grey level per pixel when considering that the autofluorescence of the bacteria increases the background fluorescence. In Figure 31a), it also appears that for the first 3 bins we can recognize different quantized peaks of the grey level distribution (red diamonds) which tend to line-up with the binned, hand counted values (black line).

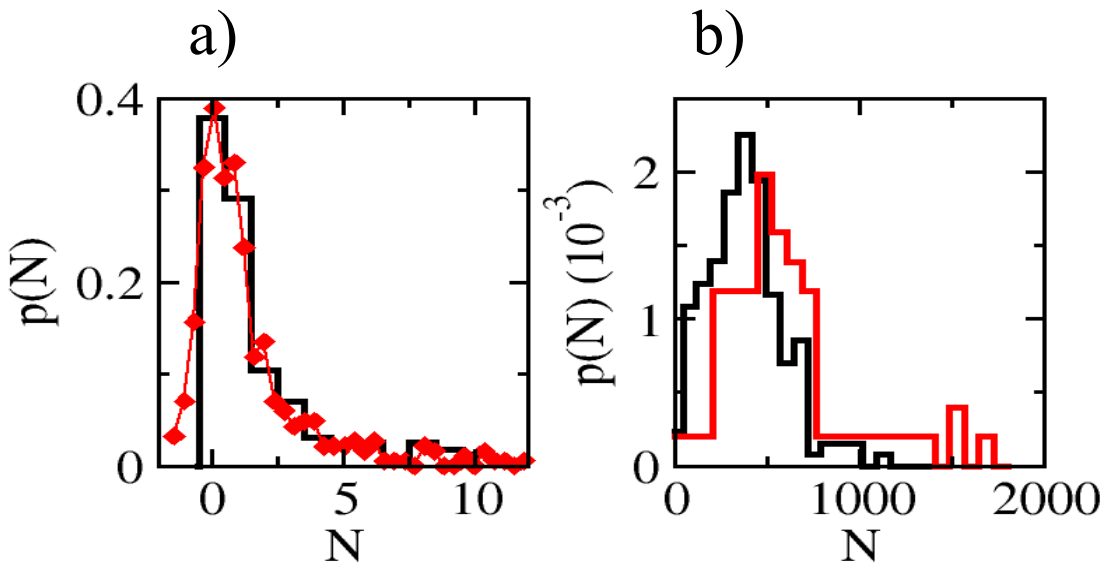

Figure 31 Microscope measurements of average receptor number.
a) The black line is the distribution of phage per bacteria measured by hand counting. The red line is the distribution of phage per bacteria measured by outlining the ROI(region of interest) and summing over the grey value of each pixel. b) The receptor distribution for Ymel (black line) and LE392 (red line) as was measured using summation of the grey value of each pixel and the calibration of the glucose grown cells.

The same measurement procedure described above for calculating the grey level fluorescence for individual bacteria attached with phage was repeated for fully induced Ymel and LE392. Using the calibrated values of Φ and φ found using the uninduced LE392, we calculated the receptor distributions of induced Ymel (172 bacteria, black line) and LE392 (64 bacteria, red line) shown in Figure 31b). The average receptor number calculated for Ymel is $\langle N \rangle = 350$ and $\sigma = 260$ where for LE392 is $\langle N \rangle = 575$ and $\sigma = 390$. While the average receptor

numbers are in agreement with the values displayed Table 2 the width of the distribution is overestimated. This is attributed to the additional measurement noise associated with the microscope measurement technique.

4.2 CHEMICAL PERTURBATIONS

The lamB gene is located in a genetic network that is silenced in the presence of glucose. When the environment changes such that maltose is present, the bacterial population responds to the new carbon source through induction of the maltose regulon allowing the bacteria to metabolize maltose. The induction of the maltose regulon does not only occur in the presence of maltose; expression of the lambda receptor protein varies greatly in different carbon sources due to endogenous induction of the regulon, examples of the different levels of regulon induction were presented in Table 3 when LE392 and Ymel were in the presence of glucose, glycerol and maltose (Schwartz 1976, Boos and Shuman 1998).

The steady state receptor PDFs for LE392 are presented in Figure 32 in M9 media supplemented with different carbon sources. LE392 expresses 600 receptors in maltose (blue line), 2 receptors in glucose (green line), between 25 and 100 in glycerol (red line) and between 10 and 1000 in glucose depending on the concentration of external cAMP. It is known that the malK promoter (which controls lamB) is activated by the presence of the induced activator malT and the cAMP/CRP complex. The induction by glycerol has previously been explained as being due to the fact that the activator of the maltose operon maltotriose is endogenously expressed activating the malT protein. Growth in glycerol then increases the internal cAMP levels which causes expression of the lambda receptor protein at intermediate levels even in the absence of the

external maltose or maltodextrins (Boos and Shuman 1998). The level of expression of the lambda receptor protein not only varies in the presence of different carbon sources but also varies greatly strain to strain. For example under highly expressed conditions the average number of receptors for Ymel is ~300 when grown in either glucose or maltose (Moldovan et. al. 2007). A third classical strain HfrG6 (obtained from the Yale *E. coli* Genetic Stock Center; Schwartz 1976) expresses ~600 receptors when grown in maltose and still maintains a basal level of ~100 when grown in glucose (data not shown).

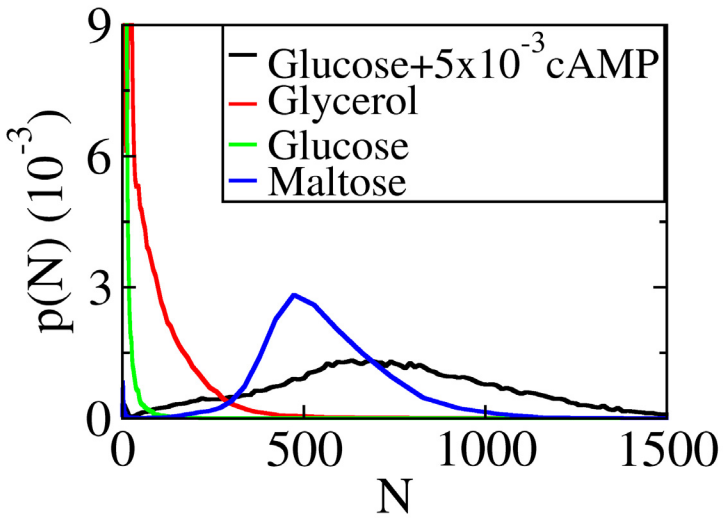

Figure 32 The maltose operon can be tuned to a variety of expression levels.
As can be seen in the graph in the presence of glucose there is very little lamB expression, but with the addition of different carbon sources or cAMP the expression of lamB can be finely tuned.

To measure the dynamic rate at which the maltose regulon in *E. coli* cells responds after an environmental change, the functional receptor distribution was measured after a sudden introduction of uninduced (glucose-grown) cells into an inducing environment (maltose, cAMP, glycerol etc.). The distribution of functional receptors after intervals of uninterrupted regrowth was assayed. After 3 hours of growth, the cells were washed and resuspended in fresh media and diluted to keep the cell concentration low and to ensure the nutrient level remained high. In Figure 33a), the raw flow cytometry data showing the forward scatter and green fluorescence for

a maltose perturbation is presented. The glucose grown cells show little green fluorescence (panel i), but after perturbation quickly begin expressing a large number of functional receptors which is reflected in the increasing green fluorescence (panel ii). The steady state is reached within 2 hours (panel iii). Normally forward scatter value is interpreted as a measurement of cell size. While this is in general a valid approximation, small changes in forward scatter are not necessarily related to a change in cell size (Shapiro 2003). While in the raw data, the forward scatter is highly correlated with fluorescence for cells with high green fluorescence, this does not seem to be due to a change in cell size. This is because the cell autofluorescence distribution grown in any carbon source and all mutants resistant to phage infection never show a forward scatter value greater than ~32 units. The forward scatter value only increases to 64 units when the cells are adsorbed with many fluorescent or non-fluorescent phage.

Figure 33b) shows the dynamics of phage receptor creation in four different perturbation media. The circles represent the receptor dynamics of cells which were perturbed with glucose+0.5 mM cAMP (purple), glycerol (black), maltose (red and cyan), and glucose+5 mM cAMP (blue). Notice that for the maltose (red and cyan) and glucose+5mM cAMP (blue) the average receptor number increases until it saturates at a steady state value greater than 500 receptors. While the maltose cells remain in a steady state, the average receptor number of the cells in glucose+5mM cAMP decreases at times >2 hrs. This is due to the depletion of the cAMP in the medium. The average receptor number greatly decreases at hour 3 until the cells are diluted into fresh glucose+5mM cAMP after hour 3 where the average receptor number increases once again.

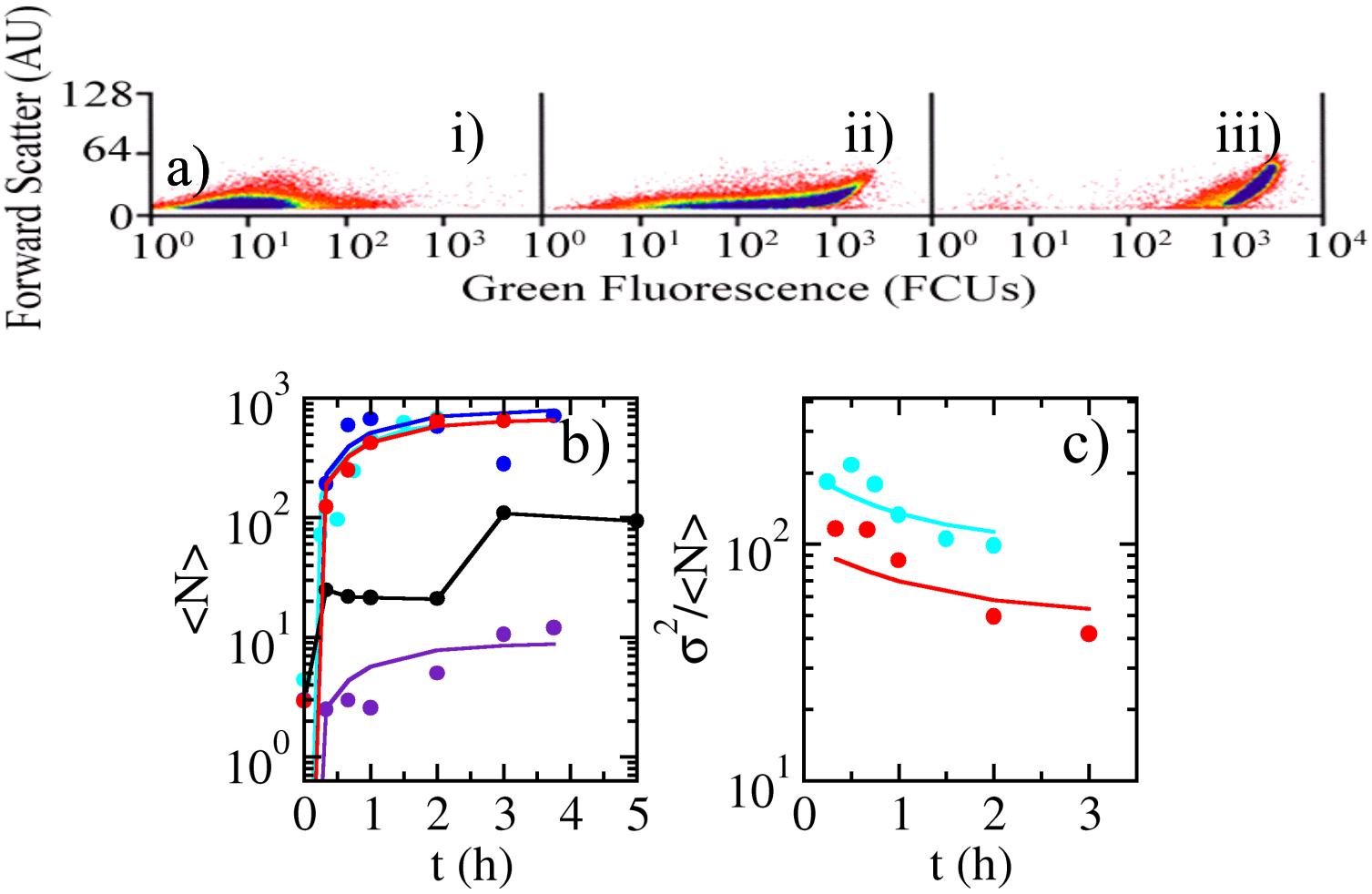

Figure 33 Chemical perturbations in different media.
(a) Cells grown in glucose were perturbed by transfer into maltose supplemented media. The receptors were assayed and run on the flow cytometer. This is the original flow cytometry data showing the forward scatter and green fluorescence. The dynamic increase of functional receptors is evident between panel i-iii. panel i) is the glucose grown cells, panel ii) is 20 minutes after maltose perturbation and panel iii) is 2 hours after maltose perturbation. b,c) Cells grown in glucose were chemically perturbed in order to induce lambda phage receptors at varying levels of expression. The perturbing media was glucose+0.5 mM cAMP (purple), glycerol (black), maltose (red and cyan), and glucose+5 mM cAMP (blue). All lines (except glycerol perturbation, black) are fits to equation 59a in b) and equation 59b in c).

While most theories of noise propagation in the process of protein expression only consider the steady-state distribution, Thattai and van Oudenaarden (2001) showed that if one assumes that the mRNA molecules equilibrate independent of their protein product, reach a Poisson distribution and the mRNA degradation rate is much larger than the protein degradation rate, for a single gene that is turned on at t=0:

$$< N >= \frac{\kappa_r \beta}{\kappa_p}(1 - e^{-\kappa_p t}) \quad (59a)$$

$$\frac{\sigma^2}{< N >} = \frac{(1 - e^{-2\kappa_p t})}{(1 - e^{-\kappa_p t})}\beta + 1 \quad (59b)$$

In these equations, σ is the standard deviation of the measured distribution, κ_r is the rate of transcriptional bursts ($\rho = \frac{\kappa_r}{\kappa_p}$; is the number of bursts per cell cycle), β is the number of receptors per burst and $\kappa_p (= \ln(2)/T_p)$ where T_p is the half-life of the protein. Most proteins (such as LamB) have a long half-life and the degradation is dominated by dilution during cell division, therefore T_p just corresponds to the length of the cell-cycle. In Figure 33b) the chemical perturbation curves were fit with equation 59a. Because the cell cycle time in M9 media is known, $\kappa_p (\approx 1 h^{-1})$ was set to this value. All chemical perturbation curves were fit except for the glycerol perturbation (black) because two distinct steady states were found. The values found from the fit are as follows, for the maltose perturbation (red and cyan) it was found that $\rho\beta \approx 700$ receptors/cell cycle, the glucose+5mM cAMP was ρβ=800 receptors/cell cycle, the glucose+0.5mM cAMP ρβ=9 receptors/cell cycle. In Figure 33c), the maltose perturbation curves were also fit with equation 59b to determine ρ and β separately. It was found using this fit that $\beta \approx 50$ receptors/burst and $\rho \approx 13$ bursts/cell cycle (red) and $\beta \approx 100$ receptors/burst and $\rho \approx 7$ bursts/cell cycle (cyan). Averaging over three separate runs, it was found that $\beta \approx 80 \pm 30$ receptors/burst and $\rho \approx 9 \pm 4$ bursts/cell cycle. The numbers found using this perturbation analysis can be compared with the steady-state analysis described below.

A useful parameter for steady-state analysis is the coefficient of variation:

$$\eta = \frac{\sigma}{< N >}, \quad (60)$$

The standard use of the coefficient of variation is as a measure of the natural variation of a particular protein amongst a population of bacteria. η as a function of $\langle N \rangle$ for a protein has been measured previously for promoters of varying activities expressing the green fluorescent protein (GFP) in bacteria but GFP is generally not measured in actual protein numbers but in relative fluorescence values (Ozbudak et. al. 2002). Bar-Even et. al. (2006) fused GFP with naturally expressed proteins. The investigators then used known average values of the naturally expressed proteins to calibrate how the number of proteins related to the fluorescence of the GFP-fusion proteins in *Saccharomyces cerevisiae* (yeast). The integral autofluorescence of a cell, though, is equal to ~1000 GFP molecules and only GFP concentrations >~1000 proteins/bacteria are detectable by this flow cytometer. At high expression levels (>1000 proteins/cell) Bar-Even et. al. (2006) showed that for naturally expressed proteins:

$$\eta^2 = A\langle N \rangle^{-1} \qquad (61)$$

For a Poisson process it is expected that A=1 in equation (61) but it has been shown that protein expression is not strictly a Poisson process because of transcriptional (Golding et. al. 2005) and translational (Cai et. al. 2006, Yu et. al. 2006) bursting. Protein expression then can be modeled as a Poisson process with bursting, in which case, $\eta^2 \alpha \langle N \rangle^{-1}$ should hold if the increase in average protein number is due to an increase in the rate of bursting or the noise is due to low-copy number mRNA fluctuations (Bar-Even et. al. 2006).

The expression of proteins under a highly repressed promoter has been previously studied at the single cell level (Yu et. al. 2006, Cai et. al. 2006, Friedman et. al. 2006). For uncorrelated burst events an equation can be derived describing the expression distribution if the number of reporters per burst is described by an exponential distribution. While an exponential distribution is continuous, it was shown in Cai et. al. (2006) and Yu et. al. (2006) to be a valid approximation

for the number of reporters per burst for the lac promoter in a repressed state. Using these approximations, the number of proteins in a population is described by the gamma distribution:

$$p(N) = \frac{N^{\rho-1} e^{-N/\beta}}{\beta^{\rho}\Gamma(\rho)} \tag{62}$$

Both of the parameters β and ρ have a specific physical meaning in this derivation. The parameter ρ is the average number of bursts per cell cycle while β is the average number of reporters per burst. The gamma distribution unlike the Poisson distribution is a two parameter distribution. The two parameters β and ρ can be determined independently:

$$\begin{aligned} \rho &= \eta^{-2} \\ \beta &= \eta^{2} < N > \end{aligned} \tag{63}$$

This model is valid for the steady state distribution in both a repressed or induced state, but cannot accurately be applied to a transient distribution.

We can graph the data presented in Figure 33 so that it can be analyzed by the formulism presented in the previous paragraph. This allows us to observe two regions of noise, the highly repressed and highly induced region. In Figure 34a) and b), the black circles are the distributions measured during the chemical perturbations. The proportionality of $\rho=\eta^{-2}$ to <N> seen from <N>=100-1000 is expected for high protein numbers and is in agreement with the work of Bar-Even and coworkers (the blue line that ranges from <N>=100-1000 in Figure 34b) is a straight line with a slope of 1). Unlike previous experiments, though, our experiment has sufficient sensitivity to observe a second noise regime at low average receptors numbers, and we find that when <N> is less than ~100 molecules the scaling behavior changes dramatically.

Figure 34a) shows that in the highly repressed region ($\langle N \rangle$~1-100) β increases linearly (ρ is constant) and for $\langle N \rangle$>100, β becomes constant while ρ increases linearly with $\langle N \rangle$. In order to quantitatively compare these results with the formulism of Cai et. al. (2006) and

Friedman et. al. (2006), the distributions which persisted for more than a few generations were given the description of steady state or quasi-steady state in the case of the glycerol cells where two distinct distributions were found. These distributions were then fit with a gamma distribution Eq. (62) and the values found for ρ and β, were plotted in Figure 34 (red circles). The two different methods of calculating ρ and β were consistent and qualitatively similar across the entire range of measurement. The glucose grown LE392 cells where $\langle N \rangle$ ranges from 2 to 4 did show quantitatively different results because while the gamma distribution does fit well the majority distribution Figure 34c), it does not accurately mimic the long minority tails measured in the actual distribution as can be seen in Figure 34d). The values calculated using the fit to the gamma distribution (red circles) were then fit with the equation:

$$\rho = A < N >^{B} \tag{64}$$

Where it can be seen that from $\langle N \rangle$ =2 to $\langle N \rangle$ ~100, ρ=0.8 is constant and when $\langle N \rangle$ >100 ρ is proportional to $\langle N \rangle$, with A=0.017 and B~1. Correspondingly, for the regime $\langle N \rangle$ =2 to $\langle N \rangle$ ~100, β is proportional of $\langle N \rangle$ with $\beta = 1.3 \langle N \rangle$ (A=1.3, B=1) for the regime where $\langle N \rangle$ >100, β=60 proteins/burst. Comparing with the values we find using the transient analysis, here we find that in the maltose environment ($\langle N \rangle$ =600 receptors), $\beta \approx 60$ proteins/burst (compared with $\beta \approx 80 \pm 30$ receptors/burst calculated using the transient analysis) and $\rho \approx 10$ burst/cell cycle (compared with $\rho \approx 9 \pm 4$ bursts/cell cycle). Both values found using the transient and steady-state analysis are consistent.

The regime from $\langle N \rangle$ =2 to $\langle N \rangle$ =100 is interesting because β is increasing linearly. Hidden within the parameter β, is both the transcriptional bursting and translational bursting (Friedman et. al. 2006). There are two explanations for an increase in β. First, the increase

could be due to an increase in the number of proteins created per mRNA transcript, which is at the level of translation.

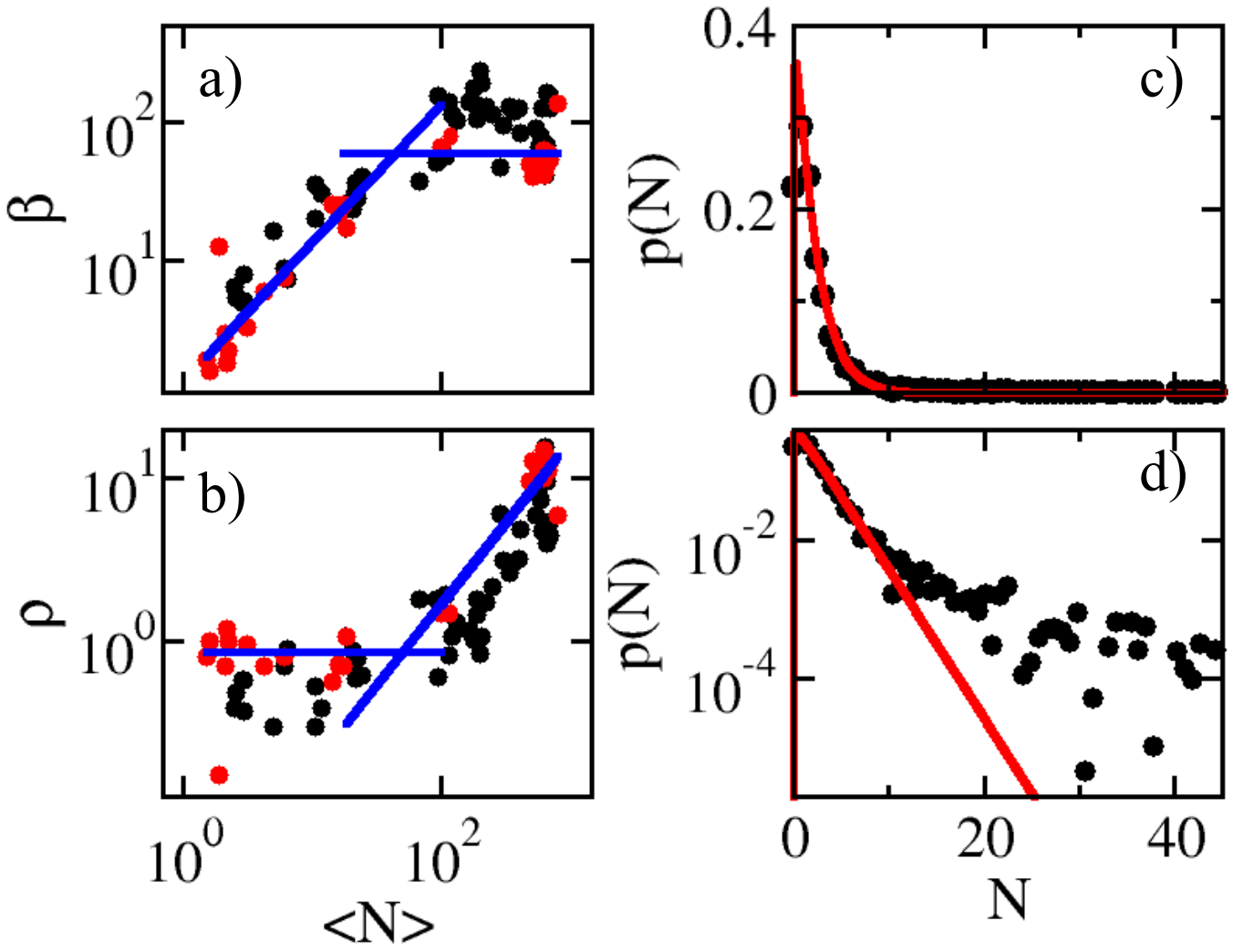

Figure 34 Studying the dominant source of noise under chemical perturbation.

(a) and (b) The black circles are all chemically perturbed distributions calculated using $\beta = \frac{\sigma^2}{< N >}$ and $\rho = (\frac{\sigma^2}{< N >^2})^{-1}$. The red circles are distributions which remain in a steady-state or quasi-steady state over several generations and β and ρ were calculated by fitting the flow cytometry data with a gamma distribution. The steady-state distributions generally fit a gamma distribution well and calculation of β and ρ were consistent using both methods except for the glucose distributions <N><~3 receptors where a small subset of cells with a large number of proteins create a long tail (black circles) (d) which is not accurately mimicked by the gamma distribution (red line) even though a gamma distribution fits the majority of the population well (c).

Second, we know that transcriptional bursting exists (Golding et. al. 2005) and the increase in β could reflect an increase in the amount of time that a promoter remains "on" and continually creating mRNA before being turned "off". We know that the increase in $\langle N \rangle$ in this regime is due to an increase in internal cAMP within the cell. The cAMP/CRP complex is known to be a transcription activator (Busby and Ebright 1999). Therefore it is most likely that the linear increase of β with $\langle N \rangle$ is due to the larger number of cAMP/CRP complexes increasing the average "on" time of the promoter.

It should be emphasized, here, that in this experiment we can only measure the number of functional receptors per cell and not the number of transcribed monomers. There are many processes between the transcription of a monomer and the expression of a functional receptor on the membrane. A recent experiment showed that kinetic assembly of the maltoporin trimers is so fast at 37 °C that the intermediates (such as LamB monomers) are vanishingly small (Ureta et. al. 2007). But which process is required to make the receptor "phage functional" is unknown.

Some experiments from the 1970s suggested that the functional receptors are not inserted constantly throughout the replication cycle of a bacterium but only during the late stage of replication. This was found for both LamB (Ryter et. al. 1975) and for the protein TSX which is the receptor of T6 phage (Leal and Marcovich 1975). It could be useful to also quantify the mRNA distribution using a method such as FISH (Fluorescent *in situ* Hybridization) in order to determine that the noise vs. mean relationship we are observing is dominated by the transcriptional and/or translational events and not from other sources of noise (Maamar et. al. 2007).

4.3 EXPLANATION OF PHAGE PERTURBATION EXPERIMENTS

In the previous section, we extensively characterized the activity of the maltose promoter for the majority of the bacterial population in different chemical environments. In this section, we focus on a constant chemical environment (M9 media+maltose at 37° C) and study the activity of a minority population of cells that manage to survive in the presence of a high phage pressure. The analysis of the chemical perturbations done in the previous section will be important to compare the protein production activity of the majority cell population to the activity of the minority cell population.

In Chapter 3.0 there was discussion about the importance of the spreading term in the equation,

$$\dot{\bar{\gamma}} = -P\sigma_{\gamma}^{2} + D(t) \qquad (65)$$

when considering the population dynamics of *E. coli* and phage. When phage are present, the killing term ($-P\sigma_{\gamma}^{2}$) decreases the average receptor number of the bacterial population and competes with the spreading rate of the distribution D(t). It remains an interesting possibility that these two competing effects may result in a quasi-steady state in the adsorption rate.

Like physical systems in a steady-state, when the receptor distribution is in a steady-state the changes in microstates of the system cannot be measured because the average spreading rate D(t)=0. For example, diffusion is impossible to observe when a dye/water mixture is well mixed, but it is easily observed when one drop of dye is placed in a tub of water. In these experiments, we want to study how the bacteria switch between subpopulations while the nutrient environment of the bacteria remains stationary. In order to do this, we perturb the steady-state distribution and measure the change in the distribution as it relaxes back into its

stationary state. If the phage pressure is negligible, ($P << \frac{\lambda}{\gamma_o}$) during the period of distribution relaxation, then measuring the change in the number of receptors is a direct measure of D(t).

In this experiment, the phage play two distinct roles. The first role is as a perturbation. As was discussed previously, phage adsorb preferentially to high receptor number bacteria and therefore high receptor number bacteria are selectively killed pushing the receptor distribution to smaller numbers. The second role that the bacteria play is as "antibody" labeling for receptors using the technique describe in detail in Section 3.1. We differentiate between the two different roles played by the phage by dyeing the phage two different colors. The perturbing phage are labeled with AlexaFluor 633 (red, excitation max: 632 nm, emission max: 650 nm). The phage that play the role of the receptor antibody are labeled with AlexaFluor 488 (green, excitation max: 495 nm, emission max: 519 nm). In some experiments, after the killing with red phage, a dye called propidium iodide (PI) was added for a period of 35 minutes. PI is a fluorescent dye which can only enter dead cells or cells with a compromised membrane, once the dye integrates into the bacterial genome its fluorescence increases 20-30 fold similar to the popular dye ethidium bromide (Ericsson et. al. 2000). PI dyes dead cells a bright orange color. The following protocol was used for the phage perturbation experiments.

1) Figure 35a,d,e): Perturbative phage are added at intermediate concentrations. Times of perturbation (when red phage are present in the system) are represented as negative times in the response curve in Figure 36.
2) Figure 35f) The perturbative phage are washed out of the media and fresh warm media is added to the bacterial population along with a final concentration of 5 μg/ml of PI. (In some experiments, PI was not added and only red phage were used to distinguish between debris and live bacteria). After 35 minutes the PI is washed out

of the reaction. Any dead cells or cells with a compromised membrane will have PI integrated into the DNA and RNA inside the cell. The uninfected bacteria regrow and are continually washed and diluted into fresh warm media after intervals of uninterrupted regrowth, allowing the cells to grow with minimal phage pressure and without reaching nutrient saturation. This corresponds to positive time in Figure 36.

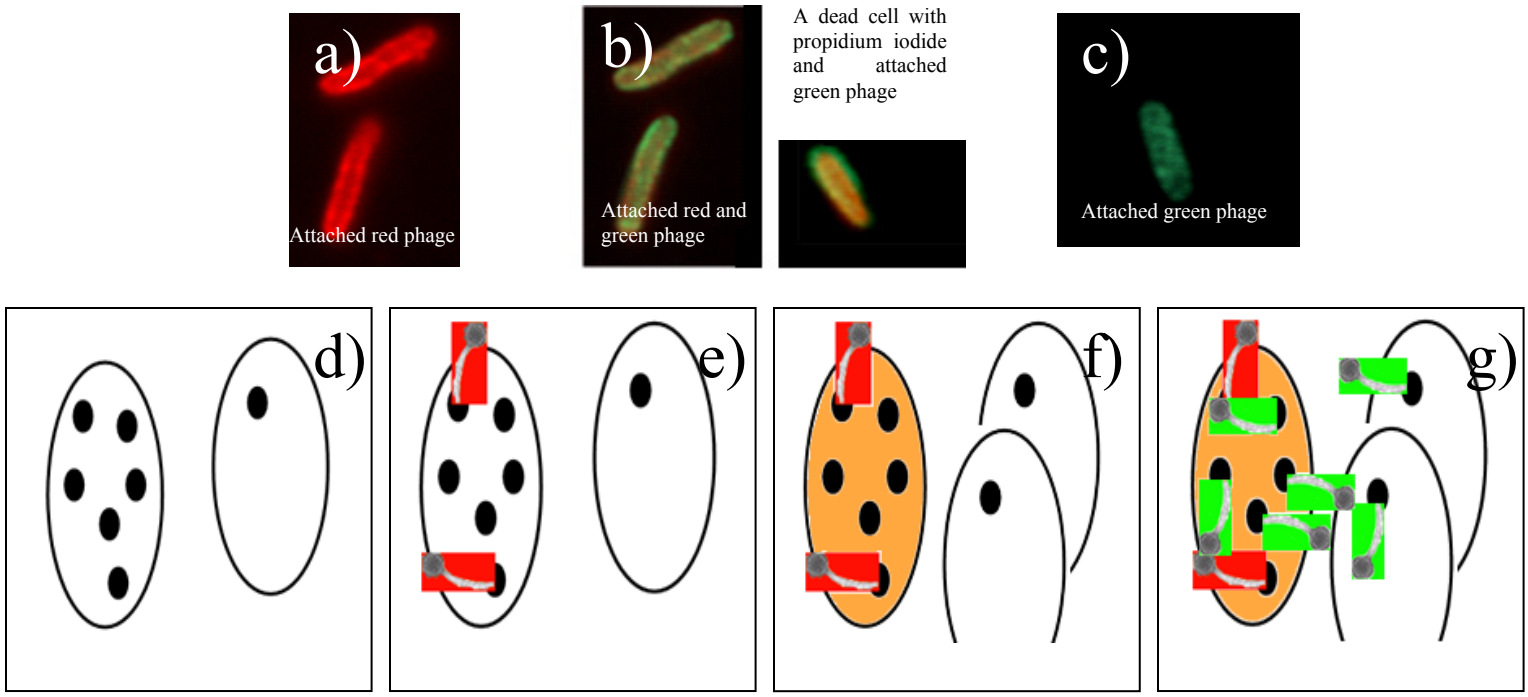

Figure 35 Cartoon explaining the phage perturbation experiment.

3) Figure 35f) The perturbative phage are washed out of the media and fresh warm media is added to the bacterial population along with a final concentration of 5 µg/ml of PI. (In some experiments, PI was not added and only red phage were used to distinguish between debris and live bacteria). After 35 minutes the PI is washed out of the reaction. Any dead cells or cells with a compromised membrane will have PI integrated into the DNA and RNA inside the cell. The uninfected bacteria regrow

and are continually washed and diluted into fresh warm media after intervals of uninterrupted regrowth, allowing the cells to grow with minimal phage pressure and without reaching nutrient saturation. This corresponds to positive time in Figure 36.

4) Figure 35b, c, g) At different time points while the cells are growing, a sample is removed from the experiment and is assayed for receptors with antibody (green) phage. The bacteria which have attached red phage and contain PI inside the cell are debris (Figure 35b). Bacteria that have no attached red phage and show no PI fluorescence but only green antibody phage are the live bacteria in the system (Figure 35c).

5) The background phage concentration is kept at $<5x10^5$ phage/cm^3 in order to minimize the effect of background phage on the regrowing population.

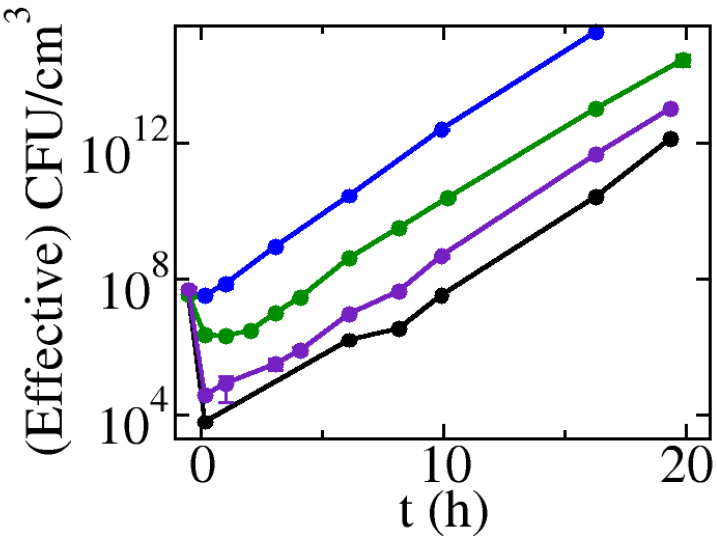

Figure 36 Killing curves from the perturbation experiment.
At negative times the perturbative phage are mixed with the bacteria at intermediate concentrations and the receptor distribution is disturbed due to selective killing. At positive times the bacteria are removed from the phage pressure and allowed to regrow in fresh media far away from nutrient saturation (through repeated dilutions). The different curves were exposed to different phage pressures, $P(0)=2x10^8$ (green), $P(0)=2x10^9$ (purple) and $P(0)=5x10^9$ cm^{-3} (black), all for a period of 0.5 h. The blue line is a population of cells that grew never having been exposed to phage. At each time point a sample was removed from the population and assayed with green phage for the receptor distribution. Notice, the perturbed bacterial populations regrow with a growth rate approximately equivalent to cells which had never been exposed to phage.

Figure 36 shows the change in bacterial concentration as a function of time during several perturbation experiments. The blue line is a population of cells that were never exposed to phage and allowed to grow far away from nutrient saturation ($B<2x10^7$ cm^{-3}). The negative times in Figure 36 are times at which red phage are present. The phage are washed out of the medium at t=0 and the cells are allowed to regrow without phage pressure and far from nutrient saturation through washing and dilution every 4-8 hours.

4.4 FLOW CYTOMETRY DATA AND ANALYSIS

After sampling as described above, the cells were placed on ice until run on the flow cytometer. Figure 37 shows an example of an experiment where the cells were never perturbed by phage but allowed to grow exponentially without reaching nutrient saturation (blue line in Figure 36) and intermittently assayed for the receptor distribution. All cells were run on the flow cytometer at approximately the same time. Notice that between hour 0 and hour 16 there are only small changes in the shape of the distribution which correspond to natural variations in the distribution over time. Cells can be left on ice for periods up to 24 hours before being run on a flow cytometer without variation in the resulting measured distribution.

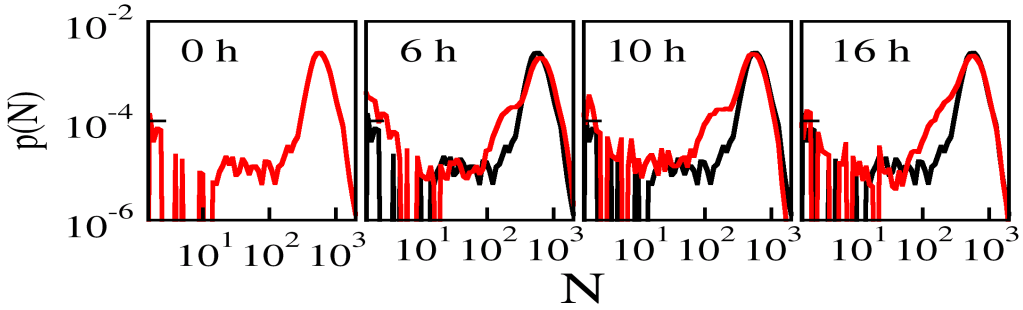

Figure 37 The natural receptor distribution variation.
Cells that were never previously exposed to phage pressure were grown with saturating nutrients and far away from population saturation for a time of 16 hours. At several time points the cells were assayed for the receptor distribution. The distributions did not show large variation and remained in the steady state.

In the phage perturbation experiment, the difficult step is determining which bacteria run through the flow cytometer are debris and which bacteria run through the flow cytometer are the live bacteria of interest. In this experiment there are three methods for determining debris from live bacteria. The first filter is the forward and side scatter. The forward and side scatter determines whether the object will be counted and are used to gate the bacterial population. In this particular experiment the value in the "APC" (FL8) (far red) and the "TexasRed" (FL3) (orange) emission channels also determines whether or not the object is debris or live bacteria. Any object adsorbed with a red phage was previously infected and is therefore considered debris. In the PI experiments, any object with a compromised membrane will allow PI to enter and therefore is also considered debris. In the flow cytometer, though, while it is simple to deconvolute the far red signal from the autofluorescent signal, the system does not have significant resolution to determine the difference between a bacterium with small red autofluorescence and several attached red phage versus a bacteria with no attached phage and a large autofluorescence. Therefore we use the value of the red fluorescence to ensure that the red fluorescence of the population of cells that are counted as live bacteria is equivalent to the red autofluorescence of the bacterial population never having been exposed to phage. For experiments without PI, when the average value of the red fluorescence has decreased down to the value of the autofluorescence, the majority of the measured population is the live bacterial population. Even after bacteria have burst, the remnants of the cell can still be counted by the flow cytometer and the debris remains the majority until the live bacterial population has regrown. The time series in Figure 38 corresponds to the black line in Figure 36. At each time point, though, not only is the red fluorescence value describing the debris in the system measured, but also the green fluorescence value of each bacterium which describes the number

of free receptors. An accurate description of the live bacteria cannot be determined, though, until the debris is only a minimal background in this system due to debris degradation and the continual growth of the live bacterial population.

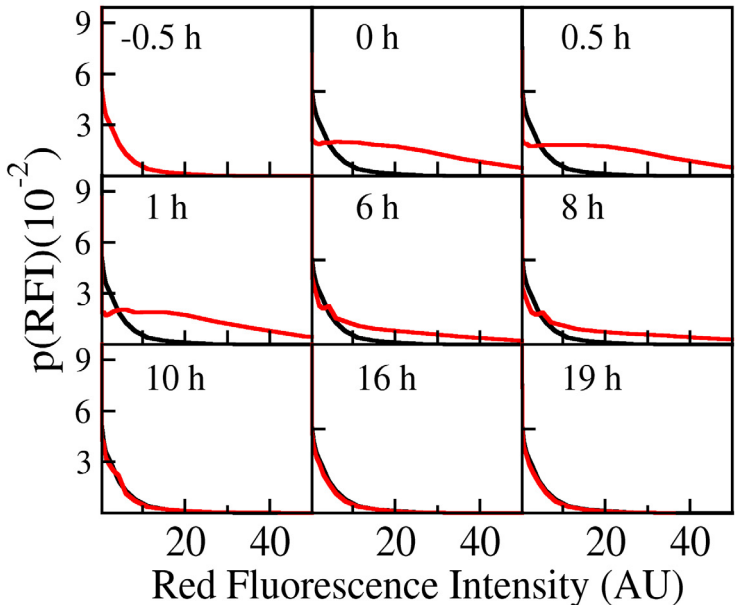

Figure 38 Evolution of bacteria with attached red phage.
The debris remains the majority of the counted points until t>8 h were the red fluorescence is equivalent to the autofluorescence of the cells. No PI was used in this experiment.

In the case of Figure 38, above, that is at t>8 h. Another indication that the sample is composed mostly of live bacteria is the increase in the number of bacteria which are counted using the forward and side scatter in a constant volume of liquid. This point also corresponds to t>8 h in Figure 38. This point accurately reflects the distribution of the receptors in the live bacterial population. As can be seen in Figure 39, the distribution is greatly disturbed from its original PDF even after 19 hours of uninterrupted regrowth. Figure 39 is a very large disruption which is expected when more than three orders of magnitude (~99.98%) of the original population was killed.

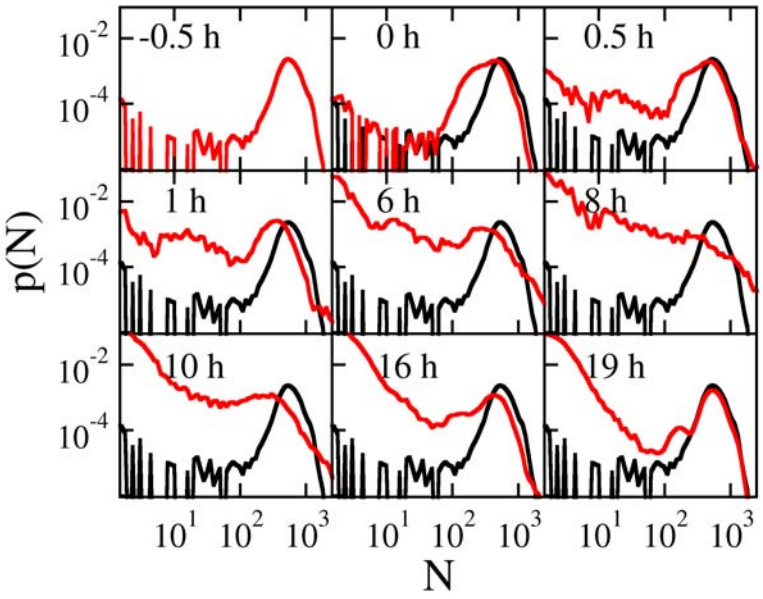

Figure 39 Green fluorescence distribution for the large perturbation (black line in Figure 36)
The green channel measurements for the same experiment as seen in Figure 38. The green channel represents the free receptor distribution in the experiment. Even after 19 hours of uninterrupted regrowth the distribution has not completely recovered. While the majority population >100 receptors has evolved into a distribution similar to the steady state, the minority population <100 receptors is still much larger than in the steady state.

On the other hand, the fluorescence of the PI in the FL3 channel has the resolution to determine the difference between the live population and dead population. Looking at the population of cells without PI, we find that the red fluorescence distribution is equivalent to the autofluorescence of the cells (Figure 40a). The green channel then accurately measures the receptor distribution of the live cells. In this experiment where the cells were killed for ½ hour with $P(0)=1x10^9$ cm^{-3} approximately 1-2 orders of magnitude of the original bacterial population was killed. As can be seen in Figure 40b), the receptor distribution is greatly perturbed but evolves back (within the natural variation of distributions) in <~8 hrs. This relaxation time is very long compared to the chemical perturbation which moved from 2 receptors to the steady state average of 600 receptors in ~2 hours.

Two parameters we can extract easily from these distributions are the standard deviation σ and the mean <N>. In the results section analysis of these two parameters are used to describe the dynamical change of the receptor distribution after a perturbation as it evolves back into its natural steady state.

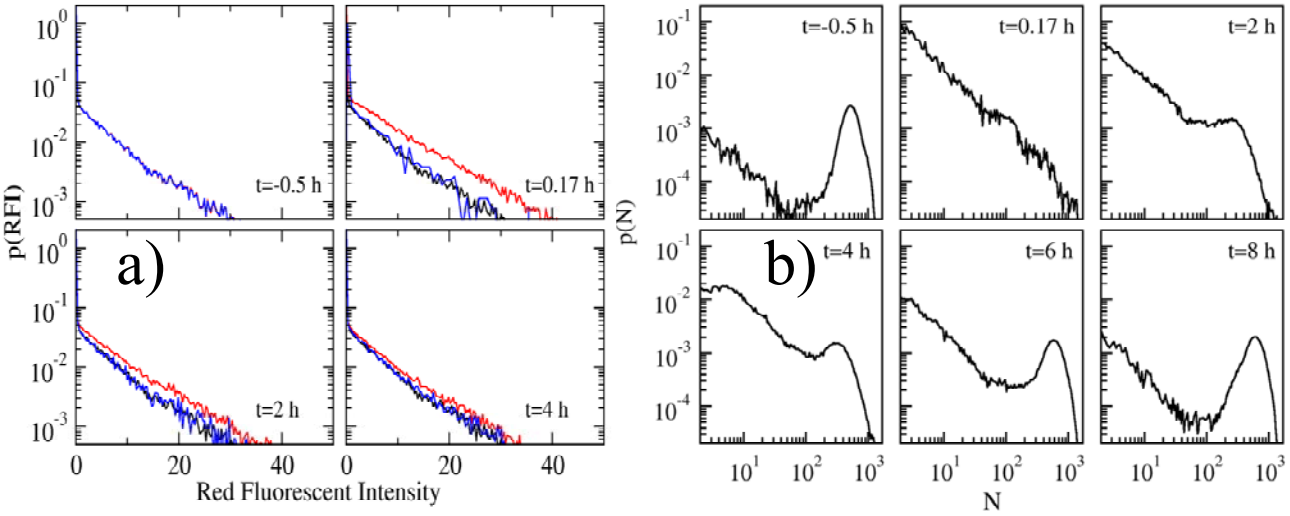

Figure 40 PI distinguishes between live and dead cells (this experiment; P(0)=1x10^9 cm^{-3}).
a) The red fluorescence of cells with no attached phage (black line) is the autofluorescence of the bacterial population. While the red fluorescence of the population of the cells increases after a perturbation due to attached red labeled phage (red line), the red fluorescence of the population of cells that is considered the live population by discrimination with PI generally has the same red fluorescence as the autofluorescent cells (blue line) independent of regrowth hour. Any distribution showing large red fluorescence is thrown out b) The receptor distribution is still perturbed after 6 hours of uninterrupted regrowth but after 8 hours of uninterrupted regrowth the receptor distribution has evolved back to its original position.

4.5 RESULTS

In these perturbation experiments, we study the LamB production in the minority subpopulation of bacteria that survive despite the presence of viruses. In Figure 41a), we can see the relaxation of a chemical perturbation experiment and phage perturbation experiments with varying levels of phage pressure. The blue triangles in Figure 41a) correspond to an experiment performed over 16 hours in which a distribution was not perturbed but allowed to exponentially grow far away from nutrient saturation. The deviation of the steady state distribution is small over a long period of time (16 hrs which corresponds to ~26 generations.) For the phage perturbed experiments, the larger the perturbation, the longer the period of relaxation (green circles, P(0)=2x10^8 cm^{-3}; pink circles P(0)=1x10^9 cm^{-3}; purple circles, P(0)=2x10^9 cm^{-3}) . The period of relaxation is much longer than the glucose to maltose chemical perturbation which is presented as the red squares. The lines in Figure 41a) correspond to a fit to an exponential, and are included to help guide the

eye. The relaxation rate of the phage perturbed distributions are similar, approximately independent of the phage pressure during perturbation, but the relaxation rate is slower than the chemical perturbations.

In a set of experiments, LE392 was transformed with the pTAS1 plasmid which confers ampicillin resistance and constitutively expresses the LamB protein. The cells were then subjected to the similar perturbation experiments as the cells without the plasmid. The bacteria transformed with pTAS1 show less persistence in their killing curves (Appendix). Similarly, in Figure 41b) it is shown that for similar phage pressures more cells are killed when LE392 contains the plasmid rather than without the plasmid. The response of the LE392/pTAS1 bacteria will be discussed in more detail in Figure 43.

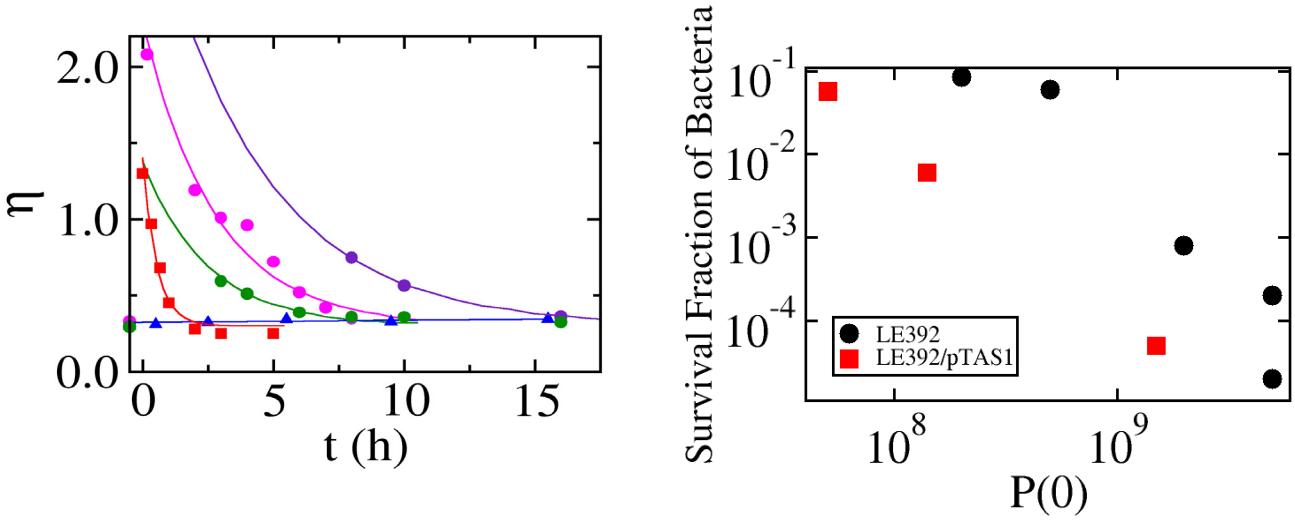

Figure 41 Perturbed distributions relax back to original distribution.
(a) The perturbed LE392 distributions (circles) do evolve back into the steady state distribution but only after many generations of regrowth. For example, after killing only ~90% of the initial distribution (green line) the distribution does not evolve to the steady state until ~6 hrs after phage pressure was removed. The color coding in the figure corresponds to the color coding in Figure 36 except for the pink circles which were killed with $P(0)=1x10^9$ cm^{-3}. The red squares are the relaxation after the glucose to maltose chemical perturbation. The relaxation rate is ~4 times greater than the phage perturbed distributions. The lines in the figure are fits to an exponential, they are only included to help guide the eye. (b) The survival fraction of bacteria after a ½ hour perturbation with varying P(0). For similar phage pressures, more cells in the population of LE392/pTAS1 cells were killed.

In Figure 42, we reproduce the chemical perturbation data from Figure 34 except we have focused specifically on the region in which the chemically perturbed distributions vary as $\eta^2 \propto < N >^{-1}$. The black circles represent how the coefficient of variation squared changes with <N> during chemical perturbations. The blue squares in Figure 42 are values of the coefficient of variation squared calculated from the phage perturbed distributions. Notice these distributions are wider than the chemically perturbed distributions. These distributions vary as approximately $\eta^2 \propto < N >^{-2}$. This indicates that the distributions become broad for small changes in the mean number when exposed to a short burst of phage and that they do not keep the same distribution shape as they relax into the steady state.

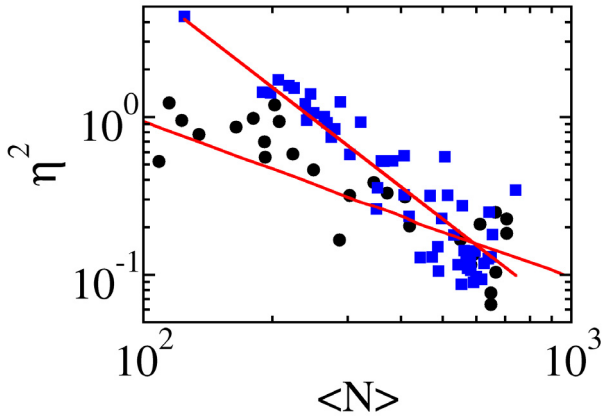

Figure 42 Comparing the width of chemically and phage perturbed distribution.
For chemically perturbed distributions vary as $\eta^2 \sim <N>^{-1}$ while phage perturbed distributions are wider for similar changes in <N>, the relationship of $\eta^2 \sim <N>^{-2}$ holds.

A second method of describing the dynamics of the system is to study the amount of time it takes the population to increase its mean value of receptors. First we define the average receptor velocity $(\frac{\Delta N}{\Delta t})$ and average receptor number (N_{av}) between two points which are consecutive in time:

$$\frac{\Delta N}{\Delta t} = \frac{< N >_2 - < N >_1}{t_2 - t_1} \qquad (66a)$$

$$N_{av} = \frac{< N >_1 + < N >_2}{2} \tag{66b}$$

Here, N_2 is the average receptor value at some time t_2, N_1 is the average receptor value at some time t_1, where $t_2>t_1$ and consecutive with t_1. While the average receptor number and average receptor velocity are useful for comparing perturbations with similar steady state values, we also define a normalized receptor velocity to compare chemical and phage perturbed distributions with different values for the steady state <N>:

$$\frac{\Delta \overline{N}_0}{\Delta t} = \frac{\frac{< N >_2 - < N >_1}{N_{av}}}{t_2 - t_1} \tag{67}$$

In Figure 43a), the normalized receptor velocity is plotted as a function of the distance away from the steady state. This distance is defined as $N_d=N_s-N_1$, where N_s is the average value of the steady state distribution. For chemical perturbations, N_s is defined as the average value of the distribution once it has relaxed into its steady state. For phage perturbations, it is defined as the value of the distribution before the phage perturbation. Presented in Figure 43a) are the receptor velocities for phage perturbation experiments performed with LE392 (black circles) and LE392/pTAS1 (red circles). While, a larger percentage of LE392/pTAS1 cells were killed for similar phage pressures than the LE392 cells (Figure 41b)), the recovery of the receptor distribution was highly similar to the LE392 cells. The receptor distributions for both LE392 and LE392/pTAS1 evolved back with the same receptor velocities for equal distances away from the steady state. In Figure 43b), the receptor velocities of the phage perturbed distribution are compared with the receptor velocities of the chemical perturbation from glucose to maltose (purple triangles). Notice during the glucose to maltose chemical perturbation, the average receptor number increases much more quickly than the phage perturbed distributions. At a distance of $N_d=400$ receptors the normalized receptor velocity of the maltose perturbed cells is

approximately one order of magnitude larger than the receptor velocity of the phage perturbed cells. The cells with few receptors do not switch to the maximum expression state with the same probability as the majority of the population when the maltose regulon is becoming induced. This implies that the mechanism which maintains the cells in the low expression state despite the presence of maltose is not just a stochastically uninduced regulon.

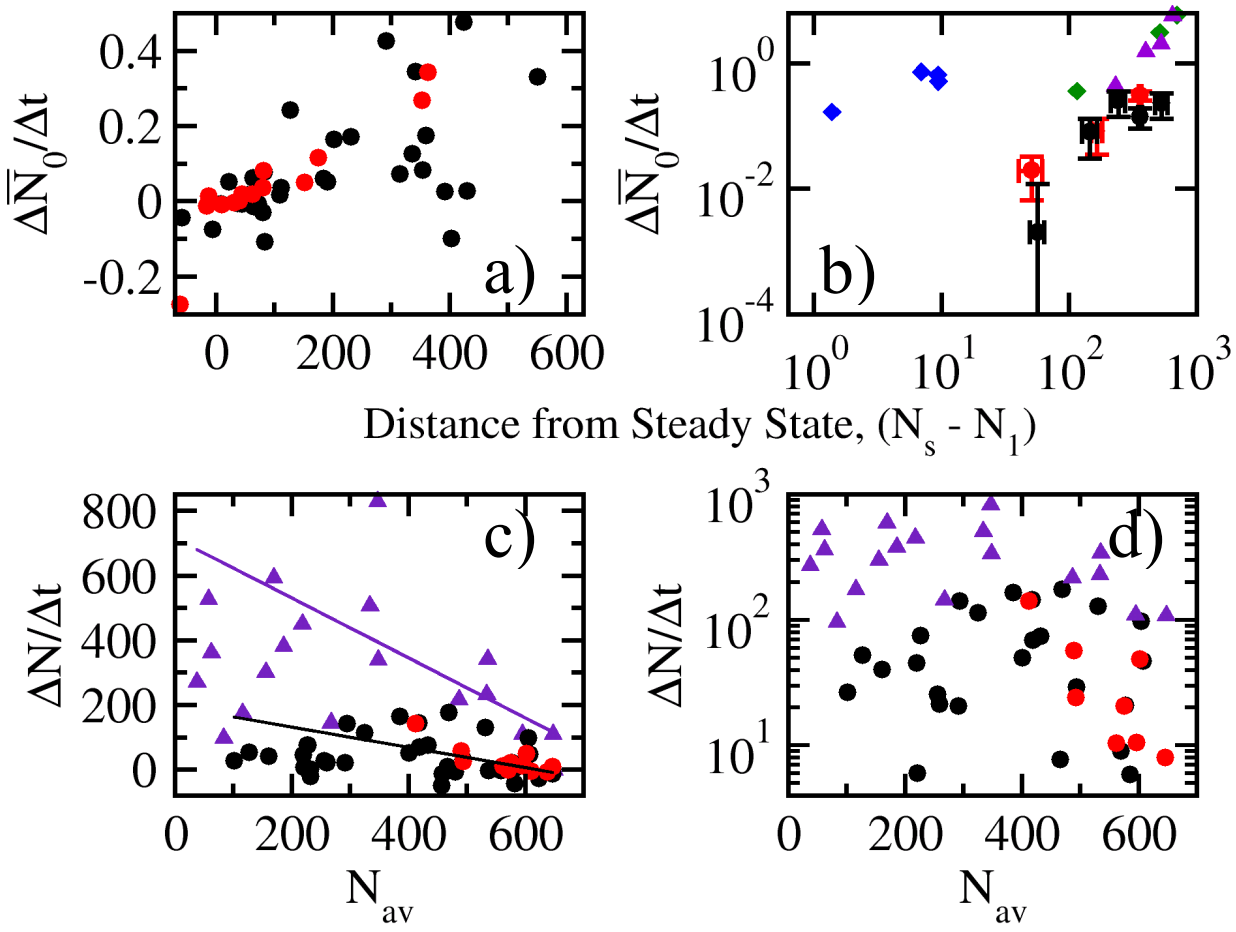

Figure 43 Receptor velocity as a function of the distance from the steady state.
(a) The normalized receptor velocities (with units of h^{-1}) measured after a phage perturbation for LE392 (black circles) and LE392 (red circles) (b) The receptor velocities after a chemical perturbation of maltose (purple triangle), glucose+5mM cAMP (green diamonds), and glucose+0.5 mM cAMP (blue diamonds). The data presented in a) were averaged over four equal sized bins for comparison with chemical perturbations,. (LE392 (black squares) and LE392/pTAS1 (red squares)). c) The non-normalized receptor (with units of receptors/hour) velocity is compared for the maltose perturbation and the phage perturbations. The lines are fits to equation 68. (d) is the same data from (c) but reproduced on a log graph to emphasize the phage perturbed data .

While defining a normalized velocity allows us to compare the phage perturbation with the different chemical perturbations, it is more quantitatively useful to examine the non-normalized receptor velocity as is done in Figure 43c). Both the chemical (purple triangles) and phage perturbed velocities (circles) are highly non-linear. For the chemical perturbations this is attributed to the lag period of the response of the maltose regulon and the inability to describe the system when $\sigma \sim <N>$. It was found, though, that the chemical perturbed distributions do show a linear region when N_{av} is larger than σ which corresponds to $N_{av}>200$ receptors. For a population of cells with a constant receptor production rate and where receptor degradation is dominated by dilution (Thattai et. al. 2001, Cai et. al. 2006, Friedman et. al. 2006) :

$$\frac{d<N>}{dt} \cong \frac{\Delta N}{\Delta t} = \omega - \kappa_p <N> \qquad (68)$$

Where $\omega(=\kappa_p \rho \beta)$ is the constant rate of receptor creation and κ_p is the dilution of the receptor due to cell division. When fitting the maltose data (purple triangles), we find values of $\omega \approx 700$ receptors per hour and $\kappa_p=0.9\ h^{-1}$, as is expected they are reasonably consistent with values found using other methods. When fitting the perturbed distributions, for $N_{av}>400$ receptors, though, it was found that $\omega \approx 200$ receptors per hour and $\kappa_p=0.3\ h^{-1}$. But from the killing curves we know that the dilution rate (or the growth rate) is always $\kappa_p \approx 1\ h^{-1}$. Therefore, ω or the rate of receptor production per cell must also be a function of <N>. This implies that after killing the majority of the cell population, there exists a population of cells with a heterogeneous receptor production rate and describing the system as having one constant value of receptor production is no longer valid. The population relaxation is not that of a homogeneous population but of a population of cells with a set of heterogeneous (or stochastic) ω's. This heterogeneity becomes manifested in the homogeneous model as a slow receptor production and dilution rate.

4.6 CONCLUSIONS

In both experiments, the population of cells is exposed to an environmental perturbation and the functional receptor distribution is assayed as the distribution relaxes into the steady state of the current chemical environment. The biological difference between the carbon source and phage perturbation experiments is that in the chemical perturbation experiment, we study the majority population as the genetic network is induced so that the increase in receptors is due to the induction of the maltose regulon. In the phage perturbation experiment, we study the minority population of cells that despite the inducing carbon source (in this case maltose) still have very few receptors. We find that the phage selection not only selects the cells with very few receptors, but also selects the cells which switch slowly from the low expression phenotype back into the full expression phenotype. In other words, not only is the number of proteins stochastic but also the level of protein production is stochastic. The selection of the slow switchers is also consistent with the experiment in Chapter 3.0 where we found that we could capture essential features of the bacterial killing curve even in the negligible switching rate limit.

Another way to describe the slow switching phenotype found in the phage perturbation experiments is that a cell that is producing LamB proteins slowly tends to remain producing them slowly. The idea that stochastically expressed phenotypes can be passed on to the progeny for several generations was discussed in a recent experiment in yeast (Kaufmann et. al. 2007). Through both experiment and simulation, the authors found that the stochastic phenotypes can be hereditary if the bursting size of a regulatory protein is large. For example, if the burst size of the malT activator protein or the burst size of cAMP or CRP is sufficiently large, it is expected that there is significant correlation in the stochastic phenotype of mothers, daughters and granddaughters.

Important questions remain to be answered such as the molecular origin of the noise which creates the minority phenotypes. This experiment also raises many questions about the evolution of noise in individual networks. Are cells truly "hedging a bet" and the existence of a minority phenotype is programmed into the genetic code to protect against an environmental perturbation, or is the expression noise just an accidental consequence of protein expression.

APPENDIX A

A.1 NUMERICAL METHODS

A.1.1 Details of Numerical Integration

The simulation of the heterogeneous model and the average homogeneous model are presented in the main text in Figure 21b), c), e), f), and Figure 22b), c) for varying initial conditions. The $2(N_{max}+1)$ coupled differential delay equations were integrated using the 4^{th} order Runge-Kutta algorithm from Numerical Recipes in C which was adapted for use with delay equations (Press et. al. 1988). For the simulation of the heterogeneous model the initial conditions for the B_Ns were set to be the PDF that was measured in Figure 17b) multiplied by the total bacterial concentration measured at the beginning of each experimental run. For the average homogeneous model, the bacterial subpopulation B_N where $N=\langle N \rangle$ the average number of receptors of the entire population was set equal to the experimentally measured total initial bacterial concentration B_{tot}, while all other bacterial subpopulations were set to an initial concentration of 0. Because there is no switching between subpopulations in the numerically integrated model, this is equivalent to setting γ as a constant based on the average receptor values of the majority population.

To ensure that the Numerical Recipes function was implemented correctly, the well-known differential equations were numerically integrated:

$$\frac{dx}{dt} = y \tag{69}$$

$$\frac{dy}{dt} = -x \tag{70}$$

The known solutions to these two equations are:

$$\begin{aligned} x(t) &= \sin(t) \\ y(t) &= \cos(t) \end{aligned} \tag{71}$$

The output from the implementation of the 4th order Runge-Kutta algorithm is pictured in Figure 44.

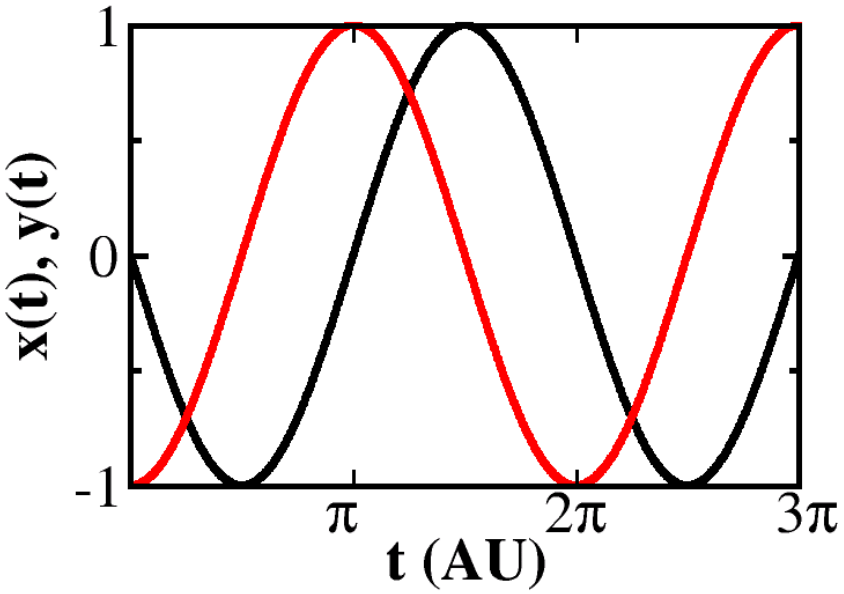

Figure 44 Numerical integration of differential equations (69) and (70).
As expected the solutions are a x(t)=sin(t) (black line) and y(t)=cos(t) (red line).

The second method of algorithm verification was to compare the numerical integration of equation (18) for $N=0..N_{max}$ with the analytical solution derived in Section 2.4. Because to derive the analytical solution, we assumed a pure log-normal distribution as the initial condition

for each B_N, a constant P_o and no switching; in order to compare the numerical integration with the analytical solution all conditions must be satisfied in the numerical integration. This numerical integration then can be compared to the simulation of the analytical solution derived in Section 2.4. The results are presented in Figure 45, the results from the analytical model (red line) and the numerical integration (black line) are nearly identical.

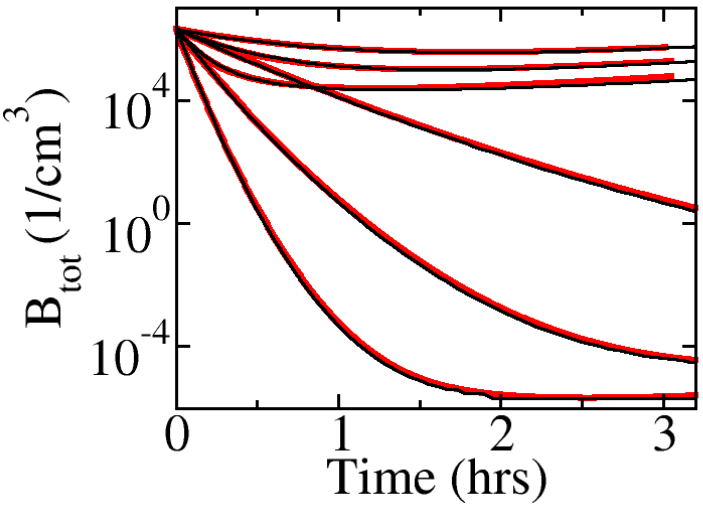

Figure 45 Comparison of analytical model and numerical integration.
The simulation of the analytical solution for a distribution with an initial log-normal distribution (red line) and the numerical integration of the full model with the same assumptions (black line) are found to be nearly identical for 2 different initial log-normal distributions and 3 different initial phage concentrations.

A.1.2 Fourier Transform Deconvolution

The theory of Fourier transform deconvolution is well established and efficient algorithms have been written (Press et. al. 1988). The basic theoretical background will be summarized here. For an integral of the form:

$$p_T(T) = \int p_F(F)\, p_A(A)\, dA \qquad (72)$$

Assuming $p_T(T)$ and $p_A(A)$ is known, and we want to find $p_F(F)$. First, if we assume that the variable F and A are uncorrelated we can write that T=F+A.

We will define the Fourier transform of a function as:

$$\tilde{p}(W) = \int p(T) e^{-iWT} dT \tag{73}$$

$\tilde{p}(W)$ is the same function but displayed in frequency space rather than in temporal space. Multiplying both sides of equation (69) by e^{-iWT} and taking the integral:

$$\int p_T(T) e^{-iWT} dT = \int\int p_F(T-A) p_A(A) e^{-iWT} dA dT \tag{74}$$

Multiplying the LHS of the equation by $1 = e^{-i(A-A)W}$, we find:

$$= \int\int p_F(T-A) p_A(A) e^{-iWT} e^{-i(A-A)W} dA dT \tag{75}$$

Rearranging:

$$= \int\int p_F(T-A) e^{-i(T-A)W} p_A(A) e^{-iWA} dA d(T-A) \tag{76}$$

Realizing that we have three separate Fourier transforms, we can fill in the functions:

$$\tilde{p}_T(W) = \tilde{p}_F(W) \tilde{p}_A(W) \tag{77}$$

Dividing:

$$\tilde{p}_F(W) = \frac{\tilde{p}_T(W)}{\tilde{p}_A(W)} \tag{78}$$

Taking the inverse Fourier transform we find:

$$p_F(F) = \frac{1}{2\pi} \int e^{iW(T-A)} \tilde{p}_F(W) dW \tag{79}$$

We have now calculated the desired PDF. Numerically, this algorithm is only useful in certain regimes. For example, a highly peaked function is very broad once it has been Fourier transformed. Therefore, in order for the inverse Fourier transform to calculate the correct PDF in temporal space, we have to keep essentially all terms in frequency space. In reality, numerical

algorithms cannot keep all terms and therefore numerical Fourier deconvolution is not a good method for the deconvolution of a highly peaked function.

In this case, the glucose distribution and the autofluorescence distribution have a large portion of overlap so neither distribution appears highly peaked compared to the other distribution. For the Fourier transform deconvolution of the glucose grown LE392 cells, the distribution for the glucose cells was placed into quantized bins along with the autofluorescence distribution and the convlv algorithm from Numerical Recipes in C was implemented in order to deconvolute the low signal from the autofluorescence distribution. The results were presented in the main text in Figure 30.

A.2 EXPERIMENTAL METHODS

A.2.1 Experimental Conditions

All experiments followed this beginning protocol unless specified otherwise. *E. coli* cells were grown overnight in M9 minimal media supplemented with maltose. The cells were then diluted 1:100 into fresh M9 media and allowed to grow to a concentration of ~10^7cells/ml. Cells prepared using this method are called exponential phase cells throughout the dissertation

A.2.2 Killing Curves

For killing curve measurements, an excess of phage was added to a set of bacterial cultures, in which we varied the initial phage concentration. We then measured the response of

the bacterial populations to determine if the results corresponded to our model calculations for times of up to 7 hours. To do this, exponentially growing cells were diluted 1:15 into fresh pre-warmed, pre-shaken M9 media to give an initial bacterial concentration of ~10^6 cm^{-3}. An aliquot was removed to determine the initial bacterial concentration. Phage were then added at a variety of initial concentrations, the cultures were mixed (vortexed) and a sample was removed to measure the initial phage concentrations using the phage plaque assay. This was done by diluting the sample and adding 0.5 ml of Ymel bacteria (grown overnight in LB), adding 2.5 ml of soft agar and pouring onto a λ plate. Throughout the dissertation, the killing curves are designated by using this measured initial phage concentration. The reaction tubes were then incubated at 37°C with shaking at 200 rpm. Every hour an aliquot is taken from the reaction tube, diluted in $MgSO_4$ buffer and plated onto LB plates to determine the viable cell concentration measured in colony forming units (CFUs).

A.2.3 Fluorescent labeling of phage

λ phage (CI857Sam7 obtained from New England Biolabs) was grown as described in the Appendix of Moldovan (2006) and purified using CsCl density gradient method. The phage were then dialyzed 3x against λ phage buffer and stored at 4 °C. To prepare for fluorescent labeling, the phage were dialyzed 3x against a pure 10 mM $MgSO_4$ pH 8.4 solution in order to get rid of all traces of the Tris buffer. 1M sodium bicarbonate (pH 8.4) was added at a volume to volume ratio of 1:10; (1 part sodium bicarbonate to 10 parts phage solution). The phage solution (generally at a concentration of 10^{12}-10^{13} phage/cm^3) was used to dissolve a dried aliquot of AlexaFluor 488 or AlexaFluor 633 (Molecular Probes), the molecule/phage ratio was

of 10^3. The mixture was shaken 150 rpm for 1 hour at room temperature (22 °C) in the dark., and finally dialyzed (3 changes of buffer for >12 hours) against λ phage buffer at 4 °C.

A.3 ESTIMATION OF MODEL PARAMETERS

A.3.1 Size of the cell (a and b)

This section will describe the use of the light microscope to determine the approximate size of the semi-major axis and semi-minor axis of the *E. coli* cells under experimental conditions. About 1 ml of the exponential phase cells was pipetted onto a poly-D-lysine coated coverslip and allowed to sit for 10 minutes. The cell suspension was rinsed off the coverslip with 5 ml modified λ-dilution buffer (10mM $MgSO_4$, pH 7.4) and the attached cells were immersed in the same buffer and viewed with a Nikon TE300 microscope under phase contrast at 100x magnification and images were recorded with a Hamamatsu C9100 CCD camera. A typical image is shown in Figure 46a. Using the SimplePCI program (v.5.3.0) an elliptical region of interest (ROI) was outlined for each cell and the maximum length and width of each elliptical cell was measured. The probability distribution of the measured values were then calculated and binned as can be seen in Figure 46b) and c) for the Ymel strain. The PDF of the radius of the semi-major axis (a) and semi-minor axis (b) of the cells were fit using a log-normal distribution and a Gaussian distribution respectively. The average value found from this fit was reported in the main text and used in all simulations. All constants were independently measured for each strain used.

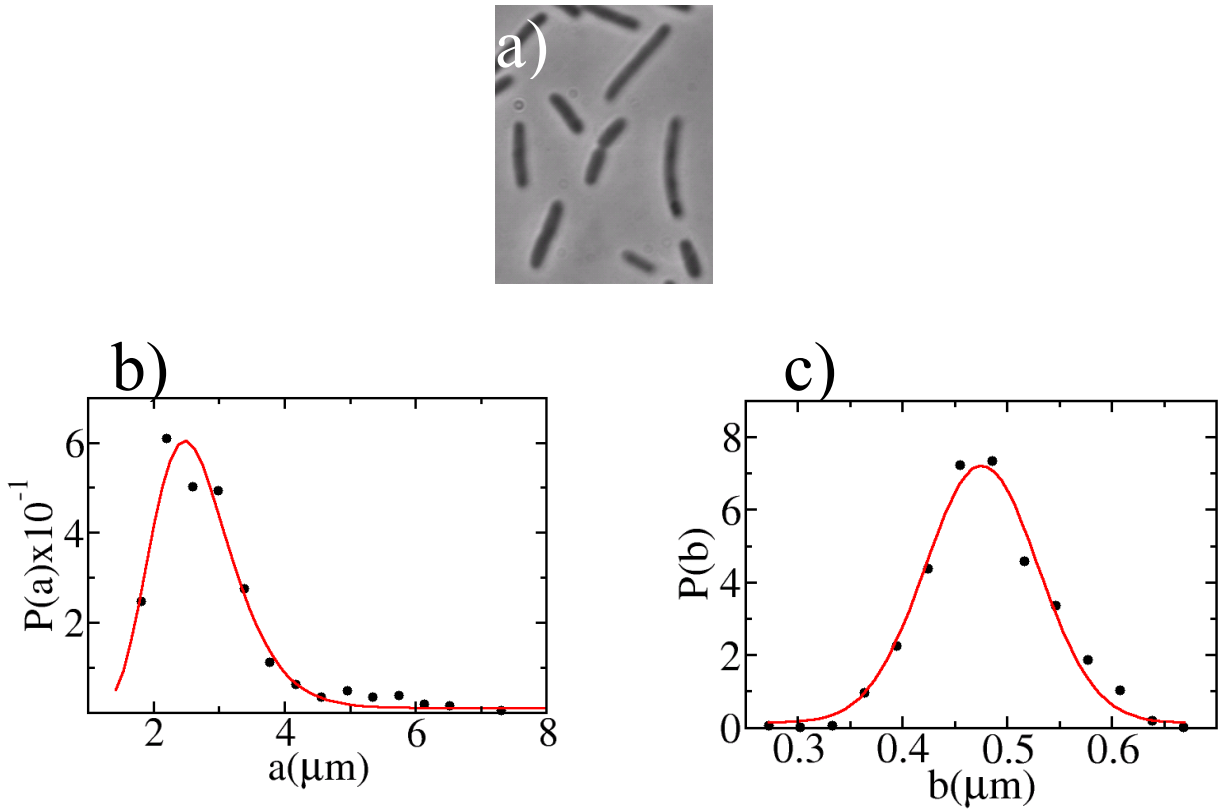

Figure 46 Measurement of the bacterial length and width.
(a) A typical phase picture taken while the strain of interest was attached to a coverslip. (b) PDF of the radius of the semi-major axis of the bacteria LE392. (b) PDF of the radius of the semi-minor axis of the bacteria LE392.

A.3.2 Maximum adsorption rate (γ_o)

The Berg and Purcell model described in Section 1.3 assumes that the receptors on the bacteria are perfect sinks. It was previously found that the adsorption rate for Ymel is comparable to that expected by a bacteria with ~300 receptors using Berg and Purcell's model when adsorption curves were performed in 10mM $MgSO_4$ media pH 7.4 (Moldovan et. al. 2007). For the population dynamics experiment, cells need nutrient supplements for growth and protein

production. Because of this requirement, adsorption experiments were performed in M9 minimal media to test the effect of the salt on the phage adsorption.

Effect of Low Salt Concentrations on Adsorption Coefficients

It has been found previously that the adsorption coefficient is highly dependent on the salt concentrations and more specifically the divalent cations such as $MgSO_4$. Adsorption curves were measured in three different conditions. The first condition was a 10 mM $MgSO_4$ solution similar to previous experiments, the second condition was standard M9 minimal media (1mM $MgSO_4$, no carbon source) and M9 minimal media supplemented with 10mM $MgSO_4$ (no carbon source). The adsorption curves were measured following the protocol that has been previously described (Moldovan 2006, Moldovan et. al. 2007).

The lack of nutrient supplements will greatly decrease bacterial growth so that the B~constant assumption used in Moldovan et. al. 2007 remains valid. Figure 47 is the graph of the adsorption curves which are performed in the B>>P limit ($\frac{P}{B} \approx 5x10^{-3}$). The blue squares were the curve that was measured in M9 media with 1mM MgSO4. Notice that that phage are adsorbed much slower than the curves in the 10mM MgSO4 solution (red squares) and the M9 with 10mM MgSO4 (black circles).

In previous work (Moldovan 2006, Moldovan et. al. 2007) it has been shown that phage adsorption is a two stage process which in the B>>P limit can be modeled as a double exponential. In Figure 47a), we show the adsorption curves with similar initial bacterial concentrations fit with the double exponential function:

$$\frac{P}{Po} = Ae^{-\frac{t}{\tau_1}} + (1-A)e^{-\frac{t}{\tau_2}} \qquad (80)$$

Both the adsorption times τ_1, τ_2 are ~4 times larger in the solution containing 1mM MgSO4 versus the solution containing 10mM MgSO4 for similar values of A. This can also be seen in Figure 47b), where only adsorption over short times <15 minutes are fit with a single exponential and once again we find that the adsorption time in 1mM $MgSO_4$ is 4 times greater than solution with 10mM $MgSO_4$. The experiments in the main text performed in the M9 with 1mM $MgSO_4$ are the killing curves in decreased salt concentration. The maximum adsorption rate in the decreased salt concentration is modeled as $\gamma_{0S} = \frac{\gamma_0}{4}$.

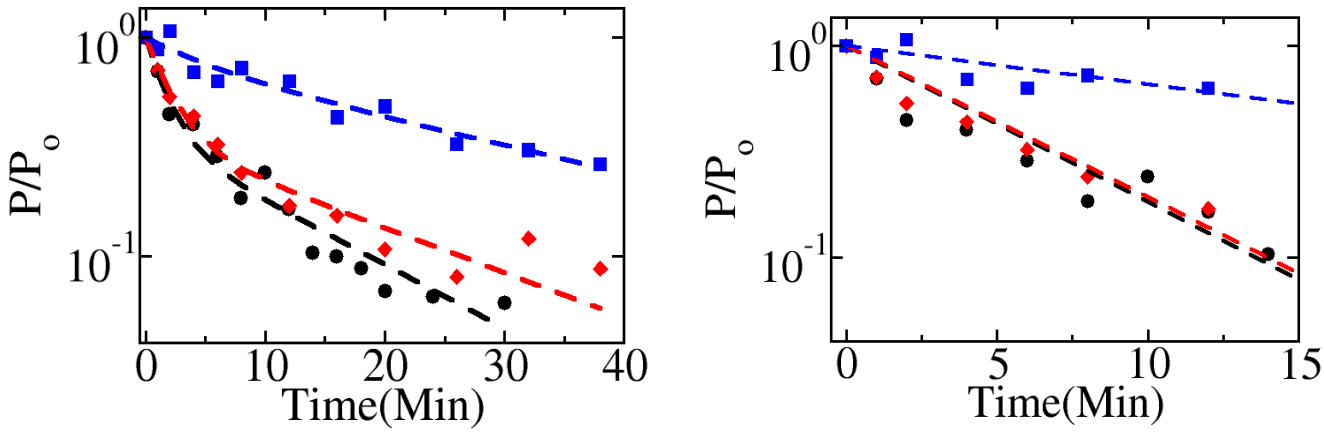

Figure 47 Adsorption measurements in different media with similar initial bacterial concentrations. The adsorption is strongest in media containing 10mM MgSO4 (red diamonds) and M9 media with 10mM $MgSO_4$ (black circles). The adsorption is ~4x slower in standard M9 media which only contain 1mM $MgSO_4$.

Double Exponential Adsorption is a Property of Wild-Type Receptors

The Ymel bacteria adsorbs phage with a double exponential behavior (Moldovan 2006, Moldovan et. al. 2007). In this work, a second strain LE392 is used which shows the double exponential behavior in adsorption. This behavior, though, is not consistent with the adsorption measurements previously reported (Schwartz 1975). In order to check if this behavior is

consistent with the wild-type protein, sequence analyses were performed on the Ymel lamB gene.

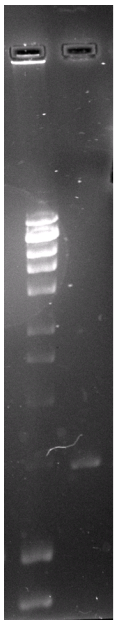

Figure 48 Amplification of the lamB gene for DNA sequencing.
The lamB gene was amplified using PCR and run on a gel (second lane) to check for length and quantity of the fragment for subsequent sequencing analyses. When compared with a GeneChoice quantitative ladder (first lane). The PCR product showed a length of ~1500 bps which is comparable to the expected 1504 bps. Subsequent analyses showed that the Ymel lamB gene is the wild-type lamB gene.

The lamB gene was amplified by colony PCR using pfuUltraII (Stratagene Cat. No. 600670) and the primers 5'CACACAAAGCCTGTCACAGGTGATG'3 and 5'CGCATCAGGCGTTGGTTGCCGAAT'3 which are located 58 bps upstream and 55 base pairs downstream respectively of the lamB gene. The product was visualized on a gel and shown to have a length of ~1500 bps as can be seen in the second lane when compared with the GeneChoice Quantitative Ladder I in the first lane in Figure 48. The expected length was 1504 bps which is in good agreement with the gel measurement. The PCR product was sequenced by automatic sequencing at the DNA Sequencing Center which is a part of the University of Pittsburgh School of Medicine Biomedical Research Support Facilities. The primers used for forward sequencing were:

5'AGAAAAGCAATGACTCAGGAGATAGA'3

5'ATGATGATTACTCTGCGCAAACTTCC'3

5'ATCTGGGCAGGTAAGCGCTTCT'3

5'CTACAATATCAACAACAACGGTCAC'3

The first 400 bps were also sequenced in reverse using the reverse primer 5'GAAGTCGATCATATGAACGTCATG'3 to ensure the accuracy of the first 50 base pairs. The sequence was then compared to the known sequence of the MG1655 strain as described in the ASAP database (Glasner et. al. 2003). We found 100% agreement between the lamB gene in Ymel and MG1655.

A.3.3 Growth Rate (λ)

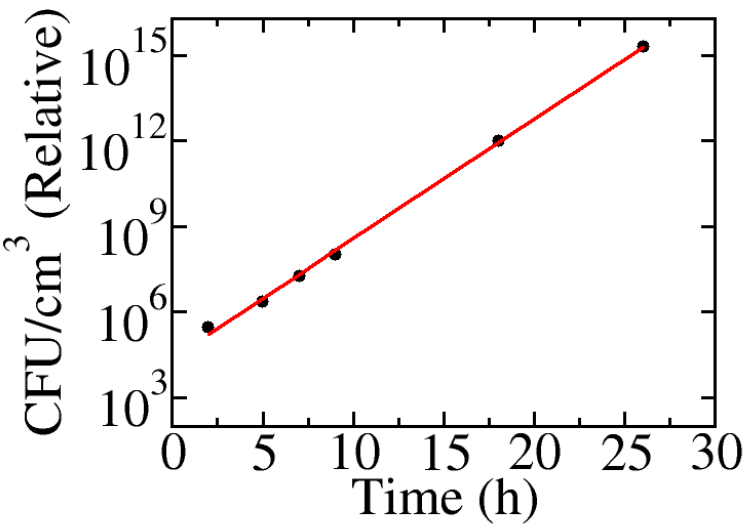

Figure 49 Measurement of the growth rate of the bacteria.
The black circles are the relative CFU/cm^3 after dilution corrections. The measurements were fit with an exponential function (red line) to find the growth rate of the bacterial strains. A typical run for the Ymel strain in which the cells were repeatedly diluted into fresh media and the relative concentration was measured over a period of 26 hours.

This section describes the measurement of the growth rate (λ) of the bacteria without inhibition by phage or lack of nutrients. Cells were grown to exponential phase. The cells were then allowed to shake at 200 rpm at 37°C for 2 hours. At certain time intervals, the colonies were diluted and plated. The experimental curve was then fit with an exponential function to find the growth rate of each cell line. A run for the Ymel strain along with the exponential fit can be seen in Figure 49, relative concentration indicates that the growth rate was measured over a period of time in which the cells were diluted into fresh warmed media in order to keep the cell growth away from nutrient saturation. The relative concentration is the extrapolated concentration if the media could hold an infinite number of cells without saturation. The value given in the text is an average of three separate runs.

A.3.4 Bursting Coefficient (m) and Latent Period (τ)

The bursting coefficient (m) and latent period (τ) were measured using the classical one-step infection procedure first introduced by Ellis and Delbrück (1939). The bacteria were grown to mid-exponential phase and mixed with λ phage at moi~1. The phage were allowed to absorb for 15 minutes at 37 °C, and the reaction was stopped by spinning down the cells at 10^4 g for 2 minutes at room temperature. The pellet was resuspended in a pre-warmed M9 medium, and the washing process was repeated again to reduce the background phage concentration. The cells were diluted 1:10 into a pre-warmed fresh medium and were kept in a 37 °C water bath. An aliquot was taken out of the sample periodically, diluted, and mixed with indicator bacteria. An infected bacterium, before bursting, will appear as one single plaque on the λ plate. However, after bursting each bacterium produces multiple phage and each of them resulting in one plaque.

As seen in Figure 50, a time delay τ after infection was stopped an step in the phage concentration, indicating nearly synchronized bacterial bursting. Using the method of Alvarez et. al. (2006), the experimental points were fit to the function

$$P = I + \frac{N}{1 + e^{-k(t-\theta)}}, \qquad (81)$$

where I is the concentration of the infected cells, N is the total number of phage produced per volume, and k is a measure of synchrony in cell bursts. The fitting procedure yields the bursting coefficient m=N/I≈13 and θ=55.5 minutes. Since the total adsorption time is 15 minutes, we assign the latent period τ=θ-15/2≈48 minutes. We found that while τ is reasonably consistent with previous observations, m is about a factor of 10 smaller than previous experiments. The low phage production is due to the minimal M9 medium used and previous measurements are in rich media (Alvarez et. al. 2006). We also found that when using glucose instead of maltose the bursting coefficient did increase by ~ a factor of 2 indicating the low burst size is due to the minimal medium and carbon source used.

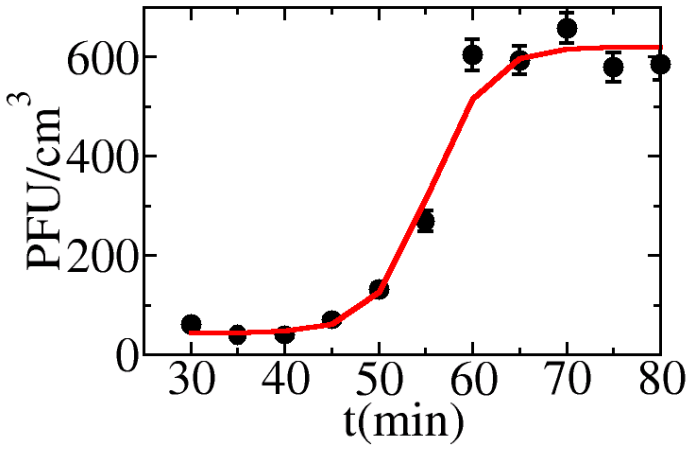

Figure 50 Measurement of the bursting coefficient and latent period.
The PFUs from time 25 minutes to 45 minutes (black circles) are the cells which had been previously infected. The PFUs from time 60 minutes to 80 minutes are the free phage after the bursting event. The ratio of these two constant numbers yields the average bursting coefficient for each strain. The beginning of the bursting event yields the latent period.

A.3.5 Debris Dissolution Rate

The simulations described in the main text are relatively insensitive to the debris degradation because the concentration of debris is low because the initial bacterial concentration in most experiments was ~10^6 bacteria/cc. This is not true when the initial bacterial concentration is greater than ~$2x10^7$ cells/cc. To estimate the debris degradation rate, LE392 cells at an initial concentration of ~$5x10^7$ were mixed with varying initial phage concentrations.

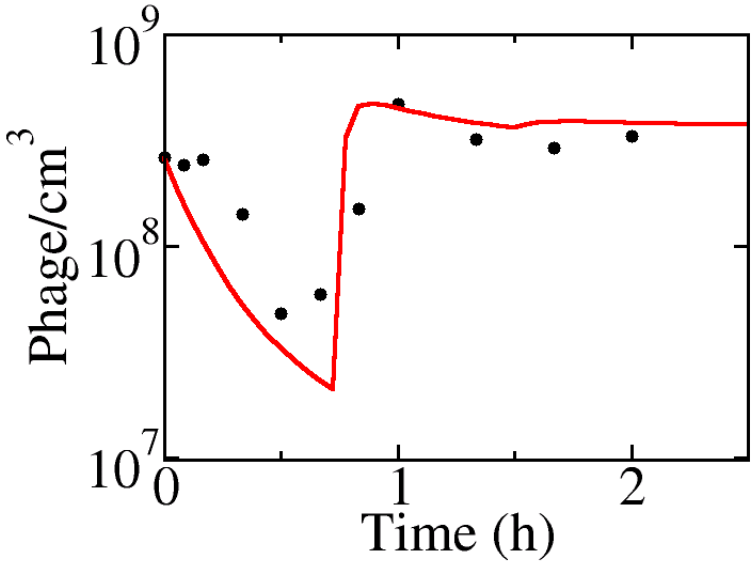

Figure 51 Measurement of the debris dissolution rate.
Phage and bacteria at high concentrations are adsorbed and the free phage concentration is measured. The heterogeneous model was then simulated and ε is varied until the simulated phage concentration (red line) and measured phage concentration (black circles) are similar.

The free phage and bacteria were measured as indicated in the Figure 51. Simulations were run and η was varied until the behavior of the simulated phage population closely resembled the experimental results. An example of both experiment and simulation can be seen in Figure 51 where the initial phage concentration ~$2x10^8$ phage/cm^3. The value of η that

allowed the best consistency between simulation and experiment consistent for most runs. H was fixed at the average value of 0.0003 which is approximately $1/\tau$, where τ is the latent period.

For the killing curves presented in the main text, though, because the debris is at a low concentration $\sim 10^6$ cm^{-3}, it was found that large variation of the debris dissolution rate for numerical integrations only minimally changed the shape of the killing curves.

A.3.6 When do we need to consider genotype mutants?

The heterogeneous model predicts that to kill all sensitive bacteria, the phage concentration must be greater than a phage concentration where the average time of adsorption for a bacteria with one receptor $1/(\gamma_1 P)$ is less than the doubling time of the bacteria and the phage concentration has to be greater than the number of receptors present ($P_o > B_{\text{tot}} \times \overline{N}$) to account for the possibility that the extra receptors per bacteria do not sink the effective phage pressure. In order to test the effects of adding an extremely large phage concentration we added 4×10^{10} phage/cm^3 to an exponentially growing bacterial population. The bacterial population was then sampled at hour intervals. As can be seen in Figure 52, the blue circles show that there is an initial immense killing of two orders of magnitude of the bacteria are killed over a period of an hour and then a slower decay where another two orders of magnitude of bacteria are killed over a period of 4 hours. After hour 5 the bacteria begin growing exponentially at a rate comparable to bacteria that are not under phage pressure. The bacteria that were plated at hour 9 do not form plaques after being regrown without pressure (the cells did not form plaques with either λ-CI857 or λ-vir). Extrapolating back to t=0, after an average of independent experiments we find that in a population of bacteria with an initial concentration of 3×10^7cm^{-3} that we find 4±3 mutants, indicating that the probability of finding a mutant is about 10^{-7}. We assume that

this is our baseline mutant background in the persister experiments and being that the initial bacterial concentration in those experiments is $10^6 cm^{-3}$ we should find a mutant in the initial population only about 10% of the time, which would only become dominate in the population after >10 hours wł

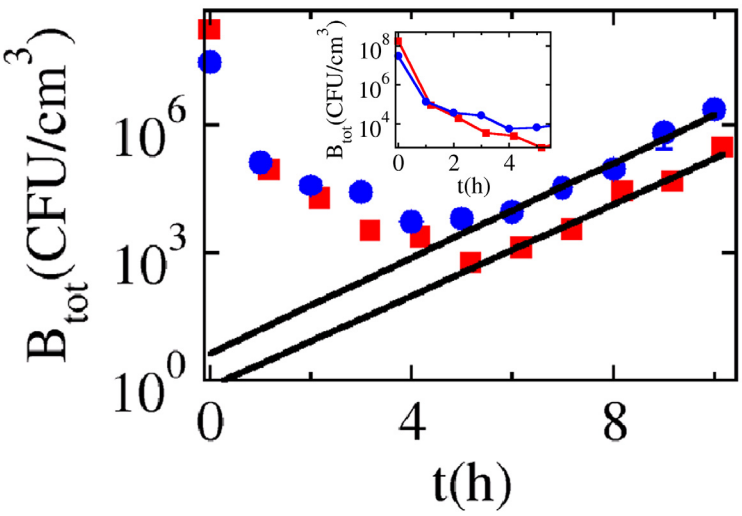

Figure 52 Testing for mutants.
The Ymel strain is bombarded with an immense phage concentration ~$4x10^{10}$ phage/cm^3. This phage concentration kills about 4 orders of magnitude of Ymel (blue circles) cells which are not sensitive when regrown without pressure. Ymel/PTAS1 (red squares) are also bombarded with a high phage concentration and show greater killing but also begin to regrow at 5 hours with cells that are insensitive to phage infection.

Ymel was transformed with the plasmid pTAS1 which was a kind gift from the Lawrence lab (Kolko et. al. 2001). pTAS1 is a plasmid which confers ampicillin resistance and constitutively expresses the maltoporin protein. The Ymel/pTAS1 cells were grown to the overnight state in M9 media with maltose and supplemented with ampicillin, the cells were diluted 1:15 and allowed to grow for ~2 hours to mid-exponential phase. A high phage concentration ~$4x10^{10}$ cm^{-3} was added and the reaction was sampled every hour. The red squares in Figure 52 are the killing curve for Ymel/pTAS1. Notice in the constitutively expressed cells, the initial killing (between hour 0 and 1) is approximately 1 order of magnitude

greater than the Ymel cells without a plasmid. The slow killing between hour 1 and hour 5 is also greater for the pTAS1 cells, killing about an order of magnitude greater than the Ymel cells without the plasmid.

To test the sensitivity of the pTAS1 cells, ten colonies from each time point on the pTAS1 killing curve were regrown and tested for their ability to form plaques on a soft agar plate. Figure 53 shows the percentage of regrown cells at each time point that formed plaques. Initially (hours 0-2) all cells were sensitive, but the percentage of sensitive regrown cells decreases in hours 3-5 until no regrown cells are sensitive at hour 6 at the time in the killing curve when the cells begin to grow exponentially at a rate comparable to that of the wild-type Ymel. Because these cells are not sensitive when regrown under lack of pressure and because the cells still show ampicillin resistance implying the cells still carry the high copy number pTAS1 plasmid, the cells are most likely insensitive to phage infection due to mutations that are not associated with the maltose regulon. This is reminiscent of the pel- mutants which have been described previously (Elliot and Arber 1978).

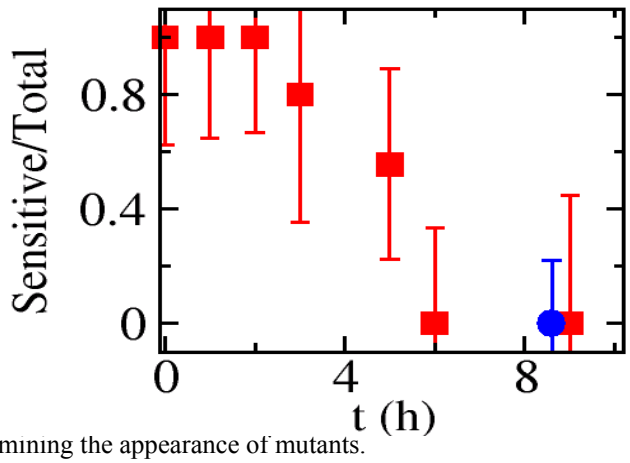

Figure 53 Examining the appearance of mutants.
The Ymel/pTAS1 cells can initially all be regrown and show sensitivity to phage infection (hours 0-2) but beginning at hour 3 a percentage of the regrown cells appear to be insensitive to phage infection until hour 6 where none of the regrown cells show sensitivity to phage infection this correlates well with the position in the killing curve where the cells begin to regrow insensitive to phage pressure. The red squares are for the Ymel/pTAS1 run and the blue circle is for the Ymel run presented in Figure 52.

A.3.7 A plasmid with the malK promoter.

In order to investigate the expression level of the malK promoter independent of the appearance of functional receptors, a plasmid was created that confers ampicillin resistance and controls expression of the Green Fluorescent Protein by the malK promoter. The pBV1114 plasmid was a gift from the Larsson lab at the Swedish Centre for Bioprocess Technology (Bostrom and Larsson 2004). It is a plasmid with confers ampicillin resistance and the malK promoter controls expression of the lacZ gene. The pELC1 plasmid was previously constructed and is a high copy number plasmid which controls the GFPmut2 (Cormack et. al. 1996) gene using the λ_{PR} promoter.

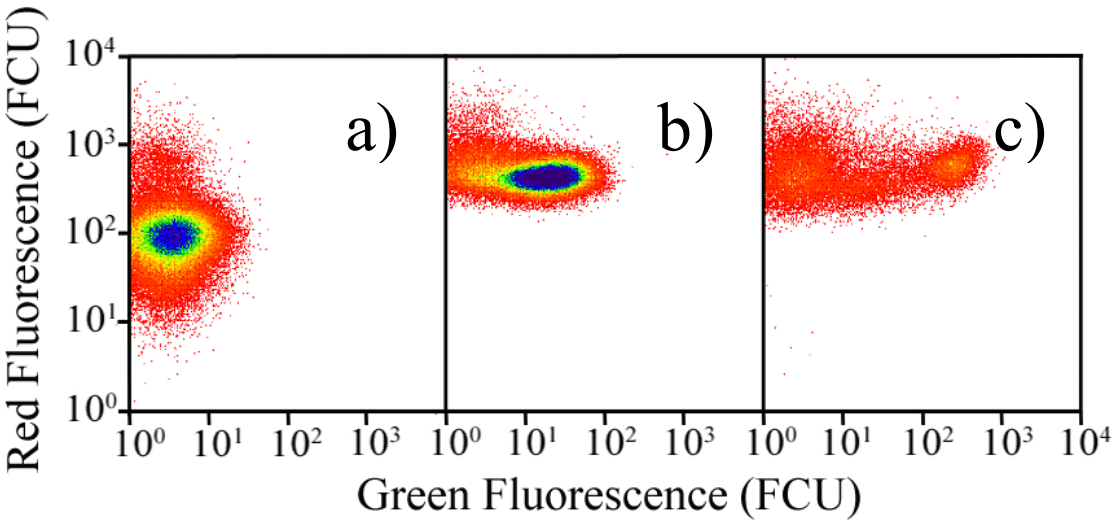

Figure 54 LE392 cells with a plasmid which controls the expression of GFP with the malK promoter. The cells are grown in glucose and assayed with red phage where it is found that the addition of the plasmid has actually increased the leakage of functional receptors in the uninduced state (a). The cells are then perturbed by changing the carbon source to maltose. After 20 minutes both the red and green fluorescence has increased (b). 3 hours after the maltose perturbation the cells are not growing quickly but for cells which expressed the green fluorescence higher than the background, there is a correlation between the green and red fluorescence (c).

The malK promoter from pBV1114 promoter was cut out of the plasmid at the EcoRI and BamHI sites and the λ_{PR} promoter on the pELC1 plasmid was replaced by the malK promoter.

The new plasmid was called pELC12. In order to replace the origin of replication to create a low copy number plasmid, the origin of replication was cut out of the pELC12 at the AccI and EcoRI sites and replaced with the pSC101 origin of replication from the pCIA2 plasmid which was a gift from the Jim Collins laboratory at Boston University (Gardner et. al. 2000). The newly constructed plasmid pELC15 is a low copy number plasmid (pSC101 generally has ~5 copies per cell) which confers ampicillin resistance and controls the GFPmut2 gene with the malK promoter. This plasmid was transformed into the LE392 cells that were used in the main text. All experiments were performed in the presence of ampicillin to ensure all cells contained the pELC15 plasmid. The functional receptors were assayed using phage labeled with Alexa Fluor 633.

Figure 54a) is the flow cytometry data of LE392 cells grown in glucose and assayed with red phage. The green fluorescence is a measure of the relative expression of the malK promoter and the red fluorescence is a measure of the number of functional receptors. The first thing to notice is that by adding the plasmid (which introduces several extra sinks for the activator malT and cAMP/CRP) the number of expressed functional receptors actually increases an interesting consequence of the perturbation of the maltose regulon network. Notice the red fluorescence when the cells are grown in glucose has an average of ~120 which corresponds to approximately 100 functional receptors per bacteria in the presence of glucose which is an order of magnitude higher than LE392 without the plasmid but is approximately the number of functional receptors expressed by the strain HfrG6 discussed briefly in the main text when it is grown in glucose. This figure also shows the green background fluorescence of the cells has increased by a factor from a value of 2 FCUs to a value of 4 FCUs which is consistent with a small leakage of GFP proteins from the plasmid. Both the autofluorescence of cells without the plasmid and no GFP

have a correlation coefficient $CC = \frac{< XY > - < X >< Y >}{\sigma_X \sigma_Y}$ ~0 where X and Y are two variables and σ_X is the standard deviation of X and σ_Y is the standard deviation of Y.

The glucose grown cells were then perturbed by placing them in media containing maltose as the sole carbon source. 20 minutes after the maltose perturbation the cells were once again assayed with red phage. The data is presented in Figure 54b) both the red fluorescence and the green fluorescence have increased. The mean red fluorescence has increased to 500 FCUs corresponding to ~500 functional receptors, the green fluorescence has also increased by a factor of 5 to 20 FCUs. The interesting aspect of this graphs is that while CC=-0.1 for the entire population, the cells whose green fluorescence has increased above the natural background have CC=0.1 so we do begin to see the expected correlation between the red and green fluorescence.

In Figure 54c), the data is presented for the same cells 3 hours after the maltose perturbation. The cells were unable to grow well in maltose when the plasmid is present, but the viable cells still expressed both red and green fluorescence. After 3 hours the cells are now expressing 600 functional receptors which is about equal to the maximum in the cells without the plasmid. The green fluorescence has also increased to 70 FCUs. For the entire population, CC=0 and there seems to be no correlation but once again just looking at the cells that express green fluorescence above the background it is found that CC=0.4 meaning that we have found a correlation between our functional receptor assay and the internal expression of protein.

BIBLIOGRAPHY

Alvarez, L.J., P. Thomen, T. Makushok and D. Chatenay. 2007. Propagation of Fluorescent viruses in growing plaques. *Biotechnol. Bioeng.* 96:615-621.

Balaban, N.Q., J. Merrin, R. Chait, L. Kowalik, and S. Leibler. 2004. Bacterial Persistence as a Phenotypic Switch. *Science* 305:1622-1625.

Bar-Even, A. J. Paulsson, N. Maheshri, M. Carmi, E. O'Shea, Y. Pilpel and N. Barkai. 2006. Noise in protein expression scales with natural protein abundance. *Nat. Gen.* 38: 636-643.

Berg, H. C. 1993. Random Walks in Biology. Princeton University Press, Princeton. 1st ed.

Berg, H. C., and E. M. Purcell. 1977. Physics of Chemoreception. *Biophys. J.* 20:193-219.

Blaxter, M. 1998. *Caenorhabditis elegans* Is a Nematode. *Science.* 282:2041-2046.

Boos, W., and H. Shuman. 1998. Maltose/Maltodextrin System of *Escherichia coli:* Transport, Metabolism, and Regulation. *Microbio. Mol. Bio. Rev.* 62:204-229.

Bostrom, M. and G. Larsson. 2004. Process design for recombinant protein production based on the promoter, P_{malk}. *Appl. Microbiol. Biotechnol.* 66:200-208.

Braun, V., and H. J. Krieger-Brauer. 1977. Interrelationship of phage λ receptor protein and maltose transport in mutants of *Escherichia coli* K12. *Biochim. Biophys. Acta.* 469:89-98.

Brooks, K., and A. J. Clark. 1967. Behavior of λ Bacteriophage in a Recombination Deficient Strain of *Escherichia coli*. *J. Virol.* 1:283-293.

Busby, S. and R. Ebright. 1999. Transcription Activation by Catabolite Activator Protein (CAP). *J. Mol. Biol.* 293:199-213.

Cai, L., N. Friedman, and X. S. Xie. 2006. Stochastic protein expression in individual cells at the single molecule level. *Nature.* 440: 358-362.

Capy, P. 2000. Is Bigger Better in Cricket? *Science.* 287:985-986.

Casadesus, J. and R. D'Ari. 2002. Memory in Bacteria and Phage. *BioEssays.* 24:512-518.

Chao, L., B. R. Levin, and F. M. Stewart. 1977. A Complex Community in a Simple Habitat: An Experimental Study with Bacteria and Phage. *Ecology.* 58:369-378.

Chapman-McQuiston, E. and X.L. Wu. Stochastic Receptor Expression Allows Sensitive Bacteria to Evade Phage Attack. Part I: Experiments. (submitted to Biophys. J., 2007).

Chapman-McQuiston, E. and X.L. Wu. Stochastic Receptor Expression Allows Sensitive Bacteria to Evade Phage Attack. Part II: Theoretical Analyses. (submitted to Biophys. J., 2007).

Charbit, A., K. Gehring. H. Nikaido. T. Ferenci. and M. Hofnug. 1988. Maltose Transport and Starch Binding in Phage-resistant Point Mutants of Maltoporin. *J. Mol. Biol.* 201:487-496.

Cormack, B. P., R. H. Valdivia, and S. Falkow. 1996. FACS-optimized mutants of the green fluorescent protein (GFP). *Gene.* 173:33-38.

Corsetti, J. P., S. V. Sotirchos, C. Cox, J. W. Cowles, J. F. Leary, and N. Blumburg. 1988. Correction of Cellular Autofluorescence in Flow Cytometry by Mathematical Modeling of Cellular Fluorescence. *Cytometry.* 9:539-547.

Crick, F. 1970. Central Dogma of Molecular Biology. *Nature.* 227:561-563.

Ellis, E. and M. Delbrück. 1939. The Growth of Bacteriophage. *J. Gen. Phys.* 22:365-284.

Elliott, J., and W. Arber. 1978. *E. coli* K-12 pel mutants, which block phage lambda DNA injection, coincide with ptsM, which determines a component of a sugar transport system. *Mol. Gen. Genet.* 161:1-8.

Elowitz, M. B., A. J. Levine, E. D. Siggia, and P. S. Swain. 2002. Stochastic Gene Expression in a Single Cell. *Science.* 297:1183-1186.

Ericsson, M., D. Hanstorp, P. Hagerberg, J. Enger, and T. Nystrom. 2000. Sorting Out Bacterial Viability with Optical Tweezers. *J. Bacteriol.* 182:5551-5555.

Friedman, N., L. Cai, and X. S. Xie. 2006. Linking Stochastic Dynamics to Population Distribution: An Analytical Framework of Gene Expression. *Phys. Rev. Let.* 97: 168302

Gardner, T.S., C.R. Cantor and J.J. Collins. (2000). Construction of a genetic toggle switch in *Escherichia coli. Nature.* 403:339-342.

Gibbs, K. A., D. D. Isaac, J. Xu, R. W. Hendrix, T. J. Silhavy and J. A. Theriot. (2004) Complex spatial distribution and dynamics of an abundant *Escherichia coli* outer membrane protein, LamB. *Mol. Microbiol.* 53:1771-1783.

Glasner, J. D., P. Liss, G. Plunkett III, A. Darling, T. Prasad, M. Rusch, A. Byrnes, M. Gilson, B. Biehl, F.R. Blattner, and N. T. Perna. 2003. ASAP, a systematic annotation package for community analysis of genomes. *Nucleic Acids. Res.* 31:147-151.

Golding, I., J. Paulsson, S. M. Zawilski and E. C. Cox. (2005) Real-Time Kinetics of Gene Activity in Individual Bacteria. *Cell.* 123: 1025-1036.

Halme, A., S. Bumgarner, C. Styles, and G. R. Fink. 2004. Genetic and Epigenetic Regulation of the FLO Gene Family Generates Cell-Surface Variation in Yeast. *Cell.* 116:405-415.

Havilio, M. 2006. Signal Deconvolution Based Expression-Detection and Background Adjustment for Microarray Data. *J. Comput. Biol.* 13:63-80.

Hershey, A.D. and Chase, M. 1952. Independent functions of viral protein and nucleic acid in growth of bacteriophage. *J Gen Physiol.* 1:39-56.

Hofnung, M., A. Jezierska, and C. Braun-Breton. 1976. *lamB* mutations in *E. coli* K12*:* growth of lambda host range mutants and effect of nonsense suppressors*. Mol. Gen. Genet*. 145: 207-213.

Leal, J. and H. Marcovich. 1975. Electron Microscopic Observations of the *tsx*^{s} Gene Expression in *Escherichia coli* K12F^{-} Cells after Conjugation with Hfr Bacteria. *Molec. Gen. Genet.* 139:203-212.

Lenski, R.E. 1988. Dynamics of Interactions between Bacteria and Virulent Bacteriophage. *In* Advances in Microbial Ecology. Marshall KC, editor. Plenum Press, New York. 1-44.

Lenski, R.E., and B.R. Levin. 1985. Constraints on the Coevolution of Bacteria and Virulent Phage: A Model, Some Experiments, and Predictions for Natural Communities. *American Naturalist* 125(4):585-602.

Levin, B.R., F.M. Stewart, and L. Chao. 1977. Resource-limited growth, competition and predation: a model and experimental studies with bacteria and bacteriophage. *American Naturalist* 111:3-24.

Lipsitch, M., E. A. Herre and M. A. Nowak. 1995. Host Population Structure and the Evolution of Virulence: A "Law of Diminishing Returns." *Evolution.* 49:743-748

Lotka, A. J. 1925. Elements of physical biology. Baltimore: Williams & Wilkins Co.

Kaufmann, B., Q. Yang, J. Mettetal, and A. van Oudenaarden. 2007. Heritable Stochastic Switching Revealed by Single-Cell Genealogy. *PLoS Biology.* 5:e239.

Kolko, M. M., L. A. Kapetanovich, and J. G. Lawrence. 2001. Alternative pathways for siroheme synthesis in *Klebsiella aerogenes*. *J. Bacteriol.* 183:328-335.

Kussel, E., R. Kishnoy, N. Q. Balaban and S. Leibler. 2005. Bacterial Persistence: A Model of Survival in Changing Environments. *Genetics.* 169:1807-1814.

Maamar, H., A. Raj and D. Dubnau. 2007. Noise in Gene Expression Determines Cell Fate in *Bacillus subtilis*. *Science.* 317:526-529.

Mader, S. 2004. Biology. McGraw-Hill, New York. 8th ed.

Mangan, S., A. Zaslaver and U. Alon. 2003. The Coherent Feedforward Loop Serves as a Sign-sensitive Delay Element in Transcription Networks. *J. Mol. Biol.* 334:197-204.

May, R. 1976. Simple mathematical models with very complicated dynamics. *Nature.* 261:459-467.

May, R. 1972. Limit Cycles in Predator-Prey Communities. *Science.* 177:900-902.

Mignotte, M., J. Meunier, J.-P. Soucy, and C. Janicki. 2002. Comparison of deconvolution techniques using a distribution mixture parameter estimation: Application in single photon emission computed tomography imagery. *Journal of Electronic Imaging.* 11:11-24.

Moldovan, R. 2006. The Interaction Between Lambda Phage and Its Bacterial Host. Ph.D. thesis. University of Pittsburgh, Pittsburgh. pp 98.

Moldovan, R., E. Chapman-McQuiston, and X.L. Wu. 2007. On Kinetics of Phage Adsorption. *Biophys. J.* 93:303-315.

Novick, A. and M. Weiner. 1957. Enzyme Induction as an All-or-None Phenomenon. *Proc. Natl. Acad. Sci. USA.* 43:553-566.

Ozbudak, E. M., M. Thattai, I. Kurtser, A. D. Grossman and A. van Oudenaareden. 2002. Regulation of noise in the expression of a single gene. *Nature Genetics.* 31:69-73.

Ozbudak, E. M., M. Thattai, H. N. Lim, B. I. Shraiman and A. van Oudenaareden. 2004. Multistability in the lactose utilization network of *Escherichia coli. Nature.* 427:737-740.

Press, W. H., S. A. Teukolsky, W. T. Vetterling and B. P. Flannery. 1988. Numerical Recipes in C: The Art of Scientific Computing. Cambridge University Press, New York.

Ptashne, M. 2004. A genetic switch: phage lambda revisited. Cold Spring Harbor Press, Cold Spring Harbor, NY. 3rd ed.

Rabinovitch, A., I. Aviram, and A. Zaritsky. 2003. Bacterial debris--an ecological mechanism for coexistence of bacteria and their viruses. *J. Theor. Biol.* 224:377-383.

Raser J. M. and E. K. O'Shea. 2004. Control of Stochasticity in Eukaryotic Gene Expression. *Science.* 304:1811-1814.

Raser, J. M. and E. K. O'Shea. 2005. Noise in Gene Expression: Origins, Consequences and Control. *Science.* 309:2010-2013.

Rosenfeld. N., J.W. Young, U. Alon, P. S. Swain and M. B. Elowitz. 2005. Gene Regulation at the Single-Cell Level. *Science.* 307:1962-1965.

Ryter, A., H. Shuman, and M. Schwartz. 1975. Integration of the Receptor for Bacteriophage Lambda in the Outer Membrane of *Escherichia coli:* Coupling with Cell Division. *J. Bact.* 122:295-301.

Schirmer, T., Keller, T.A., Wang, Y.F., and J. P. Rosenbusch. 1995. Structural basis for sugar translocation through maltoporin channels at 3.1 Å resolution. *Science.* 267:473-474.

Schrag, S.J., and J.E. Mittler. 1996. Host-Parasite Coexistence: The Role of Spatial Refuges in Stabilizing Bacteria-Phage Interactions. *The American Naturalist* 148(2):348-377.

Schwartz, M. 1975. Reversible interaction between coliphage lambda and its receptor protein. *J. Mol. Biol.* 99:185-201.

Schwartz, M. 1976. The Adsorption of Coliphage Lambda to its Host: Effect of Variations in the Surface Density of Receptor and in Phage-Receptor Affinity. *J. Mol. Biol.* 103:521-536.

Schwartz, M. 1987. The Maltose Regulon. *In Escherichia coli* and *Salmonella typhimurium.* Neidhardt FC, editor. American Society for Microbiology, Washington, D.C.

Shapiro, H. M. 2003. Practical Flow Cytometry. John Wiley & Sons, Inc. Hoboken, New Jersey. 4th ed.

Shen-Orr, S. S., R. Milo, S. Mangan and U. Alon. 2002. Network motifs in the transcriptional regulation network of *Escherichia coli. Nature Genetics.* 31:64-68.

Siegele, D. A. and J. C. Hu. 1997. Gene expression from plasmids containing the *araBAD* promoter at subsaturating inducer concentrations represents mixed populations. *Proc. Natl. Acad. Sci. USA*. 94:8168-8172.

Swain, P., M. B. Elowitz, and E. Siggia. 2002. Intrinsic and extrinsic contributions to stochasticity in gene expression. *Proc. Natl. Acad. Sci. USA*. 99:12795-12800.

Szmelcman, S. and M. Hofnug. 1975. Maltose Transport in *Escherichia coli* K-12: Involvement of the Bacteriophage Lambda Receptor. *J. Bacteriol.* 124:112-118.

Thattai, M. and A. van Oudenaarden. 2001. Intrinsic noise in gene regulatory networks. *Proc. Natl. Acad. Sci. USA*. 98:8614-8619.

Thattai M. and A. van Oudenaarden. 2004. Stochastic gene expression in fluctuating environments. *Genetics.* 167:523:530.

Ureta, A.R., R. Endres, N. Wingreen and T. Silhavy. 2007. Kinetic analysis of the assembly of

the outer membrane protein LamB in Escherichia coli mutants each lacking a secretion or targeting factor in a different cellular compartment. *J. Bacteriol.* 189:446-454

Volterra, V. 1926. Variazioni e fluttuazioni del numero d'individui in specie animali conviventi. Mem. R. Accad. Naz. dei Lincei. Ser. VI, vol. 2.

Wangersky, P. and W. Cunningham. 1957. Time Lab in Prey-Predator Population Models. *Ecology.* 38:136-139.

Weaver, R. F. 2002. Molecular Biology. McGraw-Hill, New York, 2nd ed.

Yu, J., J. Xiao, X. Ren, K. Lao and X. S. Xie. 2006. Probing Gene Expression in Live Cells One Protein Molecule at a Time. *Science.* 311:1600-1603.